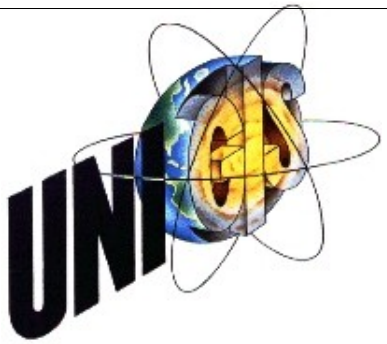

Master Thesis

im Rahmen des

Universitätslehrganges „Geographical Information Science & Systems“

(UNIGIS MSc) am Interfakultären Fachbereich für GeoInformatik (Z_GIS)

der Paris Lodron-Universität Salzburg

zum Thema

"Approaches to topographic normalization for forest type mapping in Shitai County, Anhui Province, China"

vorgelegt von

MSc Metodi Panev

10662, UNIGIS MSc Jahrgang 2012

Zur Erlangung des Grades

„Master of Science (Geographical Information Science & Systems) – MSc(GIS)”

Freiburg, February 2015

Table of Contents

Figure Index....IV
Index of Tables....VI
Abbreviations....VII
SUMMARY....1

1 INTRODUCTION....3

1.1 BACKGROUND....3
1.2 OBJECTIVES AND RESEARCH QUESTIONS OF THE MASTER THESIS....4
1.3 THEORETICAL BACKGROUND....6
1.3.1 Topographic effect....7
1.3.2 Topographic normalization....9
1.3.3 Ratio based approaches....9
1.3.4 Approaches using DEM....11
Lambertian surfaces / models....12
Non-Lambertian surfaces / models....14
Issues with the topographic normalization models....15
1.4 STUDIES FROM THE REGION....16
2 MATERIALS AND METHODS....17

2.1 STUDY SITE....17
Location....17
Vegetation....19
2.2 AVAILABLE MATERIALS....20
2.2.1 Satellite imagery....20
Rapid Eye....20
Landsat 8....22
2.2.2 Digital Elevation Model (DEM)....24
2.3 SOFTWARE....24
Quantum GIS....24
Orfeo Toolbox....24
Semi-automatic classification plug-in....25
ForestEye Processor....25
3 METHODOLOGY....26

3.1 FIELD WORK - LAND USE INVENTORY....27
3.1.1 Field Maps....29
3.1.2 GIS Project....30
3.1.3 Navigation....30
3.1.4 Delineation of land cover types....31
3.1.5 Land Cover Classification Scheme....31
3.2 DATA ANALYSIS....34
3.2.1 Atmospheric correction....34
3.3 TOPOGRAPHIC NORMALIZATION....35
3.3.1 No separation....36
3.3.2 Classes separation....36

Separation of classes using NDVI....37
Separation using slope classes....37
Separation of classes using using the illumination....37
3.3.3 Shadow removal....38
3.3.4 Effects of imagery resolution to the topographic normalization....39
3.4 LAND COVER CLASSIFICATION....41
3.4.1 Multi-seasonal image....42
3.4.2 Ancillary data....42
3.5 TRAINING AREAS....43
3.5.1 Accuracy assessment....45
4 RESULTS....47
4.1 FIELD WORK....47
4.1.1 Problems encountered during field work....48
4.2 TOPOGRAPHIC NORMALIZATION....49
4.2.1 Topographic normalization of Rapid Eye imagery....50
Visual assessment....51
Original images - no separation....51
NDVI classes....52
Slope classes....53
Illumination classes....54
Shadow masking....54
4.2.2 Topographic normalization of Landsat Imagery....56
Visual assessment - topographic normalization for the Landsat 8 Image....56
4.3 SUPERVISED CLASSIFICATION....57
4.3.1 Training areas....57
4.3.2 Classification results....58
Results - original images....58
Results - Original images topographically corrected....60
Results - NDVI classes....62
Results - Slope classes....64
Results - Illumination classes....65
5 DISCUSSION....68
5.1 TOPOGRAPHIC NORMALIZATION METHODS....68
5.1.1 Separation of the images by vegetation classes....69
5.1.2 Role of image resolution to the topographic normalization....70
5.2 LAND COVER CLASSIFICATION....71
5.2.1 Ancillary data....72
5.2.2 Training areas....73
6 CONCLUSION....74
7 LITERATURE....76
8 ACKNOWLEDGEMENT....82
9 ANNEX....83
9.1 ANNEX 1 - LAND COVER STATISTICS....83

9.2 ACCURACY ASSESSMENT....84
9.3 ERROR MATRIX....85
9.3.1 Class: original images....85
9.3.2 Class: no separation....86
9.3.3 Class: NDVI....87
9.3.4 Class: slope....88
9.3.5 Class: Illumination....89
9.4 DATASETS FOR LAND COVER CLASSIFICATION....90
DECLARATION OF AUTHORSHIP....117

Figure Index

Figure 1: Overview of error sources in remote sensing (Lunetta et al. 1991; Powell et al. 2004).....6
Figure 2: Topographic effect.....7
Figure 3: Topographic effect in the RapidEye and Landsat 8 imagery.....8
Figure 4: Comparison of a multispectral image (RapidEye bands 541) and NDVI.....10
Figure 5: Angles involved in the calculation of IL (Justice & Holben 1979; Riano et al. 2003).....11
Figure 6: Schematic presentation of the lambert's cosine law*.....12
Figure 7: Part of the Project Area which is subject of this Master Thesis.....18
Figure 8: Elevation profile of the region. The profile follows the red line on the image from S-N.....18
Figure 9: Differences in resolution between the RapidEye image (left) and the Landsat 8 iage (right).....20
Figure 10: Spectral characteristics of the different bands for the RapidEye images.....21
Figure 11: Time-line of Landsat Missions (USGS 2014).....22
Figure 12: Flow chart of the work steps as part of the master thesis.....26
Figure 13: a) overview of the Sampling Plots in the Project Area and the Study Area; b) scheme of a sample plot including the intended delineation of land use types; c) Land use types coded according to the delineated land use.....28
Figure 14: Color composites of the study area (a - true color composite bands 321; b - false color composite 541).....29
Figure 15: Atmospheric correction module - ForestEye processor.....34
Figure 16: The Topographic correction module of the ForestEye Processor.....35
Figure 17: The classification option of the semi-automatic classification plugin.....41
Figure 18: Obtaining training areas from delineating the field maps. a) field map; b) Delineated training areas.....44
Figure 19: Example of the Google Earth high-resolution imagery from the study area..44
Figure 20: Schematic presentation of a typical confusion matrix (Strahler et al. 2006)..46
Figure 21: Illumination rasters: a) RapidEye spring; b) Landsat 8.....49
Figure 22: Visual assessment of the topographic correction on a complete image. The first row are examples from the spring and second row are examples from the autumn RapidEye image.....51
Figure 23: Visual assessment of the topographic correction - NDVI classes separation. The first row are examples from the spring and second row are examples from the autumn RapidEye image. The red squares show the areas which are over-corrected.....52
Figure 24: Visual assessment of the topographic correction - Slope classes separation. The first row are examples from the spring and second row are examples from the autumn RapidEye image.....53
Figure 25: Visual assessment of the topographic correction - Illumination classes separation. The first row are examples from the spring and second row are examples from the autumn RapidEye image.....54
Figure 26: Results of the object-based approach for shadow masking. a) the segments overlaid on the spring RE image; b) the red colored area presents the result of the object based classification - in this case presenting the shadows.....55
Figure 27: Visual assessment of the topographic normalization procedure for the landsat

8 image.....56
Figure 28: Color style used for the land cover classification.....58
Figure 29: Overview of the land cover classification of the original not-corrected image 58
Figure 30: Overview of the land cover classification of the original images (a - RE spring false color composites 541; b - classification of datasets containing all bands from the spring and autumn images; c - datasets with all bands with the addition of ancillary data).....60
Figure 31: Overview of the land cover classification of the images corrected by NDVI classes (a - RE spring false color composites 541; b - classification of datasets containing all bands from the spring and autumn images; c - datasets with all bands with the addition of ancillary data).....62
Figure 32: Overview of the land cover classification of the images corrected by Slope classes (a - RE spring false color composites 541; b - classification of datasets containing all bands from the spring and autumn images; c - datasets with all bands with the addition of ancillary data).....64
Figure 33: Overview of the land cover classification of the images corrected by Illumination classes (a - RE spring false color composites 541; b - classification of datasets containing all bands from the spring and autumn images; c - datasets with all bands with the addition of ancillary data).....66
Figure 34: Left over topographic effect in the classified images (a - topographically normalized image; land cover map of b - topographically normalized image; c - original not corrected image).....71
Figure 35: Comparing the effects of ancillary data to the land cover classification.....72

Index of Tables

Table 1: Spectral bands of Landsat 8 imagery.....23
Table 2: Attributes recorded on the plots center of each LUI Plot.....31
Table 3: Land Cover Classification System used for the LUI (lin4carbon 2014).....32
Table 4: Metadata used for the calculation of the illumination raster.....35
Table 5: Separation of the Rapid Eye imagery in classes according to NDVI values.....37
Table 6: Overview - results from the field work.....47
Table 7: Initial land use calculation based on the delineated inventory plots.....48
Table 8: Correlation indicies of the topographic correction for all classes. The highest 5 correlations per band are marked in bold; the lowest 5 correlations are in italic. (C-correction; M - Minnaert method; R - Rotation method).....50
Table 9: Correlation indicies of the topographic normalization for the shadow masked images. (C-correction; M - Minnaert method; R - Rotation method).....55
Table 10: Correlation indicies of the topographic normalization for the Landsat 8 Image.....56
Table 11: Separation of the trainings dataset for classification and verification.....57
Table 12: Land cover statistics for the non-corrected images (AD - ancillary data).....59
Table 13: Accuracy assessment for the not-corrected images.....59
Table 14: Land cover statistics for the not separated images (AD - ancillary data).....61
Table 15: Accuracy assessment for the not-separated images.....61
Table 16: Land cover statistics for the images corrected by NDVI classes (AD - ancillary data) 63
Table 17: Accuracy assessment for the images corrected by NDVI classes.....63
Table 18: Land cover statistics for the images corrected by Slope classes (AD - ancillary data) 65
Table 19: Accuracy assessment for the images corrected by Slope classes.....65
Table 20: Land cover statistics for the images corrected by Illumination classes (AD - ancillary data).....66
Table 21: Accuracy assessment for the images corrected by Illumination classes.....67

Abbreviations

Abbreviation	Description
AD	Ancillary data
DBH	Diameter at Breast Height
DEM	Digital Elevation Model
FAO	Food and Agriculture organization
GIS	Geographical Information System
GPS	Global positioning system
IPCC	Intergovernmental Panel on Climate Change
LIDAR	Light Detection And Ranging
LS	Landsat
LUI	Land Use Inventory
NDVI	Normalized Difference Vegetation Index
RE	RapidEye
REDD	Reducing Emissions from Deforestation and Forest Degradation
SRTM	Shuttle Radar Topography Mission
TOA	Top Of the Atmosphere
UNFCCC	United Nations Framework Convention on Climate Change
USGS	United States Geological Survey
VCS	Voluntary Carbon Standard

Summary

The aim of this master thesis is to research different approaches for topographic normalization of Rapid Eye imagery with the objective of creating accurate forest type maps of regions dominated by rugged terrain.

The study area is situated in the Shitai County, Anhui Province, China and covers the extent of one tile from a Rapid Eye image. It is predominantly hilly and mountainous area, where steep mountains are intersected by valleys. Forest are dominating the mountain slopes whereas agriculture dominates in the valleys. Most common forest types are Chinese fir (*Cunninghamia lanceolata*), *Cyclobalanopsis and Castanopsis broadleaved forests* and bamboo. Whereas tea and especially rice are dominant agricultural crops.

Three common methods for topographic normalization were used in order to compare which one compensates the topographic effect most efficient. Additionally the images were separated in vegetation classes, using several criteria (NDVI, slope and illumination) to see if the efficiency of the normalization process would improve.

Besides the RapidEye images, a Landsat image of the study area was also processed with the three methods of topographic normalization, in order to see the effect of different resolution imagery on the topographic normalization.

The normalized images were classified using a maximum likelihood classifier. In order to provide reference data for the classification, a Land Use Inventory (LUI) was carried out. The LUI was performed on a systematic 3x3 grid, with plots of 200x200m, in which the current land use types were delineated.

Ancillary data (DEM and NDVI) was added additionally to the classification, to see if the addition would improve the forest type maps and compensate for the left over topographic effect.

The results showed that the c-correction and rotation method provide better normalization compared to the minnaert method. The separation in classes is not improving significantly the normalization, and the topographic normalization of the Landsat images does not differ significantly from the RapidEye images.

The results also showed the the topographically normalized images provide better

classification results. These results are improved further with the addition of the ancillary data. Furthermore the addition of the ancillary data is compensating to some extent the topographic effect which is left over after the normalization.

1 Introduction

1.1 Background

The work done during the research for the master thesis and the final document are part of the international research project “Lin4carbon”(lin4carbon 2014). It is a Sino-German cooperation project between the University of Göttingen in Germany and the Chinese Academy of Forestry.

Remote sensing analysis related to forestry has been always an important issue. The first aerial image of a forest stand is connected with the beginnings of the remote sensing (Hildebrandt 1987).

Recently the forest type mapping though remote sensing based analyses has seen new developments. This is partly enabled to the technological development and launching new sensors which provide information on temporal, spectral and spatial resolution which enables a more efficient and on time land cover and forest type analyses. One such example is the RapidEye sensor (BlackBridge 2014). It provides high resolution (5m) multi-spectral imagery, more frequent revisiting time, and has spectral resolution which is specially fitting to requirements connected to land cover and forest type mapping (Weichelt, et al. 2013; de Sousa et al. 2012).

On political level there have also been some changes which bring forward a higher interest in forest type mapping on large areas. On important factor has been the climate change talks led by the UNFCCC. They have had the forests as one of the main focus points, through which mechanisms were developed that define exact actions. One example of such a mechanism is "Reducing emissions from deforestation and forest degradation (REDD)". Other international bodies, such as FAO, aim towards collecting of forestry related information from their member countries through large scale inventories on regional or national level (FAO 2010).

There are also approaches which aim towards standardization of procedures for procuring forestry related information and forest mapping (GOFC-GOLD 2013; Open Foris 2014).

The common thing for these approaches and mechanisms is that they all require in one form or another an accurate forest type or land cover map, possibly a historical

development of the forest and land cover for the project regions. Often are these projects on larger areas being either on regional or national level.

However, providing accurate land cover and forest type maps on large area is a challenging task. Such an activity might face a number of obstacles. The availability of satellite imagery is often a problem, especially of imagery which are cloud free and have the proper quality requirements.

The accuracy of the results can be influenced by the terrain as well. Especially in mountainous regions, high percentage of the terrain is affected by cast shadow, which also affects the results of any land cover or forest type mapping. Such aspects become even more important in remote regions, or areas which are lacking data with optimal quality and aim towards a cost efficient approach.

1.2 Objectives and research questions of the master thesis

All issues presented in the introduction are present in the research for this master thesis as well. If the aim is to create an accurate forest type map for the study region, utilizing for that purpose satellite imagery acquired from the RapidEye sensor, all error sources which can influence the accuracy of the analysis should be corrected or avoided.

In the case of the Shitai County, China, one of the main factors or error source when creating a forest type map would be the topographic effect, or the cast shadow.

The main focus of this master thesis is the removal of the topographic effect in the satellite imagery with the purpose of creating an accurate forest type map.

In this line the research question which this master thesis tries to answer are:

- Will the implementation of the topographic normalization methods: c-correction, minnaert and rotation method reduce the topographic effect on the satellite imagery?
- Will the topographic normalization give better results if it is performed for separate vegetation classes?
- Will the topographic normalization give better results if the shadows are masked

out?

- Do the topographic normalization methods perform better on Landsat imagery as on the RapidEye images, taking into account the lower resolution?
- Are topographically normalized images giving a better accuracy in a land cover / forest type classification?
- Will the inclusion of ancillary data to the land cover analysis, improve the accuracy of analysis and decreases the topographic effect?

1.3 Theoretical background

When forests are the object of a remote sensing analysis the aim would be to determine the characteristics of the forest, possibly identify the forest type and in a broader scale produce a land cover map. However a land cover map or a forest type map is the last step of the remote sensing analysis. In order to come to this output there are several steps which have to be finished. Depending on the goal of the analysis and the quality of the material, this analysis procedure might differ but the general processing steps would remain the same. The steps and components of the processing are described in standard remote sensing literature (Bhatta 2008; Liang et al. 2012; Lillesand et al. 2004; Rees 2013). One important step is the preprocessing of the satellite imagery. The preprocessing involves several techniques which would be implemented before commencing with the data analysis.

Generally, the aim of the preprocessing is to increase the accuracy by removing any errors in the imagery. Lunetta et al. (1991) gives a general overview of the sources which can cause errors during the remote sensing analysis, where "Data processing" is one of the first and main factors which have to be concerned.

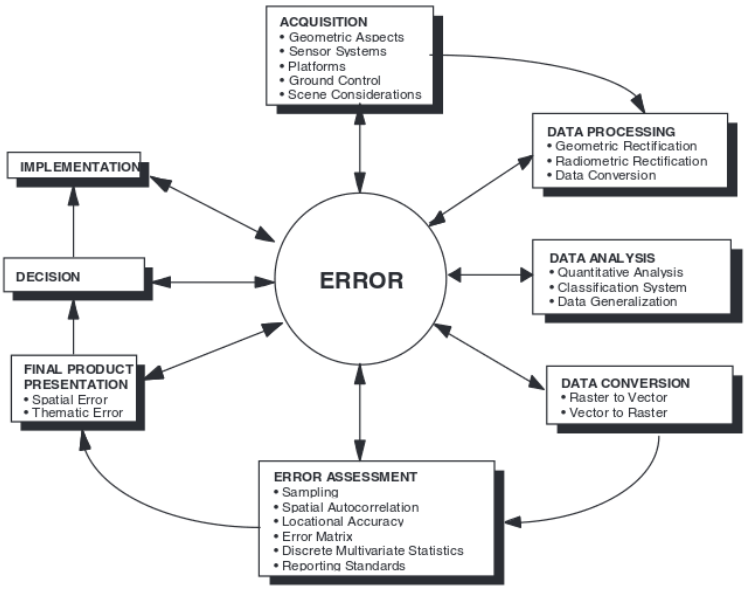

Figure 1: Overview of error sources in remote sensing (Lunetta et al. 1991; Powell et al. 2004)

There are several techniques involved here such as atmospheric correction, radiometric correction, geometric correction, techniques for image enhancement etc.

In relation to the topic of the master thesis, one essential procedure includes the removal or compensation of the topographic effect.

1.3.1 Topographic effect

The topographic effect is present in imagery produced from passive systems that depend on the solar illumination and occurs in areas with high and steep mountains.

The effect relating to this error is known as topographic effect and it can be defined as:

> ...variation in radiances from inclined surfaces compared to radiances from a horizontal surface as a function of the orientation of the surfaces relative to the light source and sensor position- (Holben & Justice 1980)

The impression of the topographic effect is clearly noticeable in the satellite images. As it can be seen from the Figure 3, the topographic effect gives an impression of relief. On the image with better resolution (RapidEye has 5m resolution as compared to the 30m resolution of Landsat 8), the topographic effect is even more noticeable.

Certainly this effect is more pronounced in areas with rugged terrain with high and steep mountains as it is the case in the study area.

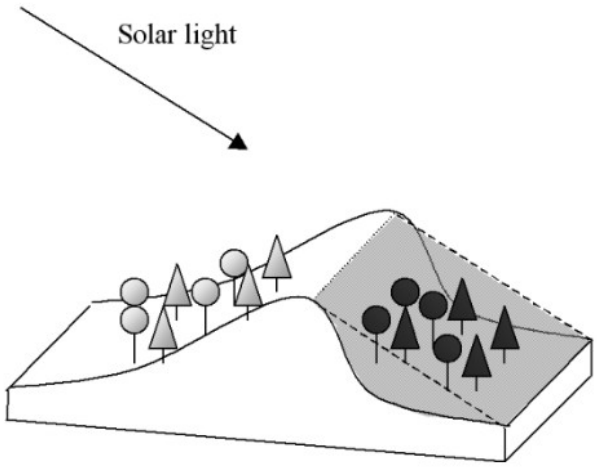

Figure 2: Topographic effect

Figure 2 can be used to illustrate the details regarding the topographic effect (Riano et al. 2003). Here the problem is schematically presented, as the trees or the forest which is situated on the slope opposite of the solar light is in shadow. Therefore although

being basically the same land cover type as the forest on the illuminated slope, it would give a different reflectance value.

The different shapes of terrain as stipulated in the definition cause also difference in the reflection of the solar radiation. Also, depending on the sun's position and the latitude of the region, some part of the terrain may be partly or completely under shadow. As an outcome same or similar land cover types show high variations in the reflectance (Riano et al. 2003) which in turn leads to misclassification of land use types. Areas of high relief are especially affected by this (Colby 1991).

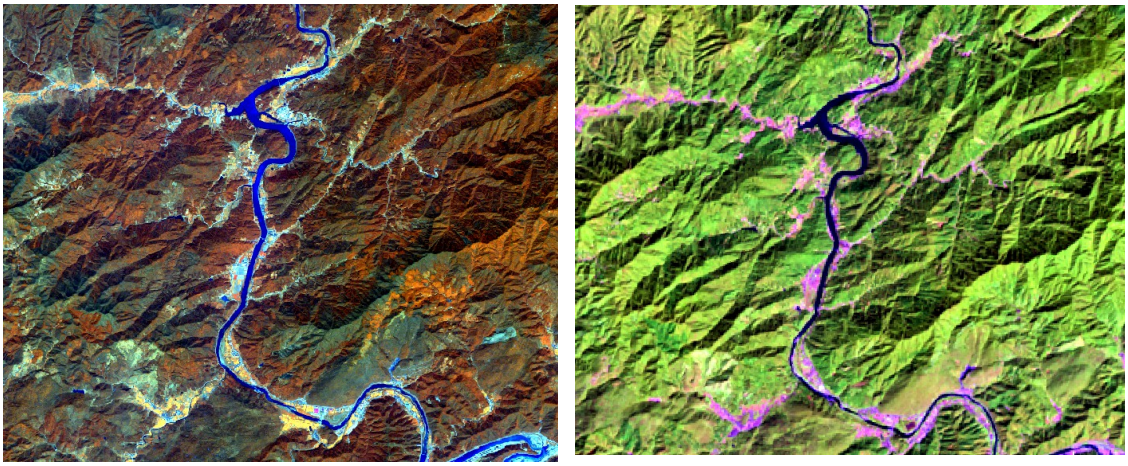

Figure 3: Topographic effect in the RapidEye and Landsat 8 imagery

1.3.2 Topographic normalization

The problems caused by the topographic effect are known as long as the remote sensing applications are used. When looking in the literature it is noticeable that there are several methods which are being used in practice which can correct or compensate this effect. A good overview of the most widely used methods is given for example by Riaño et al. (2003). He defines the term “topographical normalization” or “topographical correction” as:

> ...”compensation of the different solar illuminations due to the irregular shape of the terrain.”

There are two general categories for topographic normalization (Riano et al. 2003), (Ekstrand 1996):

- Ratio based approaches (Band rationing)
- Approach using DEM

1.3.3 Ratio based approaches

Band ratios or band transformations are transformations of multi-band (miltispectral images) where through a mathematical combination of the pixel values of the image bands a new pixel value is received (Rees 2013). Some of the most common band ratios which are used in the remote sensing are vegetation indices and are of high importance for vegetation research and monitoring. Such indices are designed to use the vegetation ratios such as the Normalized Difference Vegetation Index (NDVI). This method has been first developed by Deering (1978) and has been used ever since for images of different sensors.

The NDVI is using the red image band (R) and the infra-red image band (IR) in oder to calculate the ratio:

$$NDVI = \frac{(IR - R)}{(IR + R)} \quad (1)$$

As a results there is a new image with pixel values ranging from -1 to 1 (Albertz 2009). Usually high values 0.6 – 0.8 present dense vegetation such as temperate or tropical rain forests, moderate values 0.2-0.3 represent grass and shrub-lands, and values below 0.1 present rock, bare land, sand (Herring 2000).

The NDVI and other similar vegetation indices are based on the difference in the reflectance in the red and infra-red bad. Whereas the reflectance in the visible spectrum (red band) is low, the near-infra red has a high reflectance (Rees 2013).

Band ratios have been also used to compensate for the topographic effect (Colby 1991; Mather & Tso 2003; Riano et al. 2003). For example Colby (1991) used the Landsat TM based ration of the bands 4 and 5 to correct the topographic effect of sites with same vegetation but different topography. His results showed that the variance between the samples was lower in the ratio images than the original bands 4 and 5, therefore he concluded that band rationing does in fact partially compensate for the topographic effect.

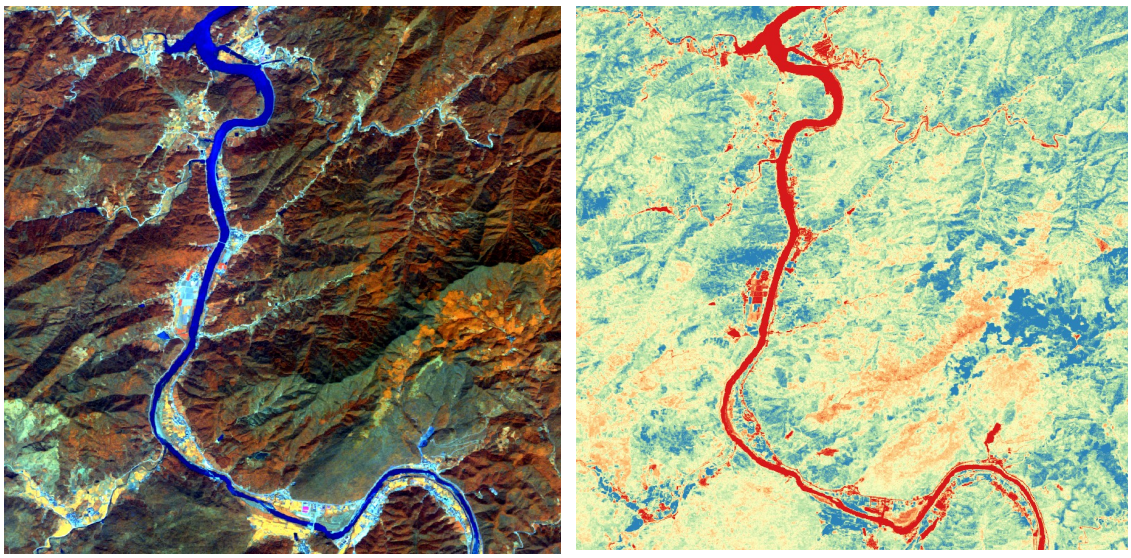

Figure 4: Comparison of a multispectral image (RapidEye bands 541) and NDVI

However the vegetation indices have their limitations. One important limitation is that a detailed land use mapping is limited due to the loss of spectral resolution (Riano et al. 2003). Usually the vegetation indices such as the NDVI are presented as one layer or dataset. This means however that the information contained in the different bands of multisprectral images is lost.

1.3.4 Approaches using DEM

Besides the band ratios, there are further approaches which are dependent on several aspects. Usually a Digital Elevation Model (DEM) which is of the same or similar resolution as the images is needed to perform the topographic normalization.

The base for the topographic correction of these models is the relative solar incidence angle or illumination (IL) condition (Tan et al. 2013). In this case the DEM is required to calcuate the incidence angle defined as the angle between the normal to the ground and the sun rays (Justice & Holben 1979; Riano et al. 2003). In the Figure below an overview is given of the angles involved in calculating the illumination.

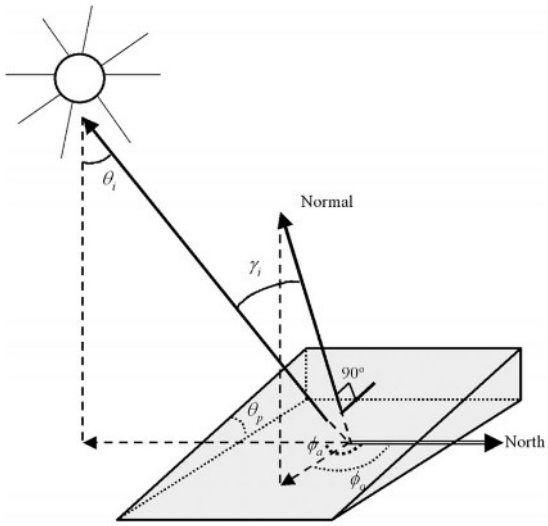

Figure 5: Angles involved in the calculation of IL (Justice & Holben 1979; Riano et al. 2003)

The values of the IL are ranging between -1 and 1. In order to calculate the IL, the following equation can be used:

$$IL = \cos\varphi_i = \cos\theta_p * \cos\theta_z + \sin\theta_p * \sin\theta_z * \cos(\phi_a - \phi_o) \quad (2)$$

Where:

- θ_p *– is the slope angle*
- θ_z *– is the solar zenith angle*
- ϕ_a *– is the solar azimuth angle*
- ϕ_o *– is the aspect angle.*

After calculating the IL the topographic normalization of the image can be done using several models. In general there are two kinds of models (Colby 1991; Ekstrand 1996;

Riano et al. 2003):

- Lambertian surface models
- Non-lambertian surface models.

Lambertian surfaces / models

Lambertian surface models takes into account a surface reflection which is fitting to the Lambert or cosine law. It has been developed by (Lambert 1760) and states that:

> ...”the radiant intensity observed from a "Lambertian" surface is directly proportional to the cosine of the angle θ between the observer's line of sight and the surface normal.”..

Basically what the Lambert' law says it that the radiation from one point is reflected equally in all directions. Below is an Figure of the lambertian surface.

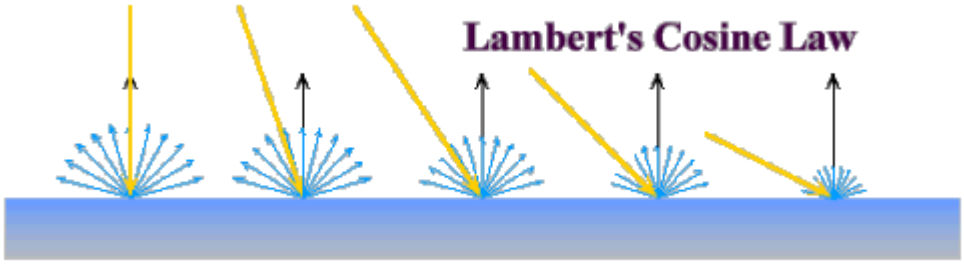

*Figure 6: Schematic presentation of the lambert's cosine law**

The lambertian models in that sense are compensating the effects caused only by the orientation of the surface. Here the radiance is proportional to the cosine of the incident angle, where the incidence angle presents the angle between the surface and the sun beam.

One of the most common methods based on lambertian surface is the **cosine method**. This method was first introduced by Teillet et al. (1982) and was later adjusted and improved by Civco (1989).

Teillet et al. (1982) expressed his model in two ways. First a more detailed model which requires information which can be easily acquired such as solar illumination angles,

* Figure source: http://escience.anu.edu.au/lecture/cg/Illumination/lambertCosineLaw.en.html (visited on 20.05.2014)

DEM but also information which require further models. This is for example the path radiance for each spectral band and additional atmospheric information.

In practice he proposes also a simplified method which can be applied if there is a lack of atmospheric information.

This model is expressed as:

$$L_H = L_r * \left(\frac{\cos Z}{\cos i}\right) \quad (3)$$

where

- L_H - *radiance observed for horizontal surface*
- L_r - *radiance observed over sloped surface*
- *Z- solar illumination angle*
- *i - incidence angle with respect to surface normal. The calculation of cos i corresponds with the calculation of IL in the equation (2) above.*

Civco (1989) adjusted this model after several researches showed an over correction of the equation (3):

$$\delta DN_{\lambda.ij} + \left(DN_{\lambda.ij} * \left(\frac{\left(\mu_k - X_{ij}\right)}{\mu_k}\right)\right) \quad (4)$$

where:

- $\delta DN_{\lambda ij}$ - *normalized radiance data for pixel* $_{ij}$ *in band* λ
- $DN_{\lambda ij}$ -*the raw radiance for pixel* $_{ij}$ *in band* λ
- μ_k - *the mean value for the entire scaled illumination model*
- X_{ij} - *the scaled illumination value for pixel* $_{ij}$

The models based on a lambertian surface are wavelength independent (Riano et al. 2003; Tan et al. 2013). This is however not the case in reality where the reflectance is diffused in many directions. In order to compensate for this there are model which do not assume a lambertian surface.

Non-Lambertian surfaces / models

Chronologically the first model that was used for compensating the topographic effect was introduced by (Minnaert 1941) in his research connected to lunar photometry. This model has since been also implemented in terrestrial conditions (Bishop et al. 2003; Blesius & Weirich 2005; Ekstrand 1996; Lu et al. 2008).

$$L_n = \frac{L * \cos e}{\cos^k i * \cos^k e} \quad (5)$$

Where

- L_n - *is the normalized radiance*
- *cos e - is the exitance angle*
- *k - is the Minnaert constant*
- *cos i - incidence angle with respect to surface normal. The calculation of cos i corresponds with the calculation of IL in the equation (2) above.*

The Minnaert constant is band dependent, and can be calculated separately for each band. Smith et al. (1980) established the procedure for this calculation. On the other hand if *k = 1*, than the model is assuming lambertian conditions (Colby 1991).

Besides the Minnaert model, the other most frequently used non-lambertian model is the **c-correction model,** established by Teillet et al. (1982)

$$\rho_{\lambda,h,i} = \rho_{\lambda,i} * \left(\frac{\cos\theta s + c_\lambda}{\cos\gamma_i + c_\lambda}\right) \quad (6)$$

A relatively newer model which is also not based on a lambertian surface, but is rather an empirical approach towards topographical normalization is the so called **"rotation model".** Introduced by Tan et al. (2010) it can be presented as:

$$L_H(\lambda) = L_i(\lambda) - a(\lambda) * (IL - IL_H) \quad (7)$$

Where :

- L_H - *is the reflectance on flat surface*
- L_i - *is the reflectance on inclined slope*
- IL_H - *is the IL for a horizontal surface*
- *a - is the intercept of the linear regression for a specific wavelength:*

$$L_i(\lambda) = a * IL + b \quad (8)$$

In a research conducted for a couple of study sites Tan et al. (2013) showed the effectiveness of the algorithm.

Issues with the topographic normalization models

The overview of the models used for topographic normalization shows that there is quite a lot of research done on this topic. All of the models have their advantages. In spite of all, until now no generic and robust method for topographic normalization is established (Allen 2000; Lu et al. 2008)

For example research shows that the c-correction model does not perform optimal in conditions of low IL, in this cases it over corrects the topographic effect (Tan et al. 2013). The cosine model has also known issues with overcorrection (Riano et al. 2003).

Furthermore research showed that the implementation of methods with lambertian assumption should be restricted based on slope. For example Smith et al. (1980) proposes in his research on ponderosa pine (*Pinus ponderosa*) that valid results are received if the analysis is restricted to slopes with less than 25° slope and less the 45° effective illumination angles.

Since the lambertian methods are based on the same factor for all bands, several authors (Riano et al. (2003); Chuvieco (2008); Teillet et al. (1982)) consider that more appropriate methods should be used which consider band dependent factors. This relates to the models based on non-lambertian surfaces. Due to this the analysis done for this **master thesis will only concentrate on non-lambertian methods,** and will look into the implementation of the c-corerction, minnaert and rotation methods.

1.4 Studies from the region

Ever since Minnaert (1941) established his first model for topographical normalization, a large number of researchers have worked on finding the optimal correction models for their imagery. This research has been wide spread in different countries and institutions. Such as for example Teillet et al. (1982) did his research in Canada; Civco (1989); Tan et al. (2013) in USA; Riaño et al. (2003) in Spain; Shepherd & Dymond (2003) in New Zealand etc. It can also be said that most of these researches worked in conditions where optimal data quality was available, which certainly improved the efficiency of their research.

However this issue has been researched in China as well. In recent years there are several publications carried out by Chinese researchers or in China which have the topographic normalization as central topic. Such are for example the studies from Gao & Zhang, (2009b) who worked on Land Use and Land Cover Classification using Landsat 7 imagery for the watershed of the Yangjia river in China; Lu et al. (2008) used the Minnaert model for topographic normalization on a study site in Lin'An County, northwest Zhejiang province of China; Wen et al. (2009) researched the bi-directional reflectance distribution (BDRF) for topographic correction for a research site in Jiangxi province.

2 Materials and methods

2.1 Study site

The project Lin4carbon, is carried out in the municipality of Shitai in the Anhui Provice of China. This territory is covered by 6 Rapid Eye scenes. However, since the aim of the master thesis is primarily related to the development of the best suited methodology for topographic normalization, all data analysis is being limited only on one tile.

This would allow more time for a detailed analysis of different scenarios and methods, which would be performed on one tile, and in a later phase, the experts involved in the project would only need to implement the suitable methodology for the rest of the tiles.

Such a division is preferred for the additional reasons as well. Namely, the complete analysis of the datasets is dependent on several pre-processing steps. Topographic normalization is only one of them, and the rest is being analyzed by other students and experts. Only the complete results and analysis of all separate issues would allow for a complete and effective analysis of the project region.

Location

A map depicting the study area is presented in Figure 13.

Having said this, the project area itself has a size of 89,314ha. It is located about 500km west of Shanghai and covers the south part of the Anhui Provice. The region itself is on the border between the sub-tropical and temperate climate zones, with more distinct sub-tropical conditions.

More interesting for the research questions of this master thesis is the terrain. The terrain in the municipality is dominated by series of interchanging steep sloped hills and

mountains on one hand and rivers and valeys on the other. The hills have a relative height of 200-500m seen from the bottom of the valleys. Figure 7 gives a 3D overview of the study area. The dominating role of the hills and mountains is visible. Even better impression of the slopes and their role in creating a topographic effect can be seen from the elevation profile of the study region as presented in Figure 8.

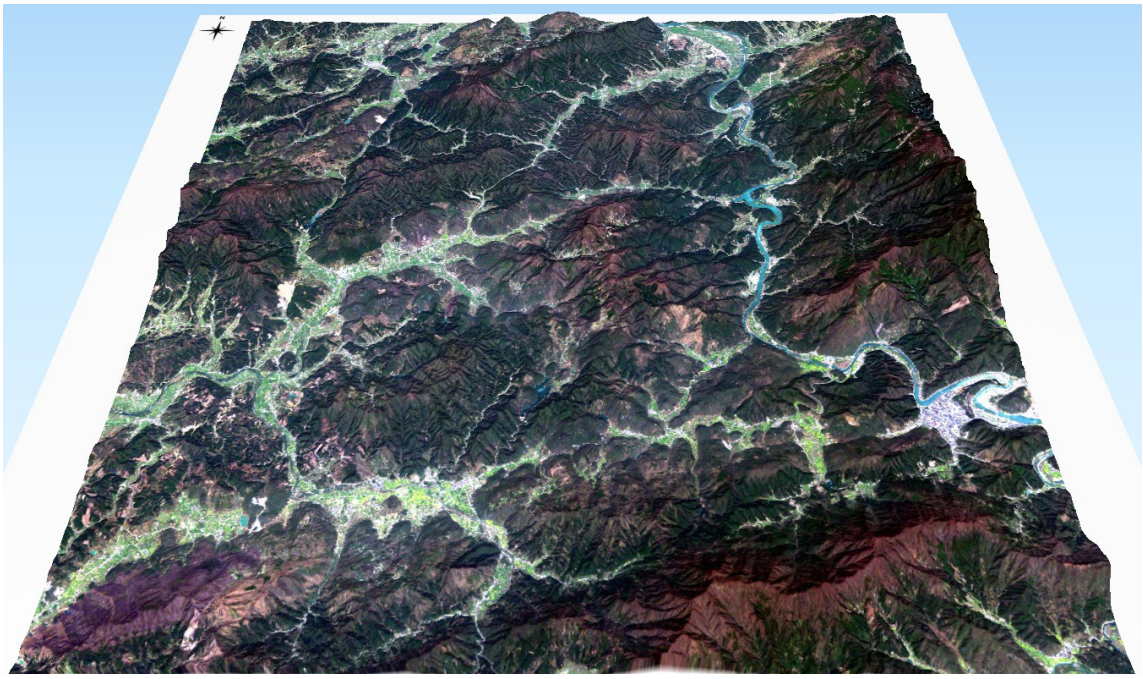

Figure 7: Part of the Project Area which is subject of this Master Thesis

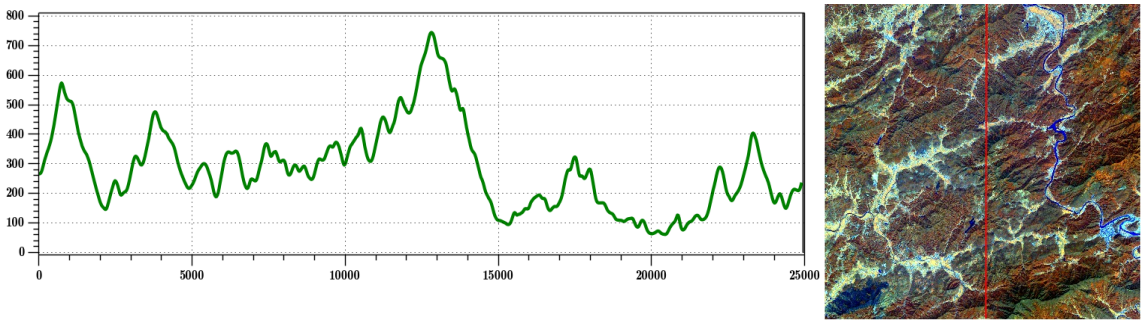

Figure 8: Elevation profile of the region. The profile follows the red line on the image from S-N

Vegetation

The dominant vegetation types in the study region are forests, shrubs or grassland and crops. Their distribution is dependent on the landscape, in most of the cases the forests are distributed on the mountain slopes, whereas the agricultural areas or crops are in the lowlands close to the rivers.

Main forest types in the region are evergreen forests where Chinese Fir (*Cunninghamia lanceolata*) and Massonian Pine (*Pinus massoniana*) are dominant; mixed broadleaved forests and bamboo grooves.

The Chinese Fir forests are wide spread in China and are used as main timber tree species in more regions. The trees of the chinese fir can grow up to 50m in height and 3m in diameter; they usually in mixed stands with broadleaved species or a s smaller pure stands on hillsides ranging from 200-2800m a.s.l. (Wu 1999).

Pinus massoniana stands are not as common as the chinese fir in the study region. The tree of the pine can grow up to 45m in height and 1,5m in diameter. They appear also either as mixed forests with broadleaved trees and chinese fir or as clear stands of pine forests

The main tree species within the broadleaved forests are *Cyclobalanopsis* and *Castanopsis*. Both of them are evergreen species and are distributed as mixed broadleaved forests.

Bamboo grooves appear normally as pure stands of bamboo. Usually they are in the vicinity of the roads. Younger bamboo appears also in a mixture with shrubs and grass, creating thick and low vegetation layer.

From the agricultural crops, rice is the main crop and is grown in the plains. Besides rice, there are also significant areas of tea as plantations, especially on slopes close to roads or other agricultural areas.

2.2 Available materials

The analysis in this master thesis is based on two major components: satellite imagery and DEM. RapidEye imagery is in the focus for the topographic normalization, whereas Landsat 8 imagery is taken as comparison to see the effects of topographic normalization on data with different spatial and spectral resolution.

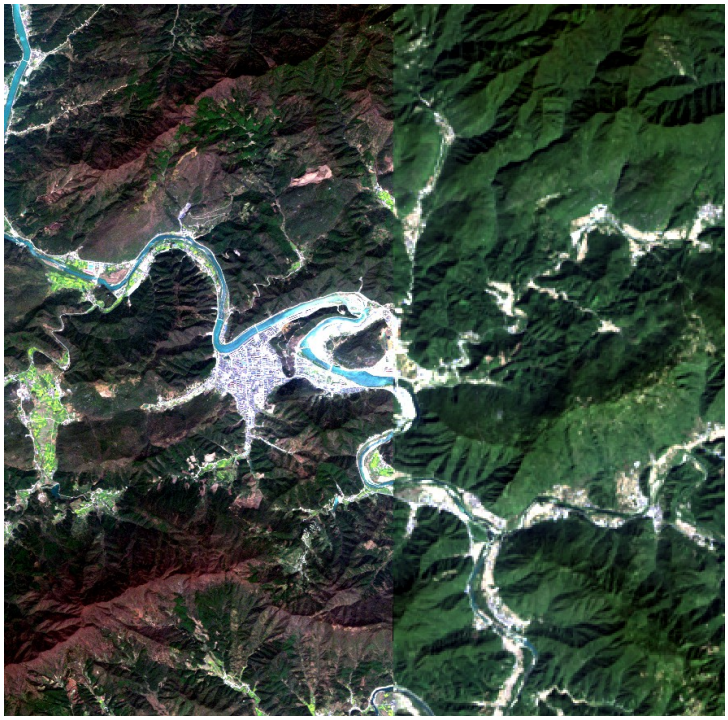

Figure 9: Differences in resolution between the RapidEye image (left) and the Landsat 8 iage (right)

All data used during this analysis was either created or converted to fit the geographical coordinate system: WGS 84 / UTM zone 50N.

2.2.1 Satellite imagery

Rapid Eye

The basic imagery utilized for the analysis is acsuired from the RapidEye satellites (BlackBridge 2014). The Blackbridge Company owns and operates an observation system which offers its services commercially. The system is composed of 5 satellites which cover an area of about 5 million km² daily.

This enables a revisit possibility for a certain spot every day (off nadir, or 5.5 days in

nadir). Such a high temporal resolution of the imagery makes it very interesting product for a number of different applications. The sensor offers a 6.5m ground sampling distance at nadir; and a digital image resolution of 5m per pixel.

Each satellites are equipped with a push-broom sensor - Jena Spaceborne Scanner JSS 56 (Weichelt, et al. 2013)

The sensor provides as output images with 5 different bands:

- Blue 440-510nm
- Green 520-590nm
- Red 630-690nm
- Red Edge 690-730nm
- Near IR 760-880nm

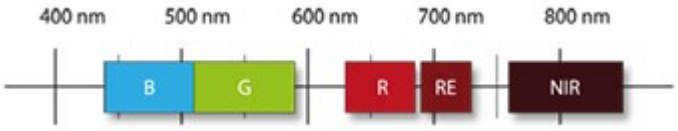

Figure 10: Spectral characteristics of the different bands for the RapidEye images

A unique characteristic for this sensor is the Red Edge band which can be useful in detecting changes in vegetation (Weichelt, et al. 2013).

Horler et al. (1983) states that the "Red Edge" is a unique effect of green vegetation resulting from 2 special optical properties of the plant tissue: high internal leaf scattering causing large NIR reflectance and chlorophyll absorption which leads to low red reflectance. The sensitivity of vegetation classes to the RapidEye's RedEdge band was shown in several studies (de Sousa et al. 2012)

The images acquired from the RapidEye system are in GeoTiff 32-bit unsigned format, have a resolution of 5m. The analysis in this master thesis is based on the Tile number: 5053016.

In order to use the differences in the season, which for the vegetation studies is certainly of importance, cloud free images of two seasons have been used: **spring** with acquisition date of 01.04.2012 and **autumn** with acquisition date of 17.10.2012. The summer images of the study region almost always have a significant cloud cover which

makes them less interesting and therefore were not used as part of the study.

Pros:

- High resolution
- Frequent return rate – enables the utilization of the images in a monitoring system which can be used for a fast / current change detection
- global coverage and extensive archive which provides multiseasonal images
- Possibility for an improved forest type recognition due to the high resolution
- Red Edge band suitable for detecting more details in the vegetation

Cons:

- Not free of charge – for larger areas the acquisition price could be problematic
- available DEMs do not fit to the resolution of the satellite images – interpolation is needed.

Landsat 8

Landsat images have been acquired as a part of the Landsat program. In a continuous development of the program new satellites have been periodically sent in earth's orbit which carried sensors with similar properties.

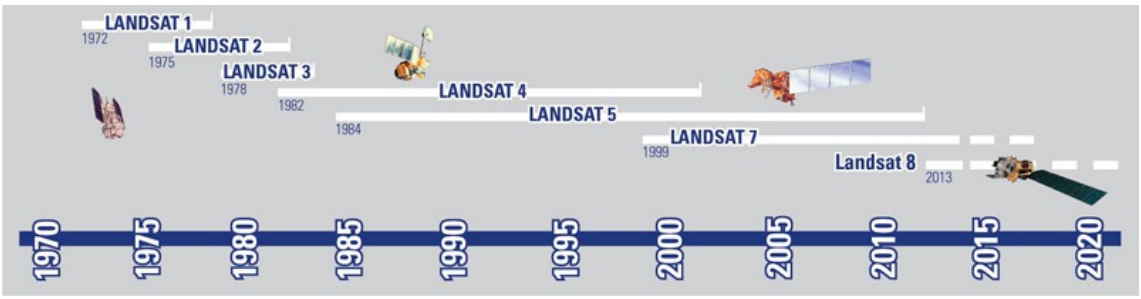

Figure 11: Time-line of Landsat Missions (USGS 2014)

For the purpose of this study Landsat 8 images have been used. In 1972 Landsat 1 was launched, and afterwards 7 more missions have been started. Meanwhile most of the missions have been discontinued. Currently only Landsat 7 and 8 are in operation.

Landsat 8 is the last of the Landsat program. It has been in operation since 11.02.2013 and is run as cooperation between USGS (United States Geological Survey) and NASA (National Aeronautics and Space Administration).

The Landsat 8 is equipped with a sensor which provides imagery with moderate

resolution of 15/30/100m. There is a difference in resolution due to the difference in information level provided by each band. Landsat 8 provides:

- 8 multi-spectral bands with 30m resolution
- 1 panchromatic band with 15 resolution
- 2 long-wave thermal infra-red bands with 100m resolution per pixel.

Landsat 8 differs from the products received by the previous Landsat missions also with the addition of new spectral band. The first spectral band covers the wavelength of 0.433 - 0.453 μm and is intended for the research of aerosols in coastal areas, whereas the previous Landsat products (for example Landsat 7) the first spectral band was blue.

The wavelengths of the different spectral bands are presented below:

Table 1: Spectral bands of Landsat 8 imagery

Bands	Property	Wavelength (micrometers)	Resolution (meters)
Band 1	Coastal aerosol	0.43 - 0.45	30
Band 2	Blue	0.45 - 0.51	30
Band 3	Green	0.53 - 0.59	30
Band 4	Red	0.64 - 0.67	30
Band 5	Near Infra Red (NIR)	0.85 - 0.88	30
Band 6	SWIR 1	1.57 - 1.65	30
Band 7	SWIR 2	2.11 - 2.29	30
Band 8	Panchromatic	0.50 - 0.68	15
Band 9	Cirrus	1.36 - 1.38	30
Band 10	Thermal Infrared (TIRS) 1	10.60 - 11.19	100
Band 11	Thermal Infrared (TIRS) 2	11.50 - 12.51	100

For this master thesis imagery from Landsat 8 was used. The study area is part of the tile with row/path: 121/39 and the image was acquired on **05.10.2013.**

2.2.2 Digital Elevation Model (DEM)

A Digital Elevation Model (DEM) presents grid data with elevation attributes which is suitable to use for analysis in raster GIS (Bhatta 2008).

DEM is an important part of the topographic normalization, since it is used for the calculation of the of the illumination as presented in equation (2). The DEM used for the purpose of this Master thesis is created by NASA's Shuttle Radar Topographic Mission - SRTM v4.1, and has a spatial resolution of 90m (Jarvis et al. 2008). Besides the SRTM DEM, there is also the ASTER GDEM (Advanced Spaceborne Thermal Emission and Reflection Radiometer) as an alternative for a DEM which is also freely available. However a recent study, conducted in South-East China, compared the accuracy of the SRTM DEM and ASTER GDEM and came to the conclusion that the SRTM DEM should be preferred when selecting between the both datasets (Jing et al. 2013).

In order to use the SRTM DEM for topographic normalization it should have similar spatial resolution as the satellite imagery. To achieve this the original SRTM DEM was re-sampled using a spline interpolation algorithm and two new DEM were created one of 5m resolution and one of 30m resolution which fit to the RapidEye and Landsat 8 imagery respectively.

2.3 Software

Quantum GIS

All GIS work needed for the data preparation, preprocessing, image enhancement etc was done using the open source GIS software - QGIS (QGIS Development Team 2014).

QGIS offers a variety of different options and modules which can be used both for vector and raster operations. For the analysis required for this Master thesis two modules / plug-ins very used for the main work steps.

Orfeo Toolbox

Orfeo Toolbox (OTB) is a software package distributed under a free software license CeCILL (CNES 2014). It can be accessed either as a separate software package or

through QGIS and offers a range of functionalities especially suited for working with raster images.

Semi-automatic classification plug-in

The Semi-automatic classification plug-in is available as an extension to QGIS (Congedo & Munafò 2012). It is a free software and offers possibilities for land cover classification of satellite imagery.

ForestEye Processor

The Forest Eye Processor is a software which has been developed by ForestEye GmbH.

It is developed with the aim of compiling different algorithms for remote sensing which would enable a fast analysis of RapidEye satellite imagery. All algorithms included in the software are previously published and known. For example the algorithms which are provided for topographic normalization are: c-correction , cosine, Minnaert, Rotation method.

This software has been used for the preprocessing (atmospheric correction). Furthermore the main analysis of the RapidEye and Landsat 8 images related to the Topographic Normalization have also been performed by this software.

3 Methodology

The activities and data analysis that was carried out for this Master thesis was done in several steps. It involved field work, digitalization, desk studies, data analysis etc. The following flow chart illustrates the order of the different work steps:

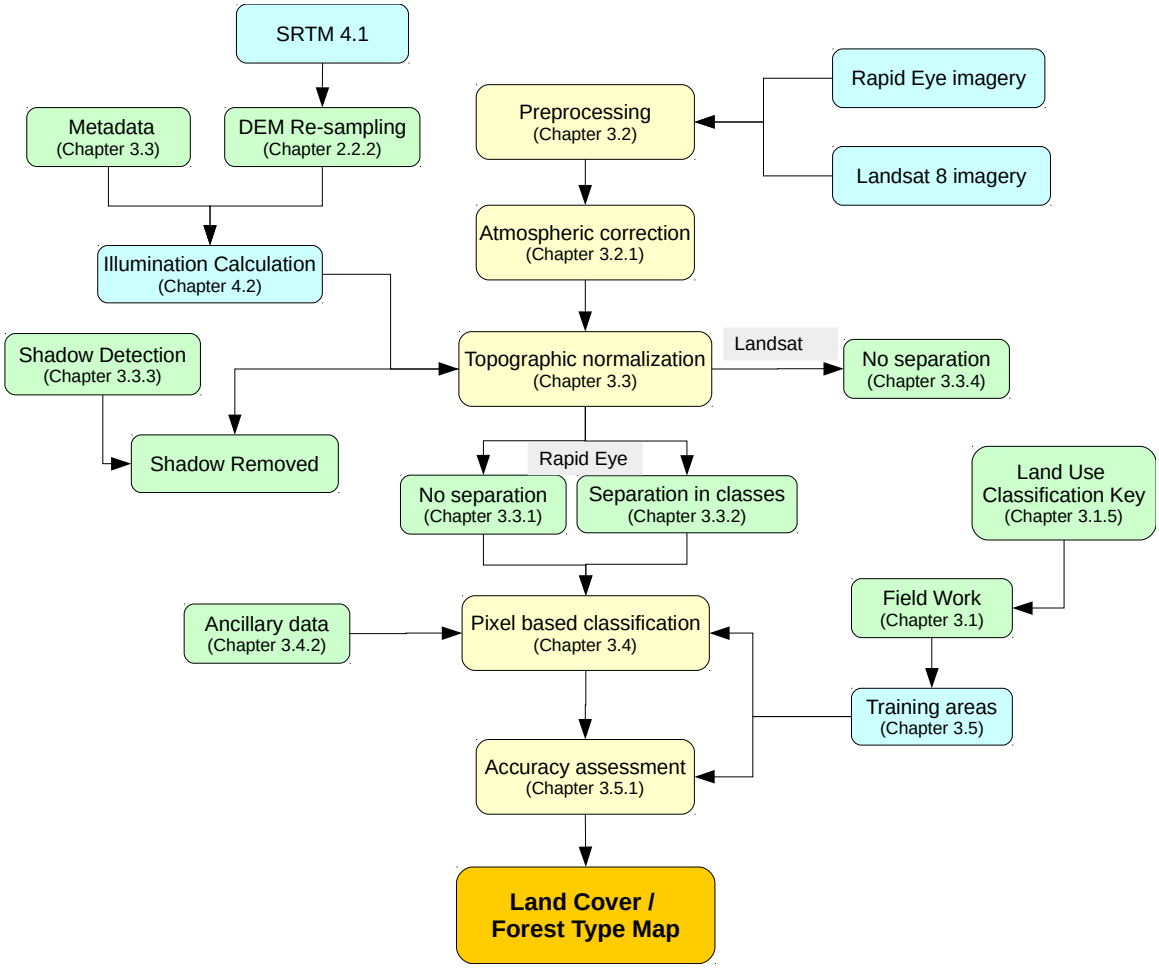

Figure 12: Flow chart of the work steps as part of the master thesis

3.1 Field work - Land Use Inventory

As part of the master thesis a four week field work on the study site in Shitai, China. The aim of the field work was to perform a Land Use Inventory (LUI) which in part was for the purposes of the Lin4carbon project, but also to serve as an exercise for collecting reference data or "ground truthing".

The ground truth or reference data can have several purposes. Lillesand et al. (2004) mentions:

1. To aid the analysis and interpretation of remotely sensed data
2. To calibrate a sensor
3. To verify information extracted from remote sensing data.

In this case the gathered data was used to help with the interpretation of the remotely sensed data and afterwards to help with the verification and accuracy calculation.

Lillesand et al. (2004) also mentions that the reference data has to be collected in accordance with statistical sampling methods. To provide a statistically sound sampling method and avoid any bias in selecting reference data, a systematic approach was used for the LUI. As part of the *Lin4carbon* project in total 100 plots were selected on a systematic grid of 3x3km. The plots are quadratic and have sides of 200x200m. In such a way the sample plots are distributed equally through the study area, this system also guarantees a sufficient amount of reference data and would cover all main land cover types.

The size of the area as well as the difficult terrain required much effort for the LUI. This combination meant that much time would be needed to perform the complete LUI. Since it would mean that the whole LUI cannot be done at once and for the purposes of only one research topic, the work was divided between a couple of students and researchers who supported each other during the work and together finished the LUI.

Below is an Figure of the LUI, the distribution of the sample plots as well as the design of the sample plots.

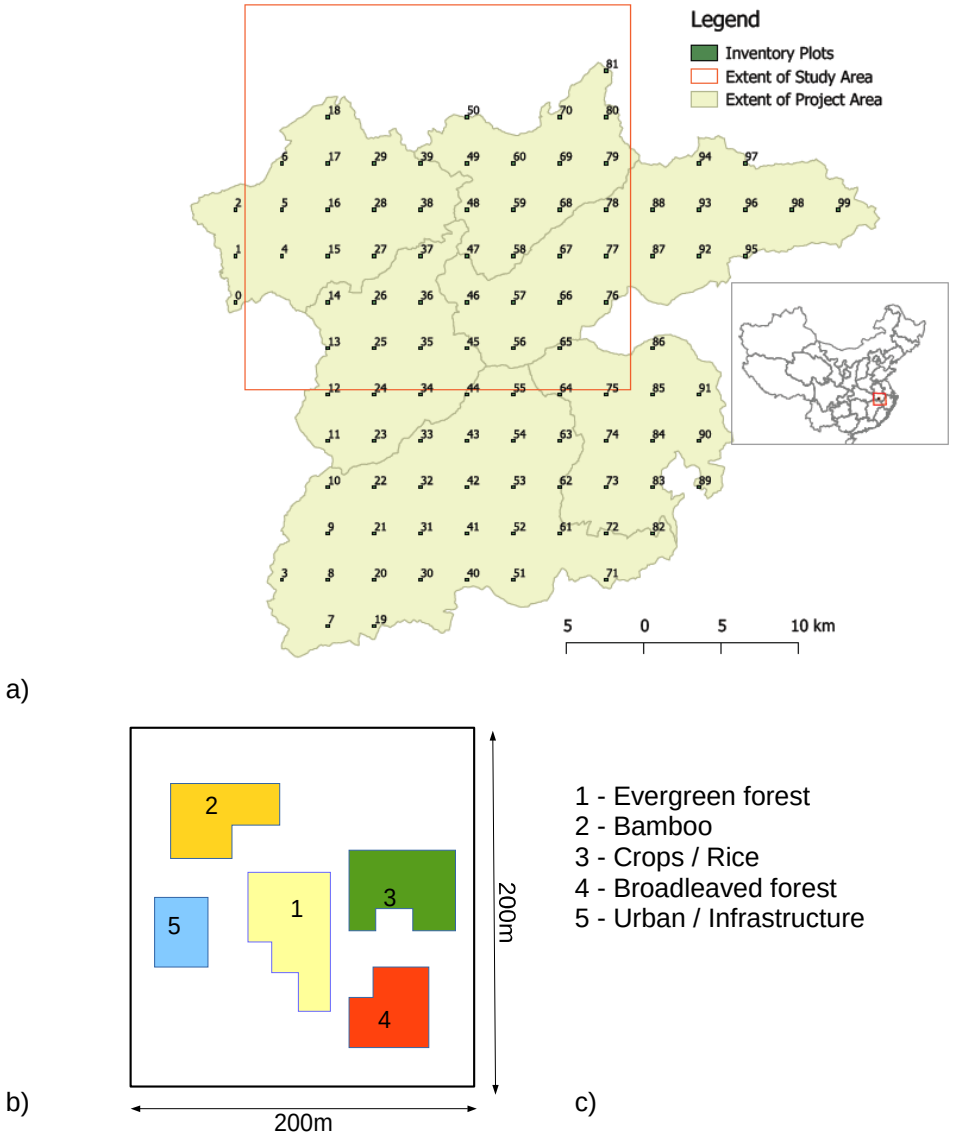

Figure 13: a) overview of the Sampling Plots in the Project Area and the Study Area; b) scheme of a sample plot including the intended delineation of land use types; c) Land use types coded according to the delineated land use

As presented in the Figure 13, the sample plots are quadratic with 200x200m sides. This size proved sufficient as most sample plots covered 2 or more land cover types.

3.1.1 Field Maps

During the preparation phase for the LUI several maps were produced which would be afterwards used in the field. Two kind of maps were produced for this purpose. One overview map of the complete project region containing the locations of the sample plots. For the actual field work and LUI detailed maps were created for each sample plot in scale of 1:4000.

Besides the boundaries of the sample plots the maps contained as background a false color composite of the RapidEye imagery. The multispectral satellite images usually contain more than three bands. For example the RapidEye image contain five bands which correlate to the different spectral values (BlackBridge 2014). However the standard computer can only display three bands which are usually marked according to the primary colors Red, Green and Blue (RGB). We can choose the reg, green and blue band from the satellite image and display a true color composite, or we can choose to display different combinations of bands according to the information needs and where such information is mostly represented. That would create a false color composite. Normally the vegetation differences are more distinct in the infra-red or near infra-red spectrum. This would mean that with the inclusion of for example band 4 or 5 from the RapidEye images, we can visually see the differences in the vegetation and especially between the forest types. Below is a Figure where the differences in visualizing color composites can be seen. The second image presents a false color composite of band 5, (Near Infra-red), band 4 (red edge), and band 1(blue). The vegetation differences are more prominent here, especially between forests and agricultural vegetation. In his relation the spring imagery provided a better distinction between the vegetation which is significant for the actual delineation in the field.

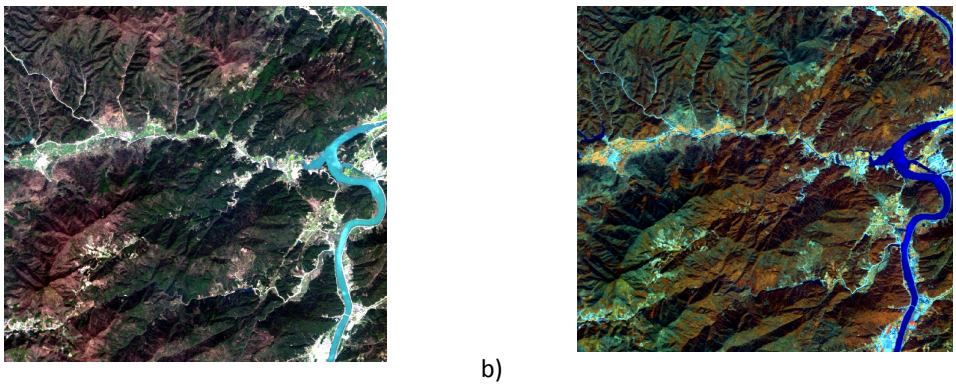

a) b)

Figure 14: Color composites of the study area (a - true color composite bands 321; b - false color composite 541)

Optimally additional information such as roads, topography, hiking paths or similar would be displayed on these maps. But, obtaining such information proved to be very difficult, and in it end unsuccessful, so as outcome the Field Maps had to be produced only with the information mentioned above.

3.1.2 GIS Project

A GIS project was set up using the software QGIS (QGIS Development Team 2014). This GIS Project contained the same information as the field maps (sample plots, project area boundaries, RapidEye imagery). The GIS project offers more flexibility in comparison to the field maps in a way that more information can be displayed, different scales, and the available information can always be exchanged or updated. For example, besides the false color composites the GIS can include true color composites (bands 3, 2 and 1 from the RapidEye imagery) and from both spring and autumn. QGIS also offers the possibility of using freely available high resolution imagery from Google Earth or Bing Maps. The flexibility of the GIS Project is especially useful when planning the navigation and routes to the sample points.

3.1.3 Navigation

The field maps and GIS project offer the basis for the navigation. Using these tool the aim is to navigate to a chosen sample plot. GPS hand-held devices, Garmin GPSmap 62stc (GARMIN INTERNATIONAL, INC; USA) and Trimble Juno (TRIMBLE NAVIGATION LIMITED; USA), were used for the navigation. As a prerequisite for the navigation the GPS devices have to contain the coordinates from the center of the sample plots and the outlines of the plot boundaries, so that when approaching the plot the position is exactly clear.

The navigation to a sample plot includes a preparation phase. This is usually done the day or the evening before the field work using both the overview map and GIS project. During this phase the aim is to choose the optimal path to the sample point. Characteristic objects can be identified, (such as clearings in the forest, river crossing etc) their coordinates can be saved in the GPS, and they can be used as way points during the navigation.

On the day of the field work, the navigation to the sample plot is started from a point chosen as most suitable to approach the sample point. It is recommended to save this point in the GPS device as it can be used as a target for tracing the way back to the

starting point.

3.1.4 Delineation of land cover types

Once the center of the plot is reached, the land cover types inside the plot can be delineated. Walking through the sample plots in each direction gives a better overview of the land cover distribution and was normally done before doing the actual delineating on the map. If a part of the plot was not accessible, an attempt has been made to reach a ground from where the land cover can be observed - i.e. opposite slope.

The delineation is done directly on the field maps. Figure 18 shows the principle of the land cover delineation. Here it is important that the delineation is done precisely, for each single land cover type without mixing the pixels.

Additionally when reaching the center of the plot the following attributes are also recorded:

Table 2: Attributes recorded on the plots center of each LUI Plot

Attribute	Description
Team	Name of the team members
Date / Time	Date and time of the measurements.
Plot slope	Slope of the plot as measured from the center
Plot asp	Aspect of the plot as measured from the center
Plot terr	Morphology of the terrain as seen from the center of the plot
LUI Nr	ID number of the LUI Plots
X / Y	Coordinates of the plot center as recorded by the GPS device
Error	the estimated error of the GPS recording in meters
HSL	Height above sea level in meters as recorded on the plot center

3.1.5 Land Cover Classification Scheme

Historically there have been several attempts to establish a standardized classification system for land use and land cover analysis. Starting with Anderson (1976) who proposes a system of two levels, where Level I contains a more general description of the land cover types and Level II which describes in more detail the general classes. His classification system contained 9 Level I classes and 37 Level II classes.

Meanwhile there is a range of different land cover and land use systems which are set up and used in different regions. Such as the Corine Land Cover in Europe (EEA 2007),

or internationally there are attempts for standardization from the side of international research bodies i.e. FAO and IPCC (Eggleston et al. 2006; Di Gregorio & Jansen 2005).

Besides the efforts done so far Di Gregorio & Jansen (2005) mention that there is a lack of internationally accepted standard for land cover and land use classification. Despite this, most of the existing systems that are in practice use a system which is divided in couple of levels which differ in details. For example the land cover from Level 1 could be Forest; Level 2 would give more details and classify it as "Broadleaved Forest"; and adding more information on Level 3 as "Beech Forest".

Such a classification system was developed also for the LUI as part of the Lin4carbon project. Below is a table showing the classification system which is based on a prior knowledge of dominant land use and land cover types.

Table 3: Land Cover Classification System used for the LUI (lin4carbon 2014)

Level 1		Level 2		Level 3	
100	Forest	110	Broad-leafed deciduous forest	111	Broad-leaved deciduous tree cover
				112	Populus tree cover
		120	Broad-leaved evergreen forest	121	Broad-leaved evergreen tree cover
				122	Cyclobalanopsis tree cover
				123	Castanopsis tree cover
		130	Coniferous forest	131	Chinese fir tree cover
				132	Massion pine tree cover
				133	Other conifers tree cover
		140	Mixed broad-leaved coniferous forest		
		150	Bamboo forest	151	Bamboo
		160	Clearing		
		170	Regeneration		
200	Natural areas	210	Shrub / herbaceous vegetation	211	Shrub
				212	Grass
		220	Open spaces	221	Bare Rock
				222	Burnt area
300	Agricultural land	310	Annual crop	311	Rice
				312	Rape
				313	Mais
				314	Cotton
				315	Beans
				316	Sesame
		320	Permanent crop	321	Tea
		330	Greenhouse		
		340	Fallow		
400	Artificial surfaces	410	Built-up area	411	Building roof type 1
				412	Building roof type 2
				413	Sealed road
500	Water bodies	510	Inland water		
600	Other	610	Barren land	611	Bare soil
				612	Unsealed road
		620	Agroforestry		
		630	Trees out of forest		

The aim during the field work was to gather information which have as much details as

it is possible to distinguish in the field, or Level 3 information. These information were added to the delineated areas as described in the previous chapter. In the further phases of the project this would give the possibility to group different classes if they are not sufficiently represented.

3.2 Data Analysis

3.2.1 Atmospheric correction

As a first step in the data analysis the satellite imagery needs to be corrected for atmospheric effects. In general the data represented on the satellite imagery in unprocessed imagery is the radiance recorded at the sensor. However, for vegetation studies the reflectance from the surface. These two values would be the same, if no atmosphere existed, but the existence of atmosphere causes additional illumination of the surface through scattered radiation (Rees 2013).

The atmospheric correction of the satellite imagery was performed in two steps:

- Conversion of the at digital values from the satellite imagery to Top of the Atmosphere (TOA) radiance;
- Conversion of the TOA radiance to surface reflectance.

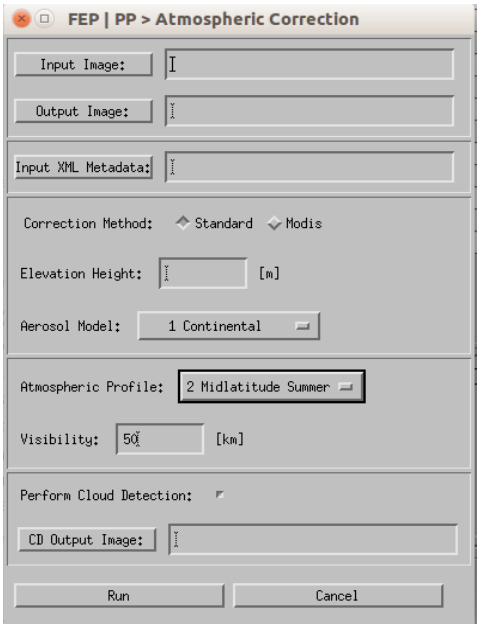

Figure 15: Atmospheric correction module - ForestEye processor

Both steps were done using the software ForestEye processor, which has a built in menu for the required pre-processing steps.

The required parameters are partly provided by the metadata file, which is available for both RapidEye and Landsat 8, and partly requires manual input.

The output of the process is presented as atmospherically corrected images. Additionally the algorithm performs cloud detection and gives as an output a raster file where the clouds are masked.

3.3 Topographic normalization

The processing of the images for topographic normalization was done using the ForestEye Processor. This software contains the most common algorithms for topographic correction. The required input parameters are:

- Satellite imagery which was atmospherically corrected
- Metafile of the satellite image - containing the key parameters for the topographic correction: sun angle and elevation
- DEM in the same resolution as the satellite imagery
- Cloud mask - as output from the atmospheric correction module
- Illumination raster.

To calculate the illumination raster the module is directly reading the metadata of the imagery. It requires however the information on solar azimuth and elevation at the time of the image acquisition.

Table 4: Metadata used for the calculation of the illumination raster

Image ID	Acquisition date	Solar azimuth	Solar elevation
5053016_2012-04-01_RE5_3A_151123	01.04.2012	169	64
5053016_2012-10-17_RE4_3A_151123	17.10.2012	177	50

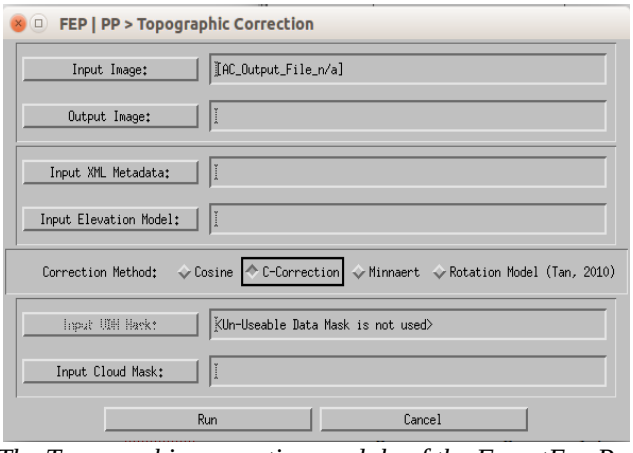

Figure 16: The Topographic correction module of the ForestEye Processor

The topographic normalization procedure could be performed directly on the image, but there are also several authors which state that the topographic normalization should

optimally be carried out separately for different vegetation classes. Such are studies from Cuo et al. (2010); Dorren et al. (2003); Riano et al. (2003).

In order to test the different approaches and see which one provides the best results, the topographic normalization would be carried out for both cases: separated in vegetation classes according to different criteria, and not separated on the whole image.

In both cases the three most common methods for topographic normalization would be used: c-correction, minnaert and rotation method (Chapter 1.3.4). The topographic normalization module from the software ForestEye would be used for this procedure. This module enables a topographic normalization of imagery with several methods. It requires a DEM and the imagery.

3.3.1 No separation

The RapidEye and Landsat 8 imagery could be directly processed after the atmospheric correction. No additional processing is required since the ForestEye Processor is directly reading in the required information from the metafiles of the imagery and calculates an Illumination raster based on the DEM.

The output of the procedure is a topographically corrected image as well as regression plots showing the correlation between the Illumination raster and the individual bands. This output would than be used as means in evaluating the effectiveness of the topographic normalization procedure.

3.3.2 Classes separation

Usually an existing or an older vegetation and land use maps are used to make the separation. However, if such a map does not exist, than there are several approaches which can be utilized in order to come to the same effect. As part of this Master thesis the following approaches have been tested and implemented:

- Separation of classes using NDVI
- Separation of classes using inclination / slope
- Separation of classes using using the illumination

As an outcome of this procedure the module produces as many rasters as there are classes. The separate classes would than be merged together using the QGIS Raster calculator, which would enable creating of only one raster per season and class.

Separation of classes using NDVI

NDVI stands for **Normalized Difference Vegetation Index.** The NDVI was already explained in Chapter 1.3.2. Besides the ratio based approaches, it has been used often to separate the satellite imagery in classes when no other information on vegetation or land cover is available (Szantoi & Simonetti 2013).

Having these data in mind, a NDVI was calculated from the atmospherically corrected images and classified in two classes representing 1) Dense vegetation or forests; 2) sparse or no vegetation. The NDVI separation was done using the thresholding tool available in the software Monteverdi (CNES 2014), and by visual assessment.

Table 5: Separation of the Rapid Eye imagery in classes according to NDVI values

	NDVI Values	
Satellite images	**No Vegetation**	**Vegetation**
Rapid Eye - Spring	-1 to 0.3	0.3 to 1
Rapid Eye - Autumn	-1 to 0.35	0.35 to 1

The satellite images were than masked by the separate NDVI classes and run through the topographic correction module in the ForestEye processor.

Separation using slope classes

The software package QGIS offers a rich menu for raster operations. One such module is the "Terrain Analysis" which contains a tool for calculation of a slope based on the DEM.

Using this tool a slope raster was calculated for the project region. Further on it has been reclassified in three classes, based on the steepness of the slope:

- Class 1: slope < 10°
- Class 2: slope 10 - 30°
- Class 3: slope > 30°

Separation of classes using using the illumination

Another approach for separating the vegetation classes is by using the difference in illumination. Basically the topographical normalization process on most of the

algorithms is based on the illumination of a Lambertian surface (Riaño et al. 2003). Such a calculation is included in the process of topographic normalization. When already calculated it can be also presented as a raster file.

Vanonckelen et al. (2013) in a study on the effects of atmospheric and topographic correction to the accuracy of land use classification, has utilized a method where the Illumination raster was divided in three classes.

The illumination was already discussed and the equation for the calculation is presented in chapter 1.3.2. For the purpose of this master theses, the illumination calculated by the topographic correction module from the ForestEye processor was used and separated in three classes. The thresholds of the different classes are based on the study from Vanonckelen et al. (2013) .

- Class 1: low illumination – cosß ≤ 0.65
- Class 2: moderate illumination – 0.65 < cosß < 0.85
- Class 3: high illumination – cosß ≥ 0.85.

3.3.3 Shadow removal

Due to the difference in the resolution between the satellite imagery and the available DEM, there is a high possibility that a part of the images would not be corrected, or that a certain amount of shadow would still remain. This remaining shadow would also have an influence on the results, in first place the effectiveness of the topographic normalization and in the classification afterwards.

One procedure to decrease such effects is to mask out the shadow areas and then carry out the topographic normalization.

The procedures for shadow detection and masking are very well known. An overview of existing approaches for shadow detection was compiled by Shahtahmassebi et al. (2013).

For the purpose of this master thesis the shadow detection has been carried out by using an object based image classification. The object based image classification is having an increasing role within the land cover analysis from remote sensing. A good overview of the existing methodologies is given by Blaschke (2010).

The image classification method used for the land cover analysis of this master thesis is

pixel based and is explained in the coming chapters. Here however, the object based classification is tested to see if it is suitable approach for detecting shadows.

The procedure was conducted in several steps:

- image segmentation using a mean-shift filter from the Orfeo Toolbox (CNES 2014). The output of this procedure is a segmented vector file based on the spectral characteristics of the image
- using the zonal statistics plug-in from QGIS (QGIS Development Team 2014) the zonal statistics was calculated for each segment and band. As outcome the vector file contains five attributes with the mean radiance values of each segment
- the segmented vector file was than rasterized (using the Rasterize tool in QGIS) creating five new bands, which are similar to the original RapidEye band with the difference that they are now composed of object / segments
- This image was in the last step classified using a maximum likelihood classifier for just two categories - shadow and no-shadow.

When the shadow raster is already classified and available it would be used as a mask during the topographic normalization process. It would be however applied only to the dataset / procedure which shows the best results for topographic normalization as described in chapters 3.3.1 and 3.3.2. The aim would be test if the topographic normalization process would improve even more when the shadows are masked out.

3.3.4 Effects of imagery resolution to the topographic normalization

One of the objectives for the master thesis is to test the dependence of the topographic normalization procedure to the resolution of the imagery. This is especially important since the available DEM are of much lower resolution as the primary imagery used in the study (RapidEye). Chapter 2.2.2 explains that the available DEM (SRTM) was re sampled from 90m resolution to 5m and 30m to fit the resolution of the RapidEye and Landsat imagery respectively. However, the resolution difference between the datasets is big, especially between the 5m of RapidEye and the 90m of the SRTM.

To test this, the topographic normalization procedure would be carried out for a Landsat 8 image (see Chapter 2.2.1). The 30m resolution of the Landsat imagery is closer to the 90m of SRTM, which might result in better topographic normalization.

The Landsat 8 image would only be processed without separation in different vegetation classes, using as well the three common methods for topographic normalization as with the RapidEye images.

3.4 Land cover classification

The land cover classification of the multispectral images can be done in two way: as supervised or unsupervised classification. Supervised classification uses information of known classes distribution to perform the classification. The known information is received from field investigations or secondary data and is used to define training data (Rees 2013)

Based on the training data, the images is examine, pixel by pixel, in order to determine the class belonging. This is why the procedure is also known as **pixel-based classification.** Additionally an algorithm is needed to assess the rules and determine which pixel belongs to which class. There are several algorithms which can be used in any supervised classification such as the minimal distance classifier, the parallelepiped classifier, maximum likelihood, spectral angle mapping etc. (Lillesand et al. 2004). One of the most commonly used is the maximum likelihood classifier, which is also implemented for analysis in this master thesis.

The maximum likelihood classifier models the probability distributions to each class, using information from the training data, from which is possible to determine the likelihood that a certain pixel belongs to some class (Rees 2013).

In order to perform the classification the Semi-automatic classification plug-in (Congedo & Munafò 2012) from QGIS was used. This tool offers to possibility to choose between a couple of classification algorithms. It also provides the option to set a probability threshold for the maximum likelihood classification. If the probability of belonging of a certain class is below the threshold this pixel will not be classified.

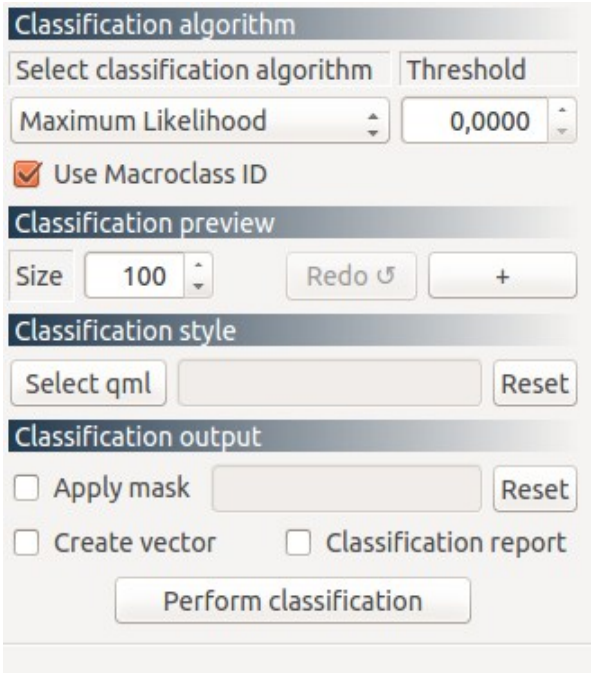

Figure 17: The classification option of the semi-automatic classification plugin

3.4.1 Multi-seasonal image

The images which are produced as an outcome of the topographic normalization procedure are single multi-band rasters representing and containing the properties of the land cover as reflectance values. Since the vegetation and the forests, go through a significant phenological change through the year, a classification of each single image representing either spring or autumn could lead towards under or overestimation of certain land cover types. This is of special interest for forest mapping since the canopy of the trees is on different stadium of development in the both seasons.

To avoid these differences, the images from the spring and autumn would be merged together, creating a multiseasonal image. This procedure is done by the module "Merge" available in the QGIS software.

3.4.2 Ancillary data

Distinguishing between vegetation classes is not always as simple especially in rugged terrain, as it is here the case. That is why the topographic normalization is being made in the first place, but there are also other procedures which provide an improved accuracy. These are for example the addition of geographical or ancillary data to the classification process. Studies performed by Jansen et al. (1990); Eiumnoh & Shrestha (2000)show an improvement of the accuracy when DEM are added to the classification process together with the bands of the satellite images. Eiumnoh & Shrestha (2000); Bahadur K.C. (2009) besides the DEM combined also vegetation ratios such as NDVI as part of the classification. They have also used object based classification (Jansen et al. 1990) or pixel based (Bahadur K.C. 2009) and in both cases there was a clear improvement in the quality and accuracy of the classification.

For the purpose of this master thesis both DEM and NDVI will be used as additional bands for during the classification.

3.5 Training areas

Richards (2012) mentions that each supervised classification has a prerequisite which is that the analyst has available sufficient known pixels for each class of interest that representative signatures can be developed for those classes. These pixels are known in the remote sensing as training data, where as the process of determining the signatures is called training. Richards (2012) also states that the training areas should represent a small proportion of the whole image which is less that 1% to 5%.

Regardless of the proportionally small area that the training data occupy, they still have to be both representative and complete (Lillesand et al. 2004). This means that if one land cover type is represented by one large area, and it contains no differences in the spectral signal, than only one training area suffices to describe it. However, if the same land cover type is spread out through the area of the image, and it is represented by different spectral classes, this land cover type would have to be covered by at least as many training areas as there are differences in the spectral signature. For example, if we have class of forest, it might include dense forest or open forest; these however differ in their spectral signature, due to which the analyst has to make sure that both cases are covered during the determination of training areas.

The training areas for this master thesis were received mainly as a result from the field work. For this purpose the field maps (see Chapter 3.1.1) after the field work were scanned; the scanned images were georeferenced; and the delineated areas were digitalized on-screen in QGIS, at the same time adding the attributes describing the land cover. During the delineation special care was taken to delineate clean pixels, meaning that one class or training area should include pixels that belong only to it. This was easier to control on the screen as it is on the paper, which is why in some cases the delineated training areas are smaller as the areas delineated on the field maps.

The Figure below shows an example of delineated training areas as outcome from the delineation made during the field work.

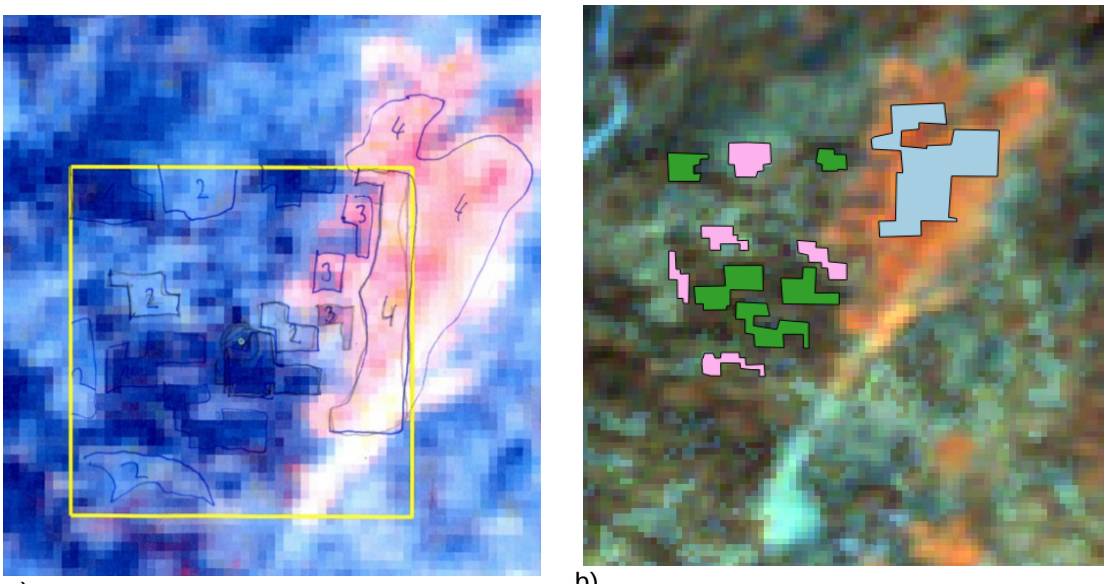

Figure 18: Obtaining training areas from delineating the field maps. a) field map; b) Delineated training areas

Additional training areas were however acquired by comparing the land cover from the RapidEye imagery with the high-resolution imagery which is freely available at Google Maps. This approach has been used in studies related to land cover analysis in cases no other sources for verification or reference were available (Nowak & Greenfield 2010; Wickham et al. 2010). Even in recent projects which aim towards production global datasets of forest/non-forest cover (Shimada et al. 2014). In this case, Google Maps were used in very limited cases. This is partly due to the bad quality of the imagery for the study region and partly due to a shift in the Google Maps imagery which occurs through the study region.

Figure 19: Example of the Google Earth high-resolution imagery from the study area

3.5.1 Accuracy assessment

Accuracy assessment is an integrative part of each land cover analysis. It is the step which verifies how successful the procedure is and expresses the degree of correctness of a map or classification (Foody 2002). It is also a measurement of how close is one classified map to the truth on the ground (Warner et al. 2009).

Congalton (2001) mentions that there are several reasons why accuracy assessment should be carried out. Those are:

- The need to know how well you are doing and to learn from your mistakes;
- The ability to quantitatively compare methods;
- The ability to use the information resulting from your spatial data analysis in some decision-making process.

Giving an overview of the history of accuracy assessment Foody (2002) mentions that there are several methods which can be used for performing accuracy assessment, but the one which is widely accepted is a confusion or error matrix. This is also supported by other authors (Lunetta et al. 1991).

Confusion or error matrices compare on a category by category basis the relationship between known reference data and the corresponding results of an automated classification The confusion matrix expresses three important indicators which describe the accuracy of the classification. **Overall accuracy** is the result of dividing the total number of correctly classified pixels by the total number of pixels; **User's accuracy** indicates the accuracy of the individual land cover classes by dividing the number of correctly classified pixes per category by the total amount of pixels classified as that category; **Producers accuracy** is calculated by dividing the number of correctly classified pixels in each category by the number of the pixels in the training dataset for that category (Lillesand et al. 2004).

A schematic presentation of a typical confusion matrix is presented in the Figure below.

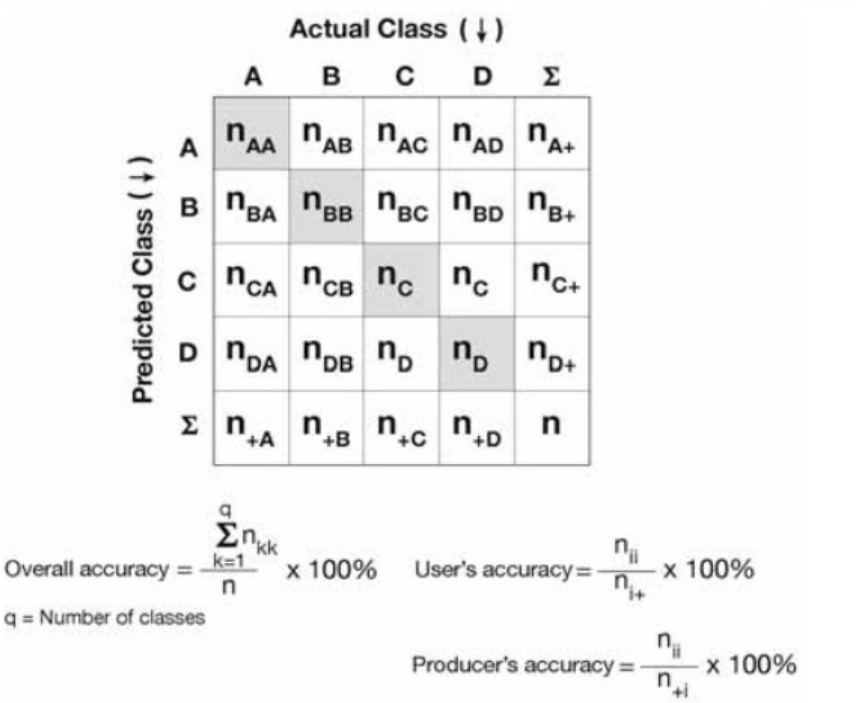

Figure 20: Schematic presentation of a typical confusion matrix (Strahler et al. 2006)

In order to carry out the process of accuracy assessment or validation, a separate dataset is required containing pixels of each land cover class. Here it is important that the dataset used for training and the one used for accuracy assessment are different, otherwise it may lead to an optimistic bias (Hammond & Verbyla 1996; Smits et al. 1999).

In the case when no independent source for verification data exists, the usual strategy is to divide the total training data set in two, one for training and one for verification.

For the purpose of this master thesis the total reference dataset which was created (as described in the previous chapter), was than divided in two parts, 2/3 of the dataset was used for training and classification; and 1/3 for verification and accuracy assessment.

4 Results

4.1 Field work

The field work for this master thesis was carried out in a period of four weeks in September and October 2013. During that time a total of 21 land use plots were visited and delineated. This component of the master thesis was a part of the total effort to do a land use inventory of the project area under the Lin4carbon project (lin4carbon 2014).

In this respect the results of the field work are presented separately for the project and study area and all conclusions and discussion is based only on the study area. The table below gives an overview of the results:

Table 6: Overview - results from the field work

	Project area	**Study area**
Total plots	100	86
Completed plots	42	38
Total area (ha)	86,314	62,500
Delineated area (ha)	119.8	36.6
Delineated area in % from total area	0.13%	0.06%
Delineated area as average of total area (ha)	1.39	0.96
Delineated area as average of plot area (%)	35%	24%

The delineated areas certainly contain land use information, which can already be calculated. This calculation could also serve as an indication of the land use on the total area. However, this is just an initial raw delineation, where the polygons in some cases contain mixed pixels and need to be cleared in the next work steps.

As i can be seen from the table below, the initial calculation of the land use from the delineated plots shows that the forest is a dominant land use type with about 50% of the total delineated area.

Table 7: Initial land use calculation based on the delineated inventory plots

Land Use	LU ID	Project area		Study area	
		ha	%	ha	%
Broad-leaved deciduous tree cover	110	31.6	26.4%	8.58	23.5%
Populus tree cover	112	1.21	1.0%	0.26	0.7%
Broad-leaved evergreen forest	120	3.05	2.5%	0.35	1.0%
Cyclobalanopsis tree cover	122	0.25	0.2%	0.25	0.7%
Castanopsis tree cover	123	0.94	0.8%	0.46	1.3%
Coniferous forest	130	7.1	5.9%	2.12	5.8%
Chinese fir tree cover	131	12.17	10.2%	3.61	9.9%
Massion pine tree cover	132	0.94	0.8%	0.25	0.7%
Mixed broad-leaved coniferous forest	140	4.07	3.4%	0.91	2.5%
Bamboo forest	150	8.88	7.4%	1.57	4.3%
Clearing	160	0.95	0.8%	0.95	2.6%
Shrub / herbaceous vegetation	210	10.03	8.4%	3.44	9.4%
Shrub	211	11.38	9.5%	3.78	10.3%
Grass	212	2.39	2.0%	1.34	3.7%
Bare Rock	221	5.26	4.4%	2.68	7.3%
Annual crop	310	0.53	0.4%	2.25	6.2%
Rice	311	7.26	6.1%		
Tea	321	7.51	6.3%	2.26	6.2%
Built-up area	410	0.15	0.1%		
Inland water	510	2.12	1.8%	0.67	1.8%
Unsealed road	612	1.8	1.5%	0.85	2.3%
Trees out of forest	630	0.16	0.1%		
		119.75	100.0%	36.58	100.0%

4.1.1 Problems encountered during field work

During the duration of the project the field work was carried out in three phases. The work done as part of this master thesis was only one of the phases. In most of the time the work was facing obstacles.

In most cases when the land use plots were situated on a slope of a mountain it took much higher effort and more time to reach the plots. This was due to the terrain form and vegetation density as well as the lack of roads or paths in the vicinity of the plots. Usually a zone of thick vegetation from shrubs, high grass, young bamboo or forest regeneration was met at the bottom of the slopes. This kind of vegetation proved to be very difficult to walk through and caused delays in the work and in some cases a couple of plots were not reached.

In a case where topographic maps were lacking, the navigation depended on the estimation from the satellite images, and also as important was the communication with the local people, who provided assistance in several cases.

Due to this reasons the aim of 100 land use plots on the total project area, was not reached.

4.2 Topographic normalization

The topographic correction on the imagery was performed as described in chapter 3.3. The complete procedure was carried out using the ForestEye Processor and was implemented on both the original images and the image classes separated according the different criteria.

In order to evaluate the effectiveness of the procedure the correlation indicies between the corrected image and the illumination raster are calculated. The illumination raster is produced during the topographic normalization and since the images are from different dates, three different illumination rasters are calculated which would fit to the illumination conditions at the moment of the image acquisition (RapidEye spring and autumn; Landsat 8). For the calculation of this rasters the equation (2) was used.

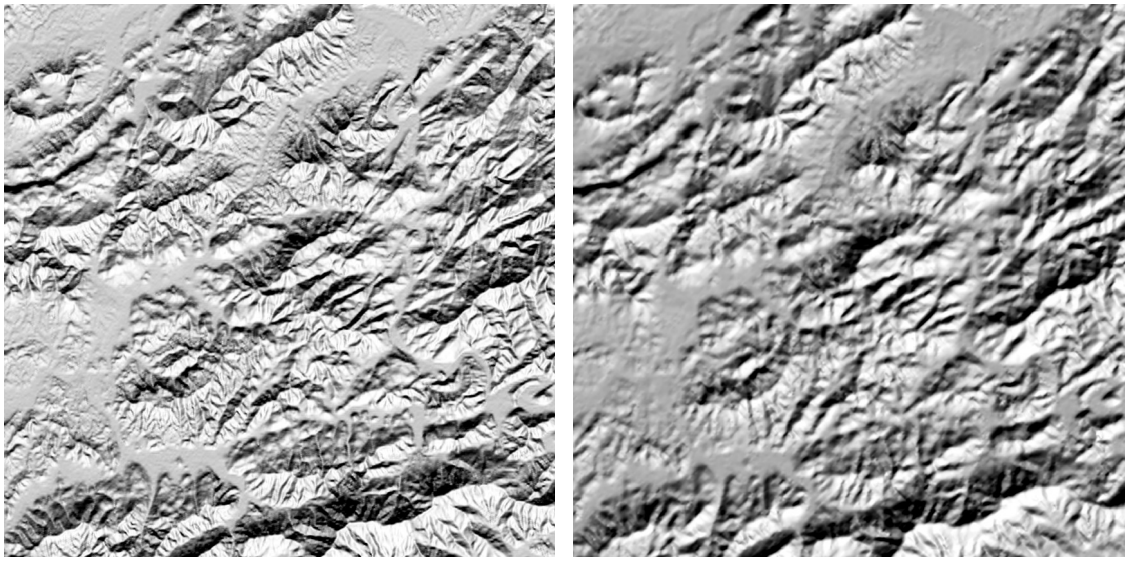

a) b)

Figure 21: Illumination rasters: a) RapidEye spring; b) Landsat 8

4.2.1 Topographic normalization of Rapid Eye imagery

Once the illumination raster is calculated the topographic correction can be carried out, and the correlation coefficients are calculated. They show the effectiveness of he correction procedure. In the table below the correlation coefficients for all classes are shown:

Table 8: Correlation indicies of the topographic correction for all classes. The highest 5 correlations per band are marked in bold; the lowest 5 correlations are in italic. (C-correction; M - Minnaert method; R - Rotation method)

Group	Class	Topographuc Correction	Bands									
			Rapid Eye Spring					Rapid Eye Autumn				
			1	2	3	4	5	1	2	3	4	5
Original image		C	0.308	0.374	0.312	0.476	0.483	0.272	0.434	0.349	0.606	0.627
		R	0.308	0.374	0.312	0.476	0.483	0.270	0.430	0.350	0.610	**0.630**
		M	0.307	0.369	0.307	0.471	0.475	0.289	0.439	0.355	0.592	0.603
NDVI	Veg	C	0.339	0.413	0.364	0.494	0.465	0.297	0.477	0.426	0.612	**0.629**
		R	0.339	0.413	0.364	0.494	0.465	0.297	0.477	0.426	0.612	**0.629**
		M	0.350	0.420	0.370	0.500	0.470	0.319	0.485	0.435	0.601	0.612
	No-Veg	C	**0.436**	**0.472**	**0.484**	**0.514**	**0.496**	**0.639**	**0.668**	**0.657**	**0.653**	0.583
		R	**0.436**	**0.472**	**0.484**	**0.514**	**0.496**	**0.639**	**0.668**	**0.657**	**0.653**	0.583
		M	0.307	0.369	0.307	0.471	0.475	**0.596**	**0.618**	**0.606**	0.604	0.542
Slope	Class 1	C	0.112	*0.127*	*0.116*	*0.131*	*0.103*	0.111	0.152	0.121	*0.191*	*0.177*
		R	0.112	*0.127*	*0.116*	*0.131*	*0.103*	0.111	0.152	0.121	*0.191*	*0.177*
		M	*0.065*	*0.071*	*0.066*	*0.072*	*0.056*	0.080	*0.111*	*0.089*	*0.136*	*0.127*
	Class 2	C	0.178	0.224	0.186	0.301	0.314	0.169	0.295	0.224	0.452	0.482
		R	0.178	0.224	0.186	0.301	0.314	0.169	0.295	0.224	0.452	0.482
		M	0.177	0.222	0.185	0.296	0.306	0.176	0.297	0.229	0.444	0.466
	Class 3	C	**0.369**	**0.514**	**0.411**	**0.645**	**0.597**	0.335	**0.573**	**0.536**	**0.724**	**0.738**
		R	**0.369**	**0.514**	**0.411**	**0.645**	**0.597**	0.335	**0.573**	**0.536**	**0.724**	**0.738**
		M	**0.371**	**0.512**	0.407	**0.639**	**0.594**	**0.347**	**0.573**	0.533	**0.711**	**0.725**
Illumination	Class 1	C	0.227	0.292	0.203	0.329	0.310	0.334	0.412	0.379	0.442	0.414
		R	0.227	0.292	0.203	0.329	0.310	0.334	0.412	0.379	0.442	0.414
		M	0.225	0.289	0.201	0.326	0.307	0.319	0.394	0.359	0.425	0.404
	Class 2	C	0.257	0.298	0.248	0.323	0.272	*0.075*	*0.136*	*0.100*	0.226	*0.243*
		R	0.257	0.298	0.248	0.323	0.272	*0.075*	*0.136*	*0.100*	0.226	*0.243*
		M	0.249	0.288	0.240	0.312	0.264	0.076	0.138	0.101	0.227	0.244
	Class 3	C	*-0.049*	*-0.020*	*-0.008*	*0.060*	*0.118*	*-0.130*	*-0.016*	*-0.041*	*0.176*	0.270
		R	*-0.049*	*-0.020*	*-0.008*	*0.060*	*0.118*	*-0.130*	*-0.016*	*-0.041*	*0.176*	0.270
		M	*-0.043*	*-0.018*	*-0.007*	*0.055*	*0.105*	*-0.134*	*-0.018*	*-0.044*	*0.177*	0.273

The table above shows the results of the topographic correction for the both rapid eye images in each class and for the three methods: c-correction, minnaert and rotation.

It can be seen that in general the topographic correction is more successful with the autumn image, which has much higher correlation coefficients as the spring image. Also, in most of the cases the correction is more successful in the infra-red and red-edge bands as opposed to the bands in the visible spectrum.

In general it appears that the best results of the correction are from the third class of the

slope separation. However, the other two classes in this separation group have correlation coefficients which are much lower.

On the opposite side, the lowest correlation coefficients are within the third class of the illumination group, which in general has low values.

It appears that the division by NDVI is giving the best correlation coefficients for both the spring and autumn images. To illustrate this, besides the correlation coefficients the regression plots can also be presented.

Visual assessment

Besides the correlation indicies, the successfulness of the topographic correction was assessed by visual assessment. All images created as a result of the topographic correction procedure are available on the DVD which is a part of the annex. In this chapter the main results will be reviewed.

Original images - no separation

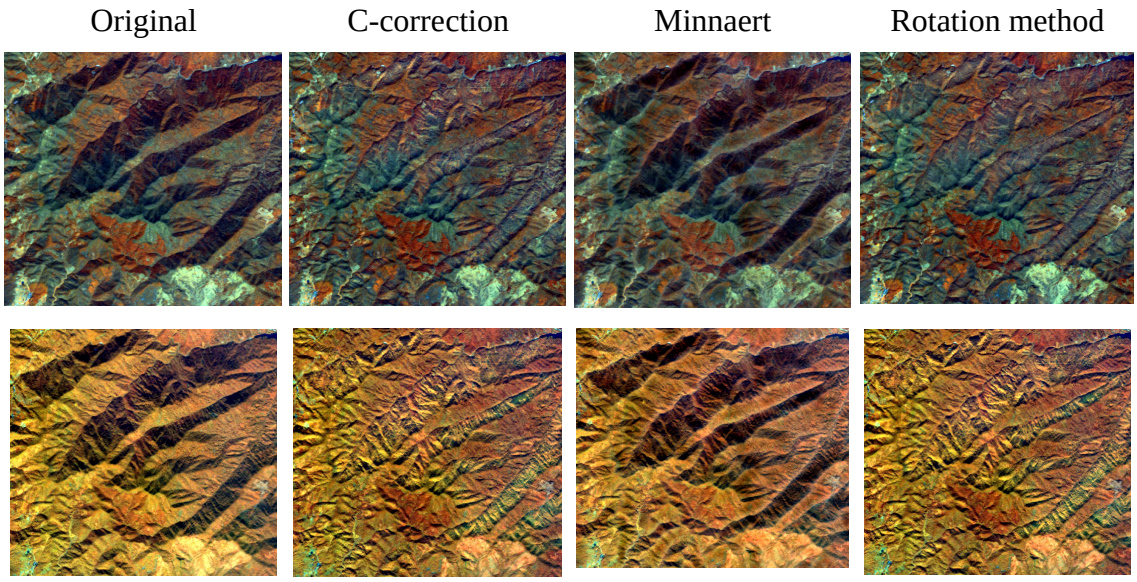

Figure 22: Visual assessment of the topographic correction on a complete image. The first row are examples from the spring and second row are examples from the autumn RapidEye image.

In the first instance the atmospherically corrected images were topographically corrected using the three methods: c-correction, minnaert and rotation method. In this case no separation in different classes was performed.

From the resulting images, it is visible that a large portion of the topographic effect is

compensated. This is true for the c-correction and the rotation method. However, the correction did not lead to a complete removal of the topographic effect. Some left over effects are noticeable on the hill and mountain ridges.

The minnaert correction method gives different results. It appears that only a small part of the topographic effects are eliminated, whereas the majority is still present on the image.

NDVI classes

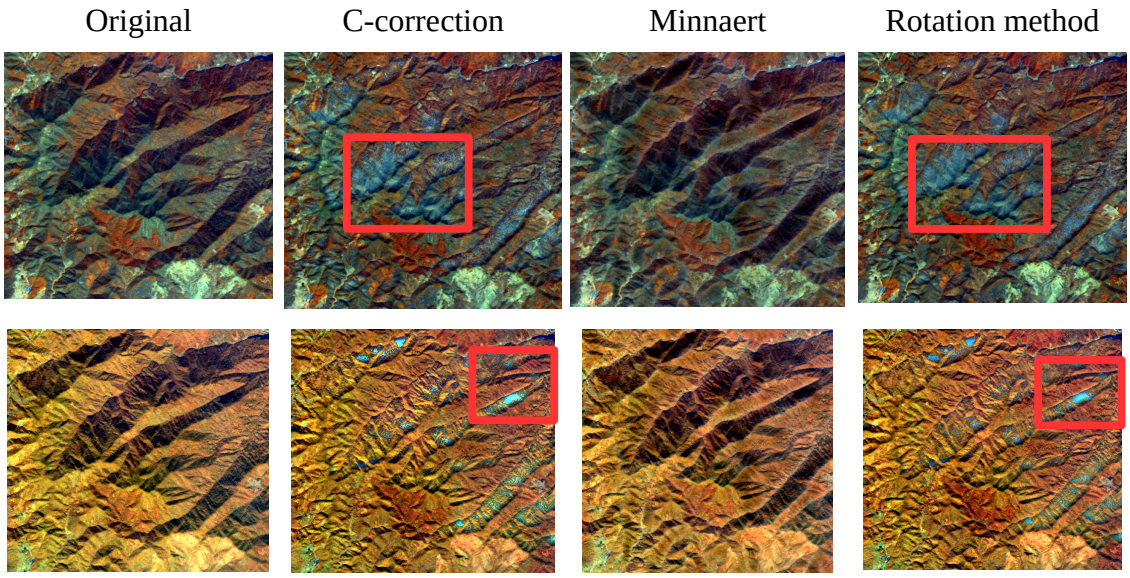

Figure 23: Visual assessment of the topographic correction - NDVI classes separation. The first row are examples from the spring and second row are examples from the autumn RapidEye image. The red squares show the areas which are over-corrected.

The results from the topographic correction of the images which were separated by NDVI classes has shown the best correlation indicies.

In the case of the visual assessment, both the c-correction method and the rotation method show good results. Most of the topographic effects are eliminated. Some are however still present, and that is more obvious in the spring image as it is in the autumn image. There is also a noticeable overcorrection related to the NDVI class representing the no forest / vegetation class. This can be seen in the examples above.

In the case of the minnaert correction, the results are very similar to the correction of the complete images. The topographic effect is not eliminated in the larger area. And additionally some distortions appear.

Slope classes

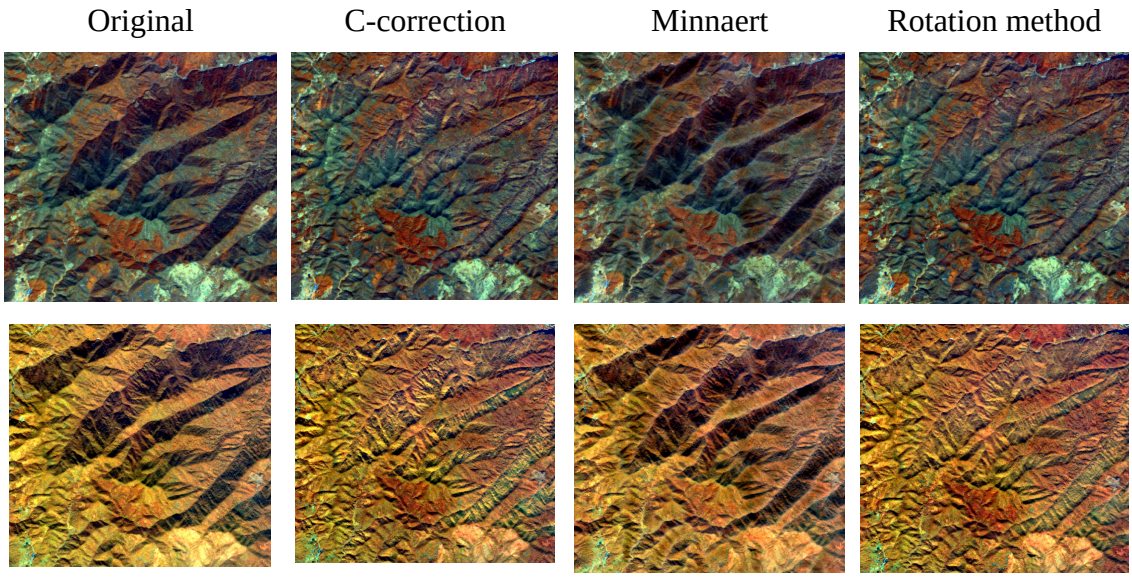

Figure 24: Visual assessment of the topographic correction - Slope classes separation. The first row are examples from the spring and second row are examples from the autumn RapidEye image.

The topographic correction of the images which were separated in slope classes showed low correlation results, except in the third class representing steep slopes.

In the case of the visual assessment, the low correlation does not show. Most of the topographic effects are eliminated with the c-correction and the rotation method, whereas the overcorrection which was present in the images corrected by NDVI classes, is not present here. The minnaert method shows again lack in the performance as most the of the topographic effects are not eliminated.

Illumination classes

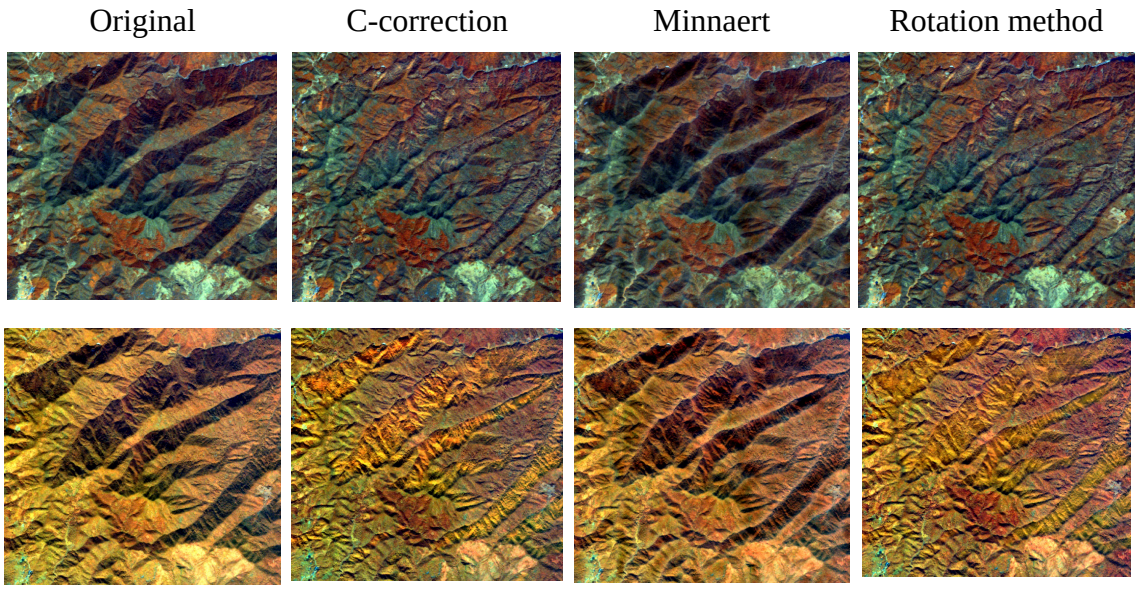

Figure 25: Visual assessment of the topographic correction - Illumination classes separation. The first row are examples from the spring and second row are examples from the autumn RapidEye image.

The images which were topographically corrected by separating them in different classes according to the illumination values, had low and even negative correlation values. This cannot be confirmed however by the visual assessment.

Again as it was the case with the other classes, the c-correction and rotation method show good results, where most of the topographic effect are eliminated. The minnaert model also here does not show good results, as most of the topographic effect are still present in the image after the correction.

Shadow masking

The topographic correction of the imagery, regardless of the class used for the correction, did not manage to eliminate completely the topographic effect. This also means that the corrected imagery contains shadowed areas. Certainly in comparison with the not corrected imagery, the shadowed areas are smaller, but still they are present and can affect the results of the land use classification.

The object-based approach for the shadow masking produced succeed to identify the biggest part of the shadows.

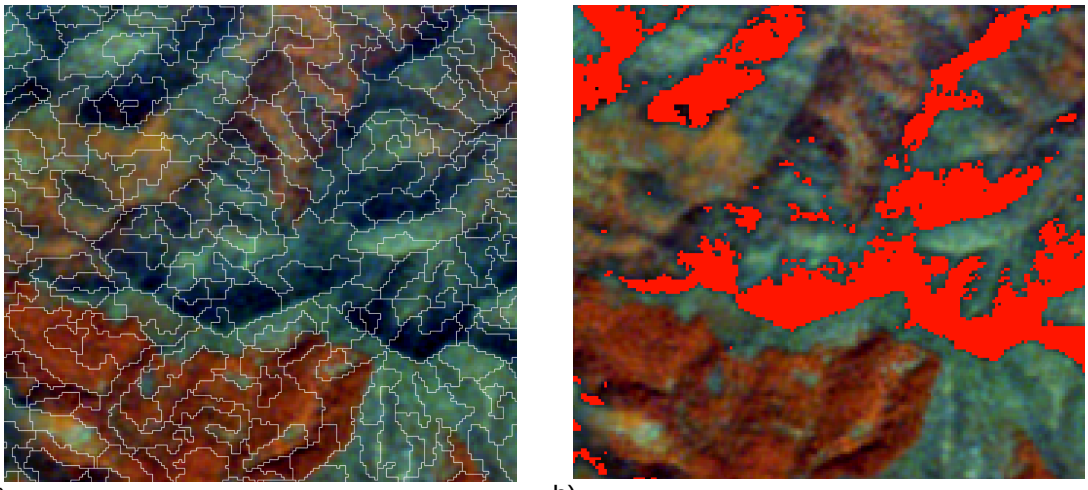

a) b)

Figure 26: Results of the object-based approach for shadow masking. a) the segments overlaid on the spring RE image; b) the red colored area presents the result of the object based classification - in this case presenting the shadows.

As a final result of the work step one raster file was created which contains two values - shadow and no-shadow. The Figure above shows an example of the final results.

The raster file of the remaining shadows, was used than as a mask in the topographic correction module of the ForestEye Processor. From table 8 as well as from the visual assessment it is apparent that the normalization of the images without their separation in classes offers a good result. Other individual classes have higher correlations, but in general they are undermined by much lower correlations or over-corrections in the rest of the image (as it is the case with the separation with NDVI classes).

Therefore the shadow raster was used as a mask in the topographic normalization procedure of the the not separated images. The table below shows the correlations which are the outcome of the procedure:

Table 9: Correlation indicies of the topographic normalization for the shadow masked images. (C-correction; M - Minnaert method; R - Rotation method)

Topographic Normalization	Bands									
	Rapid Eye Spring					Rapid Eye Autumn				
	1	2	3	4	5	1	2	3	4	5
C	*0.317*	*0.384*	*0.315*	*0.486*	*0.503*	*0.284*	*0.463*	*0.366*	*0.629*	*0.659*
R	*0.317*	*0.384*	*0.315*	*0.486*	*0.503*	*0.284*	*0.463*	*0.366*	*0.629*	*0.659*
M	*0.316*	*0.380*	*0.311*	*0.481*	*0.497*	*0.304*	*0.469*	*0.373*	*0.617*	*0.638*

4.2.2 Topographic normalization of Landsat Imagery

The topographic normalization of the Landsat image was performed without any separation in vegetation classes. Below is a table showing the correlations between the illumination raster and the individual bands of the image.

As it was the case with the RapidEye imagery, here it is noticeable that the bands 6 and 7 which are not in the visible spectrum,have higher correlations.

A comparison can be made with the RapidEye autumn image, since the acquisition dates are both in October (the correlation results of the RapidEye image are presented in Table 8). It can be seen that the correlation for the Landsat image is higher in the visible spectrum but lower that the RapidEye results in the NIR and IR sprectrum.

Table 10: Correlation indicies of the topographic normalization for the Landsat 8 Image

Topographic Normalization	Landsat 8 Bands						
	1	2	3	4	5	6	7
C-correction	*0.442*	*0.329*	*0.430*	*0.333*	*0.330*	0.554	0.535
Rotation	*0.442*	*0.329*	*0.430*	*0.333*	*0.330*	0.554	0.535
Minnaert	*0.437*	*0.341*	*0.433*	*0.341*	*0.330*	0.547	0.528

Visual assessment - topographic normalization for the Landsat 8 Image

Figure 27 presents an example of the topographically normalized images, as compared to the original Landsat image. Both the c-correction and rotation method have succeed in removing bigger part of the topographic effect, whereas the Minnaert model still leaves the biggest part of the topographic effect. Similar results were noticed from the topographic normalization of the RapidEye imagery.

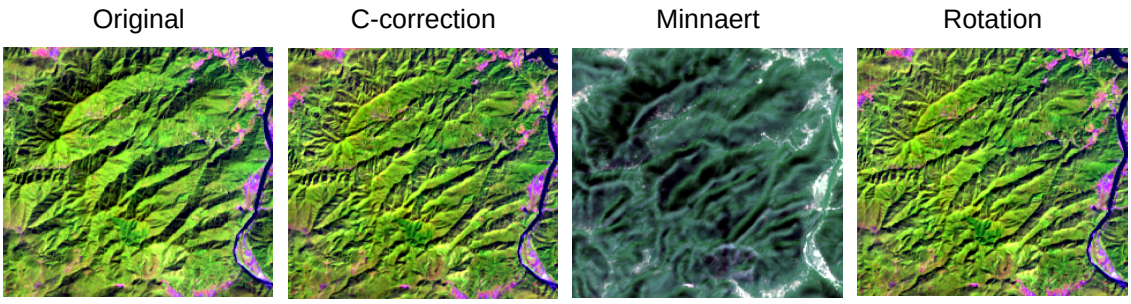

Figure 27: Visual assessment of the topographic normalization procedure for the landsat 8 image

4.3 Supervised classification

With the results from the topographic normalization and the inclusion of the ancillary data, there are in total 26 datasets which were part of the classification. The list of the datasets and its components is presented in the Annex 9.4.

4.3.1 Training areas

The acquisition of the training areas is the first step in performing the supervised classification of the images. In chapter 4.1 the delineation of the raw training areas is explained. In a further step these areas where first "cleaned" - in a process involving an improved delineation and removal of mixed pixels.

Further on, the land use classes from the raw training sets were synthesized in fewer and in some cases more general classes. This is required in cases when some classes are underrepresented and depending on the needs of the classification.

In this case nine classes were defined, corresponding to the main land use types in the study area. The training areas have been divided accordingly. At the end of this work step a data set was produced which contained all of the areas which are to be used in the classification process.

As explained in chapter 3.5.1, one aspect of the classification is the accuracy assessment. In order to provide reference areas for the accuracy assessment the total trainings data set was divided in two parts: classification dataset and verification dataset.

The table below gives and overview of the total area covered by the classification and verification datasets by land use type:

Table 11: Separation of the trainings dataset for classification and verification

Code	Land Use /Cover Type	Area (ha)	
		Classification	Verification
1	Broadleaves	9.31	2.22
2	Conifers	14.86	3.66
3	Bamboo	5.40	2.85
4	Shrubs and grass	14.46	0.87
5	Tea	1.63	0.48
6	Agricultural area	7.68	1.05
7	Water	59.33	6.11
8	Urban/Infrastructure/Roads	3.29	0.12
9	Barren land	0.29	0.09
Total Result		**116.25**	**17.45**

4.3.2 Classification results

Similarly as the presentation of the results for the visual assessment of the topographic correction (chapter 4.2.1), the results of the land cover classification will be presented for each class separately. This includes the land cover statistics, accuracy assessment and an example of the classified images. The complete error matrices for each classified image can be found in the annex and the classified images can be found in the DVD which comes as annex to this master thesis.

All the examples of the classification in the chapters below are using the color style as shown in Figure 28.

Figure 28: Color style used for the land cover classification

Results - original images

The original images, which were not corrected topographically were classified. Below are the results of the classification.

Original - not corrected | Original - not corrected | Original - not corrected + ancillary data

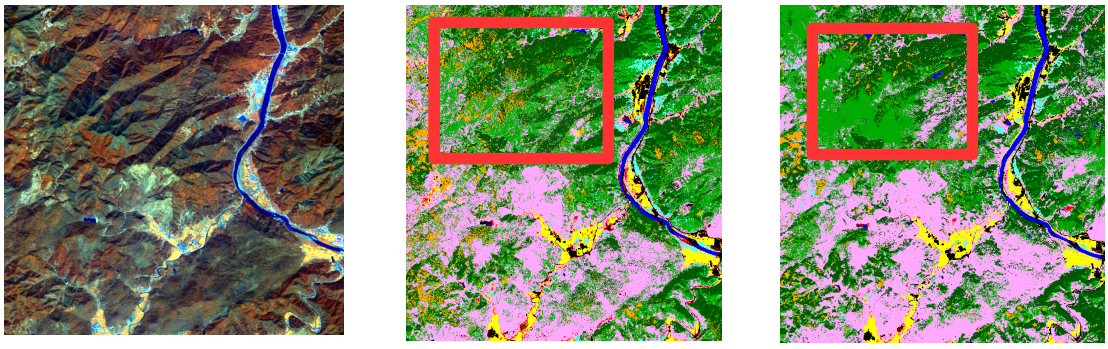

Figure 29: Overview of the land cover classification of the original not-corrected image

It can be seen that the not corrected topography is heavily influencing the land cover classification. In the red square shown in the images above, the effect is clearly visible. It is also noticeable that with the inclusion of the ancillary data in the dataset for classification, the topographic effect is partly avoided.

This difference is also shown in the over all classification, since the land cover types are differently distributed. Table 12 shows the land cover statistics. Significant changes in the area are seen within the Bamboo and Shrubs land cover types.

Table 12: Land cover statistics for the non-corrected images (AD - ancillary data)

Class	**Original**		**Original + AD**	
Topographic correctio	Not corrected			
area	ha	%	ha	%
Broadleaved Forest	15,848	25.4%	15,311	24.5%
Conifer Forest	13,232	21.2%	15,293	24.5%
Bamboo Forest	5,022	8.0%	2,565	4.1%
Shrubs and grass	17,204	27.5%	20,015	32.0%
Tea	1,221	2.0%	822	1.3%
Agriculture	4,948	7.9%	4,887	7.8%
Water	398	0.6%	488	0.8%
Urban/Infrastructure	2,349	3.8%	2,369	3.8%
Bare Land	2,277	3.6%	750	1.2%
Total	**62,500**	**100%**	**62,500**	**100%**

Table 13 shows the accuracy assessment for the not-corrected images. The overall accuracy of about 90% is relatively high, it can be also seen the the inclusion of the ancillary data has increased the accuracy of the classification. The redistribution of the land cover types (Bamboo and Shrubs) results also in a higher class accuracy for the both land cover types.

Table 13: Accuracy assessment for the not-corrected images

Class	**Original**		**Original + AD**	
Topographic corr.	Not corrected			
Overall accuracy	89.10%		91.4	
	PA	UA	PA	UA
Broadleaved Forest	66.3	77.2	67.2	81.4
Conifer Forest	84.6	86.5	87.6	86.9
Bamboo Forest	96.7	91.6	99.2	97.2
Shrubs and grass	83.4	67.6	91.2	68.8
Tea	95.9	94.5	97.4	97.4
Agriculture	92.4	97.5	93.1	97.5
Water	96.2	100	98.2	100
Urban/Infrastructure	82.6	23.3	84.7	34.8
Bare Land	100	87.8	100	97.2

The results of this class would serve as a comparison for the rest of the datasets. Optimally the topographically corrected images would result in a higher overall accuracy and better compensation of the topographic effect within the classified images.

Results - Original images topographically corrected

Expectingly the land cover classification improves when the images have been already topographically corrected. This is noticeable in the Figure 30 especially for the images corrected using the c-correction and rotation methods.

Images corrected by the minnaert method still contain a large portion of shadow cast from the topography. Since the image itself is not corrected completely the classification suffers as well. The red square in the image shows an example where the topographic effect causes misclassification, here the shadowed part of the hills are classified as bamboo. When the ancillary data is included this effect is slightly reduced.

For the images corrected by the c-correction method, there is also a difference caused when introducing the ancillary data in the classification. Especially visible is the effect on the broadleaved forests as well as the shrubs and grass.

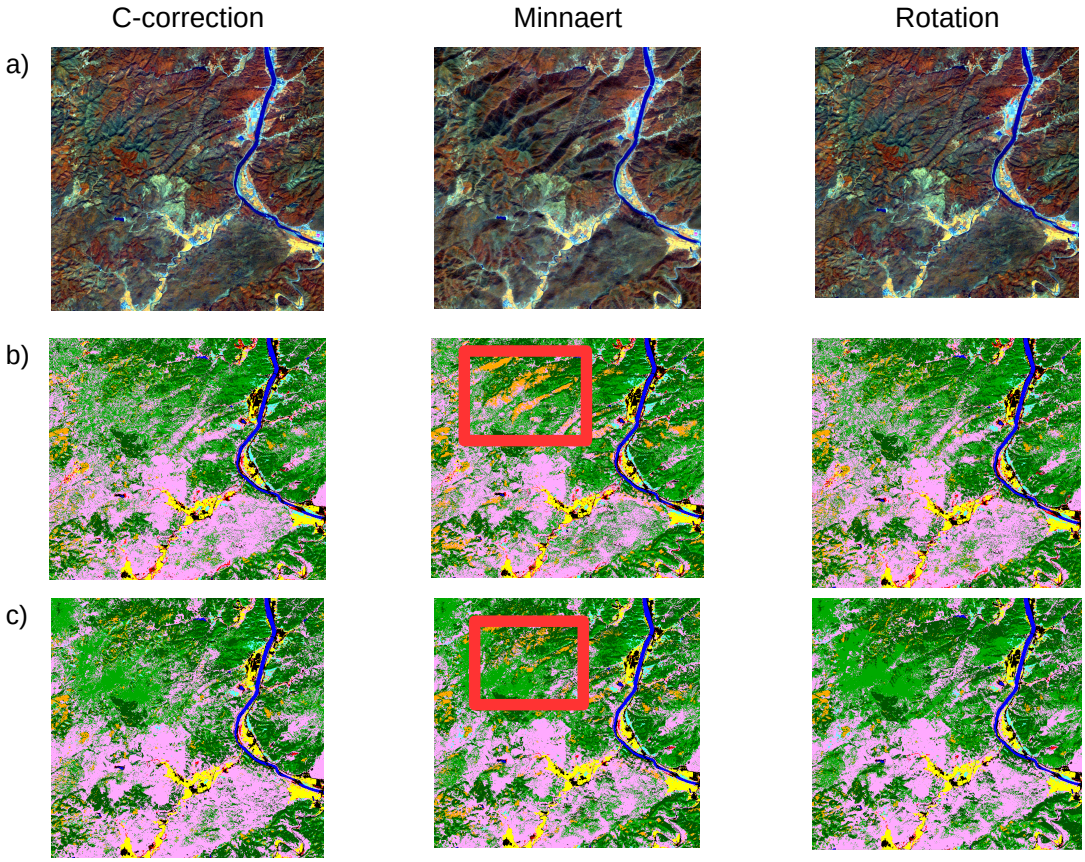

Figure 30: Overview of the land cover classification of the original images (a - RE spring false color composites 541; b - classification of datasets containing all bands from the spring and autumn images; c - datasets with all bands with the addition of ancillary data)

The land cover statistics presented in table 14 show the distribution of the land cover

types for each classified dataset. There is a visible redistribution of the land cover types between the classified datasets with and without ancillary data. For the image corrected by the c-correction method a change is noticeable between the broadleaved and conifer forests as well as a significant decrease in bare land. The images corrected by the minnaert model show a decrease in the area covered by bamboo when the ancillary data is included. Which corresponds to the partial compensation of the topographic effect.

Table 14: Land cover statistics for the not separated images (AD - ancillary data)

Class	**No separation**		**No separation + AD**		**No separation**		**No separation + AD**		**No separation**		**No separation + AD**	
Topographic corr.	C-correction				Minnaert				Rotation			
Area	ha	%	ha	%	ha	%	ha	%	ha	%	ha	%
Broadleaved Forest	15,736	25.2%	13,803	22.1%	16,527	26.4%	16,826	26.9%	15,712	25.1%	16,906	27.0%
Conifer Forest	11,909	19.1%	14,151	22.6%	12,247	19.6%	12,996	20.8%	12,182	19.5%	13,768	22.0%
Bamboo Forest	3,302	5.3%	3,269	5.2%	4,762	7.6%	3,924	6.3%	3,959	6.3%	2,508	4.0%
Shrubs and grass	20,127	32.2%	21,498	34.4%	17,786	28.5%	18,951	30.3%	19,623	31.4%	19,881	31.8%
Tea	1,302	2.1%	1,189	1.9%	1,090	1.7%	1,135	1.8%	1,042	1.7%	994	1.6%
Agriculture	5,042	8.1%	4,847	7.8%	4,948	7.9%	5,081	8.1%	4,913	7.9%	4,800	7.7%
Water	403	0.6%	446	0.7%	399	0.6%	444	0.7%	421	0.7%	442	0.7%
Urban/Infrastructure	2,426	3.9%	2,490	4.0%	2,433	3.9%	2,396	3.8%	2,300	3.7%	2,429	3.9%
Barre Land	2,253	3.6%	807	1.3%	2,308	3.7%	711	1.1%	2,349	3.8%	737	1.2%
Not classified	0	0.0%	0	0.0%	0	0.0%	37	0.1%	0	0.0%	36	0.1%
Total	**62,500**	**100.0%**	**62,500**	**100.0%**	**62,500**	**100.0%**	**62,500**	**100.0%**	**62,500**	**100.0%**	**62,500**	**100.0%**

Table 15 shows the accuracy assessment for the classified images. It is visible that there is an increase in the accuracy compared to the classification of the original images.

Also, the classified images corrected by the minnaert method show a lower accuracy, whereas the images corrected by the c-correction method show the best overall accuracy. In general the classified images where the ancillary data is included have a higher accuracy, and the lowest class accuracy is within the land cover type: Urban/Infrastructure.

Table 15: Accuracy assessment for the not-separated images

Class	**No separation**		**No separation + AD**		**No separation**		**No separation + AD**		**No separation**		**No separation + AD**	
Topographic corr.	C-correction				Minnaert				Rotation			
Overall accuracy	91.90%		92.10%		89.70%		91.10%		91.70%		91.90%	
	PA	UA	PA	UA	PA	UA	PA	UA	PA	UA	PA	UA
Broadleaved Forest	75.4	87.3	68.7	88.1	68.4	75	64	80.7	73.9	85.6	68.2	83.2
Conifer Forest	89.3	92.7	90.6	91.1	84	89	88.2	89.2	88.7	92.8	87.7	88.5
Bamboo Forest	97.9	96.9	97.5	96.4	98.5	95.5	99.3	96	98.3	95.5	99.3	96.6
Shrubs and grass	91.8	68.1	94.3	65.4	86.7	67	90.7	62.7	91.5	66.1	95.5	68.1
Tea	96.4	86.8	96.4	83.1	95.9	93.6	96.9	96	96.4	94.5	97.9	98.9
Agriculture	91.7	95.6	91.9	98.2	91.5	96.6	92.2	98.2	92.2	96.4	92.2	98.2
Water	96.4	100	98.5	100	96.2	100	98.2	100	96.5	100	98.4	100
Urban/Infrastr.	84.7	23.4	84.7	35.1	82.6	22.7	86.9	34	84.7	24.8	86.9	35.7
Barre Land	100	92.3	100	97.2	100	81.8	100	100	100	92.3	100	100

Results - NDVI classes

The classification of the images which were topographically corrected by separation in NDVI classes is shown in the Figure 31. As it was the case with the classification of the complete images (Figure 30) the classification of the minnaert corrected images is influenced by the topographic effect.

Both the images corrected by c-correction and rotation model showed an over-correction for the NDVI values representing no or low vegetation (see Table 8). This is visible in the classification as well. In the example below, marked by the red square, the over-corrected patches are shown as agricultural areas in the images corrected by c-correction and as bare land in the rotation model corrected images. These effects are however partly compensated with the introduction of the ancillary data in the classification.

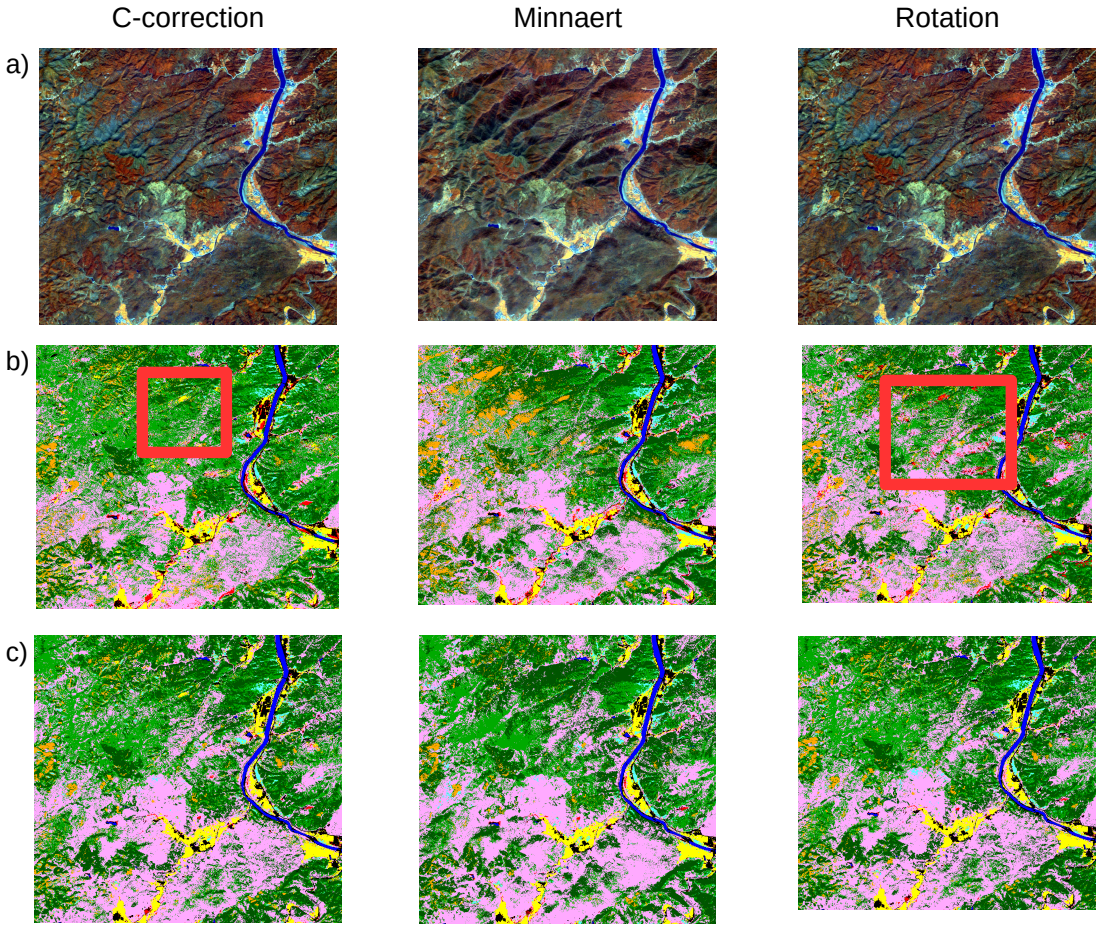

Figure 31: Overview of the land cover classification of the images corrected by NDVI classes (a - RE spring false color composites 541; b - classification of datasets containing all bands from the spring and autumn images; c - datasets with all bands with the addition of ancillary data)

The land cover statistics in this case also show a certain redistribution of the land cover types when the ancillary data is included in the classification (table 16). The trend is similar as with the classification of the images not separated in classes for the topographic correction.

Table 16: Land cover statistics for the images corrected by NDVI classes (AD - ancillary data)

Class	**NDVI**		**NDVI + AD**		**NDVI**		**NDVI + AD**		**NDVI**		**NDVI + AD**	
Topographic corr.	C-correction				Minnaert				Rotation			
Area	ha	%	ha	%	ha	%	ha	%	ha	%	ha	%
Broadleaved Forest	17,474	28.0%	15,031	24.1%	14,696	23.5%	14,678	23.5%	15,930	25.5%	15,302	24.5%
Conifer Forest	12,986	20.8%	15,316	24.5%	12,969	20.7%	15,474	24.8%	12,528	20.0%	15,741	25.2%
Bamboo Forest	3,618	5.8%	3,228	5.2%	5,111	8.2%	2,216	3.5%	4,282	6.9%	3,196	5.1%
Shrubs and grass	15,133	24.2%	19,160	30.7%	17,802	28.5%	19,875	31.8%	18,553	29.7%	18,669	29.9%
Tea	1,096	1.8%	1,139	1.8%	1,420	2.3%	1,289	2.1%	987	1.6%	993	1.6%
Agriculture	7,334	11.7%	4,978	8.0%	5,123	8.2%	5,294	8.5%	4,808	7.7%	5,011	8.0%
Water	384	0.6%	454	0.7%	400	0.6%	449	0.7%	417	0.7%	464	0.7%
Urban/Infrastructure	2,129	3.4%	2,488	4.0%	2,411	3.9%	2,440	3.9%	2,540	4.1%	2,496	4.0%
Bare Land	2,345	3.8%	704	1.1%	2,565	4.1%	747	1.2%	2,455	3.9%	629	1.0%
Not classified	0	0.0%	0	0.0%	3	0.0%	38	0.1%	0	0.0%	0	0.0%
Total	**62,500**	**100.0%**	**62,500**	**100.0%**	**62,500**	**100.0%**	**62,500**	**100.0%**	**62,500**	**100.0%**	**62,500**	**100.0%**

When looking at the accuracy assessment for this class, it is noticeable that the overall accuracy is again lowest for the images corrected with the minnaert model. Even with the addition of the ancillary data the overall accuracy is below 90%.

The addition of the ancillary data increases the accuracy in all images and the lowest class accuracy is again within the land cover type of Urban/Infrastructure.

Table 17: Accuracy assessment for the images corrected by NDVI classes

Class	**NDVI**		**NDVI + AD**		**NDVI**		**NDVI + AD**		**NDVI**		**NDVI + AD**	
Topographic corr.	C-correction				Minnaert				Rotation			
Overall accuracy	88.70%		92.2		88.80%		89.2		91.40%		92.3	
	PA	UA	PA	UA	PA	UA	PA	UA	PA	UA	PA	UA
Broadleaved Forest	68.2	81.7	70.1	87.3	66.4	75.1	59.6	76.2	71	85.1	70.6	86.4
Conifer Forest	87.4	89.4	90	89.3	83.7	87	84.9	82.5	88.3	92.8	89.4	89.5
Bamboo Forest	97.5	92	97.6	95.4	96.3	93.3	95.3	96.1	98.1	94.4	98.5	95.6
Shrubs and grass	88.7	80	92.1	72.5	82.3	63.6	90.7	61.8	88.7	64	92.6	70.3
Tea	90.4	86.1	95.9	84.1	95.9	93.6	97.4	99.4	96.4	95	95.4	94.05
Agriculture	87.6	88.2	91.2	98.2	92.4	97.3	92.6	97.8	91	96.3	91.7	97.7
Water	93	100	98.7	100	96.2	100	98.3	100	97.6	100	98.8	100
Urban/Infrastr.	78.2	16.6	89.1	34.1	80.4	22.4	86.9	35.3	89.1	26.7	86.9	34.7
Bare Land	100	35.6	100	100	100	83.7	100	100	100	83.7	100	100

Results - Slope classes

The images which were separated by slope classes for the topographic correction have showed high correlation values for the steep slopes (chapter 4.2). Also, the overcorrection noticed within the images corrected by NDVI classes is not noticeable in the images.

In the example of the classification results (Figure 32) the minnaert corrected images again show that the not compensated topographic effect has an influence on the results.

In both the c-correction and rotation method corrected images this effect is reduced, and with the inclusion of the ancillary data there is a visible improvement.

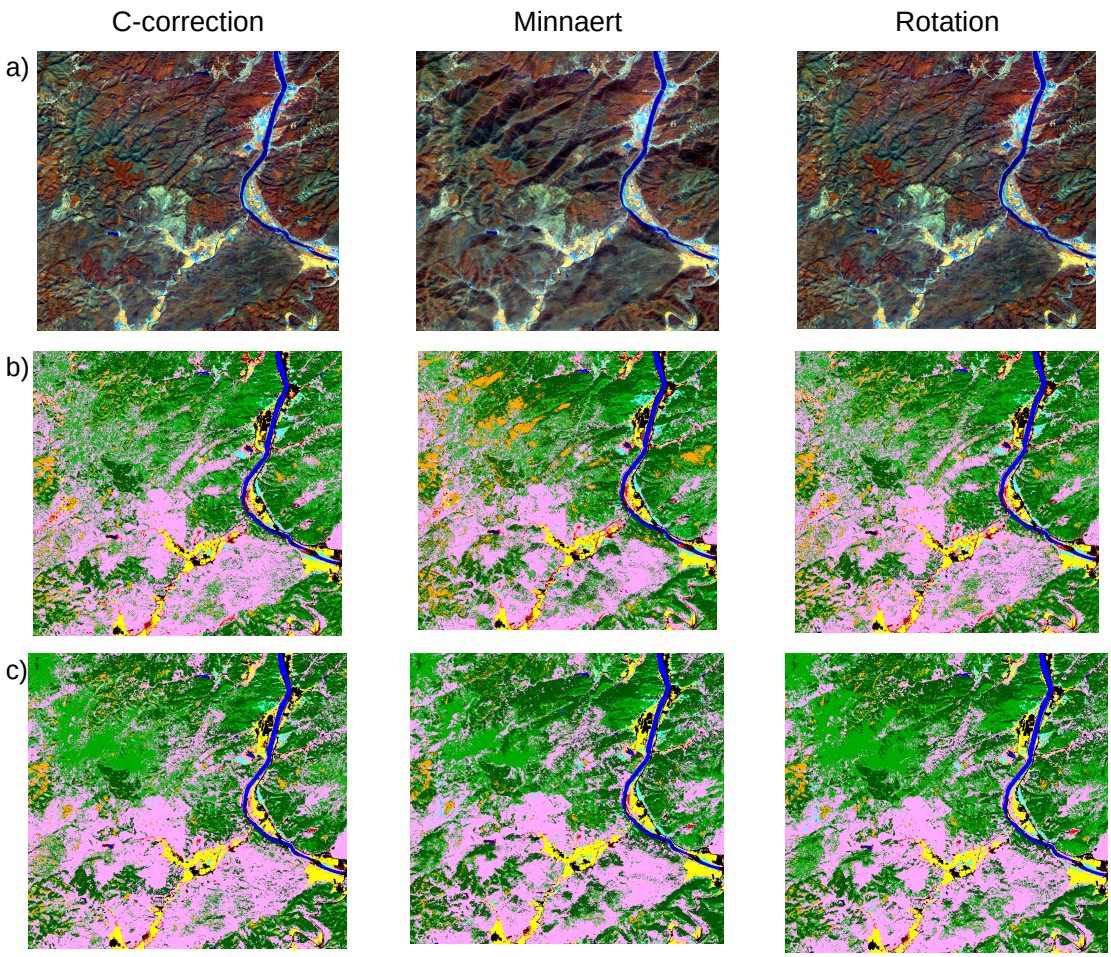

Figure 32: Overview of the land cover classification of the images corrected by Slope classes (a - RE spring false color composites 541; b - classification of datasets containing all bands from the spring and autumn images; c - datasets with all bands with the addition of ancillary data)

The land cover statistics (table 18) present numbers which are very similar to the statistics of the classification performed on the images which were not separated in classes.

Table 18: Land cover statistics for the images corrected by Slope classes (AD - ancillary data)

Class	**Slope**		**Slope + AD**		**Slope**		**Slope + AD**		**Slope**		**Slope + AD**	
Topographic corr.	C-correction				Minnaert				Rotation			
Area	ha	%	ha	%	ha	%	ha	%	ha	%	ha	%
Broadleaved Forest	15,864	25.4%	13,784	22.1%	14,721	23.6%	14,719	23.6%	15,712	25.1%	16,878	27.0%
Conifer Forest	11,921	19.1%	13,813	22.1%	12,999	20.8%	15,547	24.9%	12,205	19.5%	13,726	22.0%
Bamboo Forest	3,377	5.4%	3,253	5.2%	5,106	8.2%	2,210	3.5%	4,027	6.4%	2,468	3.9%
Shrubs and grass	19,989	32.0%	21,982	35.2%	17,677	28.3%	19,777	31.6%	19,523	31.2%	19,968	31.9%
Tea	1,282	2.1%	1,113	1.8%	1,407	2.3%	1,261	2.0%	1,036	1.7%	1,006	1.6%
Agriculture	5,028	8.0%	4,839	7.7%	5,113	8.2%	5,282	8.5%	4,922	7.9%	4,799	7.7%
Water	403	0.6%	445	0.7%	400	0.6%	453	0.7%	421	0.7%	441	0.7%
Urban/Infrastructure	2,387	3.8%	2,482	4.0%	2,414	3.9%	2,458	3.9%	2,296	3.7%	2,423	3.9%
Bare Land	2,250	3.6%	790	1.3%	2,661	4.3%	755	1.2%	2,358	3.8%	755	1.2%
Not classified	0	0.0%	0	0.0%	3	0.0%	38	0.1%	0	0.0%	36	0.1%
Total	**62,500**	**100.0%**	**62,500**	**100.0%**	**62,500**	**100.0%**	**62,500**	**100.0%**	**62,500**	**100.0%**	**62,500**	**100.0%**

The accuracy assessment presented in table 19 shows that the images which were corrected by slope classes have very similar accuracy to the not separated images.

Individually the minnaert model provides the lowest results, and c-correction the highest correlation.

Table 19: Accuracy assessment for the images corrected by Slope classes

Class	**Slope**		**Slope + AD**		**Slope**		**Slope + AD**		**Slope**		**Slope + AD**	
Topographic correctio	C-correction				Minnaert				Rotation			
Overall accuracy	91.70%		92.40%		88.90%		89.5		91.70%		91.8	
	PA	UA	PA	UA	PA	UA	PA	UA	PA	UA	PA	UA
Broadleaved Forest	75	87	70.7	88.5	67.1	75.5	60.2	77.3	73.5	85.3	67.9	83.2
Conifer Forest	88.6	92.5	90.4	90.9	84	87.1	85.5	83	88.7	92.5	87.8	88
Bamboo Forest	98.1	96.3	97.6	96.5	96.2	93.4	95.4	96.2	98.2	95.6	99.2	96.7
Shrubs and grass	91.5	67.2	94.9	67.8	82	63.8	90.7	61.9	91.8	66	95.2	68.6
Tea	96.4	87.6	95.9	83.4	95.9	94	97.9	100	96.4	95	98.4	98.4
Agriculture	91.7	95.4	91.9	98.2	92.4	97.3	92.6	97.8	92.2	96.4	92.2	98.5
Water	96.2	100	98.5	100	96.2	100	98.2	100	96.5	100	98.3	100
Urban/Infrastr.	84.7	23.4	84.7	35.1	80.4	22.4	86.9	35	84.7	24.8	86.9	35
Bare Land	100	92.3	100	97.2	100	83.7	100	100	100	92.3	100	100

Results - Illumination classes

The images which were corrected by separation in illumination classes showed the lowest correlation factors in the assessment of the topographic correction. Figure 33 show an example of the classification. The red square shows an area which is differently classified in all three cases. This is party improved with the inclusion of the ancillary data, except for the minnaert corrected images.

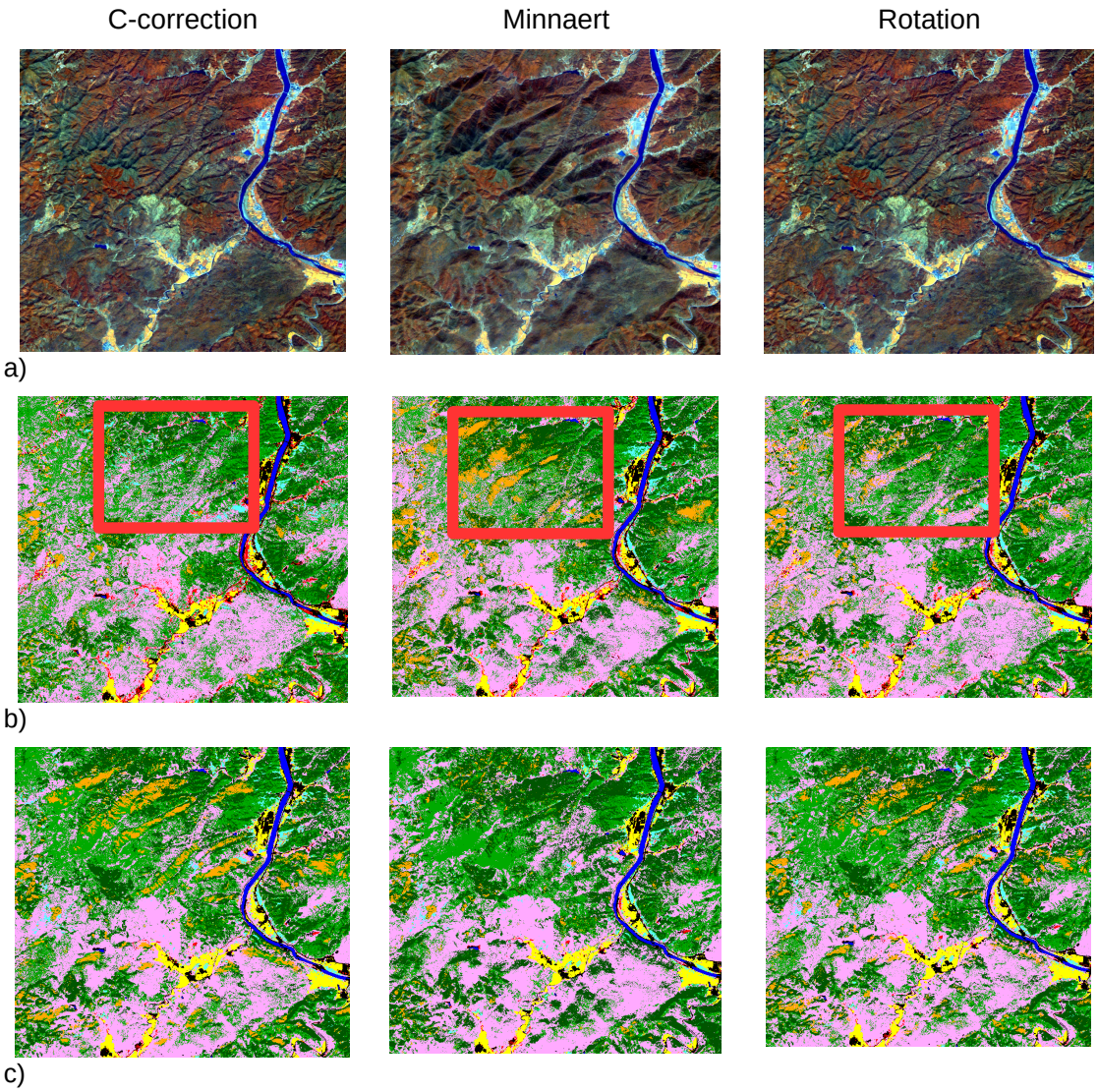

Figure 33: Overview of the land cover classification of the images corrected by Illumination classes (a - RE spring false color composites 541; b - classification of datasets containing all bands from the spring and autumn images; c - datasets with all bands with the addition of ancillary data)

Table 20: Land cover statistics for the images corrected by Illumination classes (AD - ancillary data)

Class	**Illumination**		**Illumination + AD**		**Illumination**		**Illumination + AD**		**Illumination**		**Illumination + AD**	
Topographic corr.	C-correction				Minnaert				Rotation			
Area	ha	%	ha	%	ha	%	ha	%	ha	%	ha	%
Broadleaved Forest	20,974	33.6%	16,489	26.4%	14,906	23.8%	14,888	23.8%	17,239	27.6%	16,135	25.8%
Conifer Forest	9,065	14.5%	12,469	20.0%	12,798	20.5%	15,657	25.1%	11,206	17.9%	12,753	20.4%
Bamboo Forest	2,519	4.0%	4,617	7.4%	5,112	8.2%	2,143	3.4%	3,742	6.0%	4,006	6.4%
Shrubs and grass	18,207	29.1%	19,215	30.7%	17,602	28.2%	19,641	31.4%	18,787	30.1%	19,913	31.9%
Tea	1,324	2.1%	1,255	2.0%	1,407	2.3%	1,232	2.0%	1,110	1.8%	1,243	2.0%
Agriculture	4,643	7.4%	4,910	7.9%	5,127	8.2%	5,234	8.4%	5,025	8.0%	4,856	7.8%
Water	378	0.6%	441	0.7%	400	0.6%	444	0.7%	433	0.7%	453	0.7%
Urban/Infrastructure	2,669	4.3%	2,526	4.0%	2,405	3.8%	2,449	3.9%	2,433	3.9%	2,469	4.0%
Bare Land	2,721	4.4%	542	0.9%	2,739	4.4%	773	1.2%	2,525	4.0%	637	1.0%
Not classified	0	0.0%	36	0.1%	3	0.0%	38	0.1%	0	0.0%	36	0.1%
Total	**62,500**	**100.0%**	**62,500**	**100.0%**	**62,500**	**100.0%**	**62,500**	**100.0%**	**62,500**	**100.0%**	**62,500**	**100.0%**

The classification of the c-corrected images show a big change in the land cover types for the images with or without ancillary data (table 20). Especially big difference exists in the area of broadleaved forest and coniferous forest. The differences in these land cover types are not as big within the minnaert or the images corrected by the rotation method. Looking at the accuracy of the classification (table 21), it can be seen that the minnaert corrected images have again the lowest overall accuracy. Also, the class accuracy of the land cover type urban/infrastructure is lowest in all images. All other land cover types have relatively high accuracy.

Table 21: Accuracy assessment for the images corrected by Illumination classes

Class	**Illumination**		**Illumination + AD**		**Illumination**		**Illumination + AD**		**Illumination**		**Illumination + AD**	
Topographic corr.	C-correction				Minnaert				Rotation			
Overall accuracy	89.70%		92.4		89.20%		90.6		91.04%		92.4	
	PA	UA	PA	UA	PA	UA	PA	UA	PA	UA	PA	UA
Broadleaved Forest	66.5	79.7	70.2	86.1	68.3	75.8	65	78.5	71.9	80.7	67.9	85
Conifer Forest	87.9	95.8	89.5	91.3	84.1	88.1	84.8	86.5	86.5	91	88.7	90.5
Bamboo Forest	94.2	95.9	99.5	95.7	96.5	92.7	98.7	96.6	99.1	95.4	99.5	95.4
Shrubs and grass	81.7	48.9	94.1	66	81.7	65.2	92.4	64.3	86.2	65.4	93.2	64
Tea	96.9	81	96.9	97.6	96.4	95.5	99.4	99.4	95.4	94	97.4	98.9
Agriculture	100	97.7	92.2	98.5	92.4	97.3	92.6	98.2	91.9	97.3	92.2	98.2
Water	95.9	100	98.5	100	96.2	100	98.2	100	96.9	100	98.6	100
Urban/Infrastr.	86.9	28.5	84.7	35	84.7	23	86.9	35	86.9	26.8	84.7	37.1
Bare Land	100	73.4	100	97	100	85.7	100	100	100	92.3	100	97.2

5 Discussion

Chapter 4 has presented the results of the data analysis. This chapter will discuss the results and relate them to the objectives of the master thesis as defined in chapter 1.2.

5.1 Topographic normalization methods

When looking at the results from the topographic normalization, both the statistical output as well as the visual comparison (Chapter 4.2.1) it is obvious that none of the implemented approaches has succeeded in completely removing the topographic effect from the satellite images.

This can be especially said for the minnaert model. The methods provides correlation values which are comparable with the c-correction and the rotation method. But, when looking at the images, the topographic effect is still present. As example this can be seen in the Figures 22-25. From this aspect the minnaert model is not a suitable approach for the topographic normalization of the imagery with the characteristics used in this master thesis.

Both other methods which were applied showed better results. Visually they succeeded in removing a big part of the topographic effect. However, still a certain amount of shadow from the terrain is left in the imagery.

A possible cause for the left over shadow / topographic effect in the imagery can be the difference in the resolution between the DEM and the RapidEye images. As seen in the field, the terrain in the study area is very specific. It contains micro-relief forms which make it harder to correct the image, as well as very steep slopes. The spline interpolation method which re-samples the DEM to 5m (from 90m) creates a too smooth of a surface which does not represent the frequent change in the landscape.

Similar analysis should be done with a finer DEM which better represents the specifics of the real terrain.

5.1.1 Separation of the images by vegetation classes

Three different approaches have been tested for separating the images in vegetation classes, in order to test if the topographic normalization would perform better.

Table 8 shows the correlation for all different approaches. It shows that the results of individual classes have indeed better results, as compared to the topographic normalization of the non-separated image. For instance the highest correlations are received from the class 3 of the images separated by slope classes (representing the steep slopes > 30°). This is the case with both images and all normalization methods. But, at the same time the class 1 and class 2 show one of the lowest correlations.

Similar case is with the separation of images by NDVI classes. Class 2 (representing sparse or no vegetation) has relatively high correlations for both the autumn and spring images. However, when visually inspecting the results, they show an over-correction exactly for this class.

Over-correction of the images was noticed by other authors as well. Tan et al. (2013) noticed an over-correction when using the c-correction method in areas with low illumination values. This can be the case here as well, since the over-corrected class covers partly areas which have a low illumination value.

In general, even though there is an increase with the correlation values for the images normalized by separate classes, in comparison with the images normalized without separation in classes this increase is very limited. The best values produced by separation in NDVI classes has showed an over-correction.

In this relation, it might be more time consuming and effective to avoid the separation of classes for the topographic normalization and perform the process on the complete images. If the procedure should be done for larger area it would certainly provide a faster processing of the datasets and at the same time hardly any loss in accuracy.

5.1.2 Role of image resolution to the topographic normalization

In order to test the effect of the image and DEM resolution to the topographic normalization a Landsat 8 image of the study area was used. Its resolution of 30m is closer to the original SRTM resolution of 90m. All three methods for topographic normalization which were tested for the RapidEye images have been implemented for the Landsat image as well.

The results presented in table 10 show partly higher correlations as the RapidEye spring image, but still lower or very similar to the results from the RapidEye autumn image. The visual assessment also proved a lack of improvement in the normalization process.

Instead of the image resolution it seams that a more important factor for the topographic normalization is the solar azimuth and elevation at the time of the image acquisition. This is directly related to the area covered by shadow. The results would confirm this, since the autumn image has a higher azimuth angle at the time of the acquisition, meaning that more area is illuminated as in the spring image.

5.2 Land Cover Classification

The land cover classification which aims primarily at distinguishing the main forest types, showed high overall accuracy. From the results presented in tables 13 to 21 it can be seen that most of the datasets resulted with about 90% overall accuracy. All error matrices which are related to the accuracy assessment are presented in the Annex.

When looking at the forest types, as the main goal in the mapping bamboo and coniferous forests have higher class accuracy as the broadleaved forests.

This might be related to the fact that most bamboo forests and coniferous forests appear in the field as pure stands and rarely in a mixture. On the other hand the broadleaved forests are tend to be more mixed.

Lowest class accuracy was received from the land cover type "Urban/Infrastructure".

If we look at the land cover maps which come as a result of the classification, it shows that the topographic normalization was not optimally performed. Dark areas on the images are influencing the classification and show in different land cover types as they actually are.

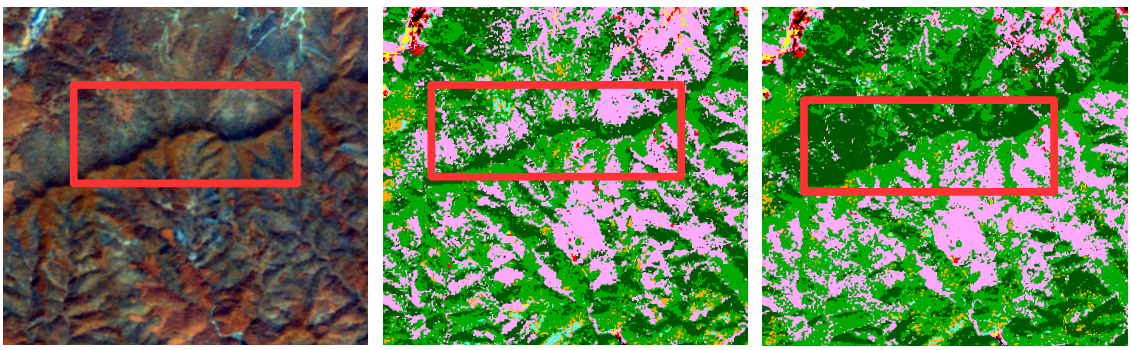

a) b) c)

Figure 34: Left over topographic effect in the classified images (a - topographically normalized image; land cover map of b - topographically normalized image; c - original not corrected image)

The red square in the Figure above shows one such effect of the left over topographic effect to the classification results. In this case the dark area of the shadow is classified as coniferous forest.

Compared however to the land cover classification of the images without any topographic correction the effect is significantly smaller.

5.2.1 Ancillary data

In the results chapter an overview of the land cover classification and its accuracy assessment was given. For each class there is also a comparison between the datasets without ancillary data and the same datasets including ancillary data.

Tables 13, 15, 17, 19 and 21 show this comparison. It is noticeable that the inclusion of the ancillary data increases the overall accuracy for every dataset as in average it is always higher 1-2% than the original dataset. Also the highest noted overall accuracy of 92.4% is a dataset which contains the ancillary data.

The effect of the ancillary data to the land cover classification is especially noticeable when directly comparing the classification outcome.

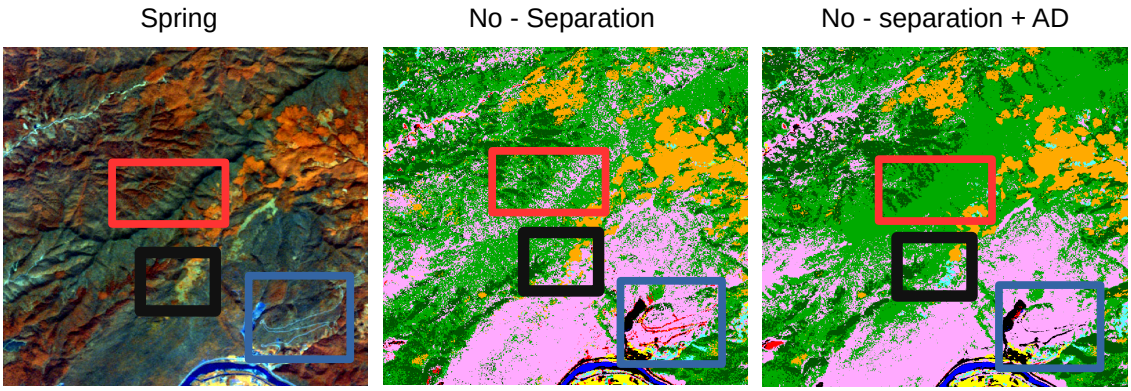

Figure 35: Comparing the effects of ancillary data to the land cover classification

In the example above there are three cases which can be seen as a direct influence of the ancillary data to the land cover classification.

The red square presents a case on the original image where the topographic effect is not completely corrected. Also, the land cover type is broadleaved forest on both sides of the slope. It is however classified as shrubs in part of the northern slope in the image not containing ancillary data. With the inclusion of the ancillary data this seems to be corrected, as the land cover type is the same on the both sides of the slope.

The black square shows an example where the land cover type changes from shrubs to tea.

The blue square shown a road leading up the slope, as a tin light blue line on the original image. It is classified as bare land on the image not containing the ancillary data, although is an asphalted road. This is corrected in the classification containing ancillary data.

This is just an Figure of the effects of the ancillary data. In general, however, the utilization of ancillary data as a component during the classification showed an improved classification and also it avoids the misclassification caused by left over topographic effects in the imagery.

5.2.2 Training areas

The creation of the training areas from the information gathered during the field work proved to be sufficient. Most of the reference areas used for the classification and verification were acquired from these information, and produced a land cover map with high accuracy.

The usability of the freely available high resolution images from google earth or bing maps were not optimal for utilization; due to several reasons such as cloud cover, poor quality and a shift in the imagery.

As already mention in chapter 4.1.1 the field work encountered certain difficulties. If similar procedure is to be carried out on a larger area, it would proportionally increase the time required for field work. In order to avoid that an alternative might be to acquire high resolution imagery for a part of the project region. This would have the aim to gather additional reference data and also to verify the classification. If it is only for a small part of the project area, it would be financially feasible and would increase the efficiency of the work.

6 Conclusion

The results from the work done for this master thesis as seen in the discussion were able to answer the questions and objectives of the research.

Three common methods for topographic normalization were implemented on the Rapid Eye imagery - c-ccorection, minnaert and the rotation method. From them the c-correction and rotation method showed similar results, whereas the minnaert method did not succeed in compensating the topographic effect in the imagery.

Several approaches were tested to see if they would increase the efficiency of the topographic normalization. These approaches were related to separating the images in vegetation classes according to different criteria; and masking out the shadows of the images. These approaches proved to improve the topographic normalization, but its effects are very limited and in some cases lead to overcorrection. Processing the whole image without separation in different classes would offer the best result.

All datasets which were topographically corrected have been classified by a pixel based classification. Nine land cover classes have been identified with three major forest types as the primary goal of the mapping. This procedure showed that the topographic normalization certainly has an effect on the land cover classification. The corrected images had increased overall accuracy. There are however leftover shadows which could not been removed by any of the topographic normalization methods. These shadows do cause a certain misclassification in the land cover maps.

Introducing ancillary data to the land cover classification proved to partly compensate for these left over effect. In general the datasets which included ancillary data in the classification provided the highest overall accuracy with about 92%. This accuracy was received from the imagery corrected by c-correction and rotation method.

The final research objective relates to the imagery resolution and its effect on the topographic normalization. For that reason a Landsat image was analyses and corrected using the same three methods for topographic normalization. However the results were not significantly better than the ones from the RapidEye images.

General remarks: The procedure used for the topographic normalization of the RapidEye imagery proved to improve the results of the land cover classification. Also, since of the aims of the project is to create a forest type map, it can be concluded that

the Rapid Eye imagery provides a good base for an accurate Forest type mapping, and has spectral properties that would allow to differentiate the main land cover types in the region.

However, in order to improve the results of the topographic normalization the same procedure should be repeated using a DEM with higher resolution. If possible a resolution which is close to the 5m of the RapidEye imagery. This would cover for the terrain specifics of the study area and possibly remove most of the topographic effects.

7 Literature

Albertz, J., 2009. *Einführung in die Fernerkundung : Grundlagen der Interpretation von Luft- und Satellitenbildern / Jörg Albertz* 4., aktualisierte Aufl., Darmstadt: WBG.

Allen, T.R., 2000. Topographic Normalization of Landsat Thematic Mapper Data in Three Mountain Environments. *Geocarto International*, 15(2), pp.15–22.

Anderson, J.R., 1976. *A Land Use and Land Cover Classification System for Use with Remote Sensor Data*, U.S. Government Printing Office.

Bahadur K.C., K., 2009. Improving Landsat and IRS Image Classification: Evaluation of Unsupervised and Supervised Classification through Band Ratios and DEM in a Mountainous Landscape in Nepal. *Remote Sensing*, 1(4), pp.1257–1272.

Bhatta, B., 2008. *Remote Sensing And Gis*, Oxford University Press, Incorporated.

Bishop, M.P., Shroder, J.F. & Colby, J.D., 2003. Remote sensing and geomorphometry for studying relief production in high mountains. *Geomorphology*, 55(1-4), pp.345–361.

BlackBridge, 2014. BlackBridge :: Delivering the World. Available at: http://www.blackbridge.com/rapideye/products/ortho.htm [Accessed April 12, 2014].

Blaschke, T., 2010. Object based image analysis for remote sensing. *ISPRS Journal of Photogrammetry and Remote Sensing*, 65(1), pp.2–16.

Blesius, L. & Weirich, F., 2005. The use of the Minnaert correction for land-cover classification in mountainous terrain. *International Journal of Remote Sensing*, 26(17), pp.3831–3851.

Chuvieco, E., 2008. *Earth Observation of Global Change: The Role of Satellite Remote Sensing in Monitoring the Global Environment*, Springer Science & Business Media.

Civco, D.L., 1989. Topographic normalization of landsat thematic mapper digital imagery. *Photogrammetric engineering and remote sensing*, 55(9), pp.1303–1309.

CNES, 2014. *Orfeo Toolbox*, CNES. Available at: http://www.orfeo-toolbox.org/otb/about-otb.html [Accessed November 30, 2014].

Colby, J.D., 1991. Topographic normalization in rugged terrain. *Photogrammetric Engineering and Remote Sensing*, 57(5), pp.531–537.

Congalton, R.G., 2001. Accuracy assessment and validation of remotely sensed and other spatial information. *International Journal of Wildland Fire*, 10(4), pp.321–328.

Congedo, L. & Munafò, M., 2012. *Development of a Methodology for Land Cover Classification in Dar es Salaam using Landsat Imagery*, Tech. rep. Rome: Sapienza University, ACC Dar Project Sapienza University. Available at: http://www.planning4adaptation.eu/Docs/papers/08_NWP-DoM_for_LCC_in_Dar_using_Landsat_Imagery.pdf [Accessed November 30, 2014].

Cuo, L., Vogler, J.B. & Fox, J.M., 2010. Topographic normalization for improving vegetation classification in a mountainous watershed in Northern Thailand. *International Journal of Remote Sensing*, 31(11), pp.3037–3050.

Deering, D.W., 1978. *Rangeland Reflectance Characteristics Measured by Aircraft and Spacecraft Sensors*, Deering.

Dorren, L.K.A., Maier, B. & Seijmonsbergen, A.C., 2003. Improved Landsat-based forest mapping in steep mountainous terrain using object-based classification. *Forest Ecology and Management*, 183(1-3), pp.31–46.

EEA, 2007. Corine Land Cover 2006 - technical guidelines. Available at: http://www.eea.europa.eu/publications/technical_report_2007_17/download [Accessed December 6, 2014].

Eggleston, H.S. et al., 2006. *2006 IPCC guidelines for national greenhouse gas inventories*, Available at: http://www.ipcc-nggip.iges.or.jp/public/2006gl/index.htm [Accessed November 10, 2014].

Eiumnoh, A. & Shrestha, R.P., 2000. Application of DEM data to Landsat image classification: evaluation in a tropical wet-dry landscape of Thailand. *Photogrammetric Engineering and Remote Sensing*, 66(3), pp.297–304.

Ekstrand, S., 1996. Landsat TM-based forest damage assessment: correction for topographic effects. *Photogrammetric Engineering and Remote Sensing*, 62(2), pp.151–162.

FAO, 2010. Global Forest Resources Assessment. Available at: http://www.fao.org/forestry/fra/67090/en/chn/ [Accessed November 29, 2014].

Foody, G.M., 2002. Status of land cover classification accuracy assessment. *Remote Sensing of Environment*, 80(1), pp.185–201.

Gao, Y. & Zhang, W., 2009. LULC Classification and Topographic Correction of Landsat-7 ETM+ Imagery in the Yangjia River Watershed: the Influence of DEM Resolution. *Sensors*, 9(3), pp.1980–1995.

GOFC-GOLD, 2013. *A sourcebook of methods and procedures for monitoring and reporting anth ropogenic greenhouse gas emissions and removals associated with deforestation, gains and losses of carbon stocks in forests rem aining forests, and forestation*, GOFC - GOLD Land Cover Project Office, hosted by Wagen ingen University, The Netherlands. Available at: http://www.gofcgold.wur.nl/redd/.

Di Gregorio, A. & Jansen, L., 2005. *Land Cover Classification System: Classification Concepts and User Manual : LCCS*, Food & Agriculture Org.

Hammond, T.O. & Verbyla, D.L., 1996. Optimistic bias in classification accuracy assessment. *International Journal of Remote Sensing*, 17(6), pp.1261–1266.

Herring, J.W. and D., 2000. NASA Earth Observatory : Available at: http://earthobservatory.nasa.gov/Features/MeasuringVegetation/measuring_vegetation_2.php [Accessed November 23, 2014].

Hildebrandt, G., 1987. 100 Jahre forstliche Luftbildaufnahme - Zwei Dokumente aus den Anfängen der forstlichen Luftbildinterpretation. *Bildmessung und Luftbildwesen*, 55, pp.221–224.

Holben, B.N. & Justice, C.O.J., 1980. The topographic effect on spectral response from nadir-pointing sensors. Available at: http://ntrs.nasa.gov/archive/nasa/casi.ntrs.nasa.gov/19810004902.pdf [Accessed June 10, 2014].

Horler, D.N.H., DOCKRAY, M. & Barber, J., 1983. The red edge of plant leaf reflectance. *International Journal of Remote Sensing*, 4(2), pp.273–288.

Jansen, L.L.F., Jaarsma, M. & van der Linden, E., 1990. Integrating Topographic Data with Remote Sensing for Land-Cover Classification. *Photogrammetric engineering and remote sensing*, 56(11), pp.1503–1506.

Jarvis, A. et al., 2008. Hole-filled SRTM for the globe Version 4, available from the CGIAR-CSI SRTM 90m Database. Available at: http://srtm.csi.cgiar.org [Accessed April 12, 2014].

Jing, C. et al., 2013. Comparison and validation of SRTM and ASTER GDEM for a subtropical landscape in Southeastern China. *International Journal of Digital Earth*, 7(12), pp.969–992.

Justice, C. & Holben, B., 1979. Examination of Larnbertian and Non-Lambertian Models for Simulating the Topographic Effect on Remotely Sensed Data. Available at: http://ntrs.nasa.gov/archive/nasa/casi.ntrs.nasa.gov/19800004282_1980004282.pdf?origin=publication_detail [Accessed June 10, 2014].

Lambert, J.H., 1760. *Lamberts Photometrie : [Photometria, sive De mensura et gradibus luminus, colorum et umbrae] (1760)*, Leipzig : W. Engelmann. Available at: http://archive.org/details/lambertsphotome00lambgoog [Accessed June 29, 2014].

Liang, S., Li, X. & Wang, J., 2012. *Advanced Remote Sensing: Terrestrial Information Extraction and Applications*, Academic Press.

Lillesand, T.M., Kiefer, R.W. & Chipman, J.W., 2004. Remote sensing and image interpretation. , (Ed.5), p.xiv + 763 pp.

lin4carbon, 2014. Sino-German cooperation project “lin4carbon.” *Lin4carbon*. Available at: http://lin2value.uni-goettingen.de/en/leftmainnavigation/arbeitspakete/lin2value.html [Accessed April 7, 2014].

Lu, D. et al., 2008. Pixel-based Minnaert correction method for reducing topographic effects on a Landsat 7 ETM+ image. *Photogrammetric Engineering and Remote Sensing*, 74(11), pp.1343–1350.

Lunetta, R.S. et al., 1991. Remote sensing and Geographic Information System data integration: error sources and research issues. *Photogrammetric engineering and remote sensing*, 57(6), pp.677–687.

Mather, P. & Tso, B., 2003. *Classification Methods for Remotely Sensed Data*, CRC Press.

Minnaert, M., 1941. The reciprocity principle in lunar photometry. *The Astrophysical Journal*. Available at: http://web.gps.caltech.edu/~vijay/Papers/BRDF/minnaert-41.pdf [Accessed June 29, 2014].

Nowak, D.J. & Greenfield, E.J., 2010. Evaluating The National Land Cover Database Tree Canopy and Impervious Cover Estimates Across the Conterminous United States: A Comparison with Photo-Interpreted Estimates. *Environmental Management*, 46(3), pp.378–390.

Open Foris, 2014. Open Foris. *Free open-source solutions for environmental monitoring*. Available at: http://www.openforis.org/ [Accessed January 17, 2015].

Powell, R.. et al., 2004. Sources of error in accuracy assessment of thematic land-cover maps in the Brazilian Amazon. *Remote Sensing of Environment*, 90(2), pp.221–234.

QGIS Development Team, 2014. *QGIS Geographic Information System*, Open Source Geospatial Foundation Project. Available at: http://qgis.osgeo.org [Accessed November 30, 2014].

Rees, W.G., 2013. *Physical Principles of Remote Sensing*, Cambridge University Press.

Riano, D. et al., 2003. Assessment of different topographic corrections in landsat-TM data for mapping vegetation types (2003). *IEEE Transactions on Geoscience and Remote Sensing*, 41(5), pp.1056–1061.

Riaño, D. et al., 2003. Assessment of different topographic corrections in Landsat-TM data for mapping vegetation types (2003). *IEEE Transactions on Geoscience and Remote Sensing*, 41(5), pp.1056–1061.

Richards, J.A., 2012. *Remote Sensing Digital Image Analysis: An Introduction*, Springer Science & Business Media.

Shahtahmassebi, A. et al., 2013. Review of shadow detection and de-shadowing methods in remote sensing. *Chinese Geographical Science*, 23(4), pp.403–420.

Shepherd, J.D. & Dymond, J.R., 2003. Correcting satellite imagery for the variance of reflectance and illumination with topography. *International Journal of Remote Sensing*, 24(17), pp.3503–3514.

Shimada, M. et al., 2014. New global forest/non-forest maps from ALOS PALSAR data (2007–2010). *Remote Sensing of Environment*, 155, pp.13–31.

Smith, J.A., Lin, T.L. & Ranson, K.L., 1980. The Lambertian assumption and Landsat data. *Photogrammetric Engineering and Remote Sensing*, 46(9), pp.1183–1189.

Smits, P.C., Dellepiane, S.G. & Schowengerdt, R.A., 1999. Quality assessment of image classification algorithms for land-cover mapping: A review and a proposal for a cost-based approach. *International Journal of Remote Sensing*, 20(8), pp.1461–1486.

De Sousa, C.H.R. et al., 2012. Analysis of rapideye's red edge band for image segmentation and classification. Available at: http://mtc-m18.sid.inpe.br/col/sid.inpe.br/mtc-m18/2012/05.18.13.14/doc/137.pdf [Accessed November 29, 2014].

Strahler, A.H. et al., 2006. Global land cover validation: Recommendations for evaluation and accuracy assessment of global land cover maps. *European Communities, Luxembourg*, p.51.

Szantoi, Z. & Simonetti, D., 2013. Fast and Robust Topographic Correction Method for Medium Resolution Satellite Imagery Using a Stratified Approach. *IEEE Journal of Selected Topics in Applied Earth Observations and Remote Sensing*, 6(4), pp.1921–1933.

Tan, B. et al., 2010. An illumination correction algorithm on Landsat-TM data. In *Geoscience and Remote Sensing Symposium (IGARSS), 2010 IEEE International*. IEEE, pp. 1964–1967. Available at: http://ieeexplore.ieee.org/xpls/abs_all.jsp?arnumber=5653492 [Accessed April 11, 2014].

Tan, B. et al., 2013. Improved forest change detection with terrain illumination corrected Landsat images. *Remote Sensing of Environment*, 136, pp.469–483.

Teillet, P.M. et al., 1982. On the slope-aspect correction of multispecral scanner data. *Canadian Journal of Remote Sensing*, 8(2), pp.84–106.

USGS, 2014. Landsat Missions Timeline. Available at: http://landsat.usgs.gov/about_mission_history.php [Accessed November 29, 2014].

Vanonckelen, S., Lhermitte, S. & Van Rompaey, A., 2013. The effect of atmospheric and topographic correction methods on land cover classification accuracy. *International Journal of Applied Earth Observation and Geoinformation*, 24, pp.9–21.

Warner, T.A., Nellis, M.D. & Foody, G.M., 2009. *The SAGE Handbook of Remote Sensing*, SAGE.

Weichelt, H. et al., 2013. *The RapidEye Red Edge Band*, BlackBridge. Available at: http://www.blackbridge.com/rapideye/upload/Red_Edge_White_Paper.pdf [Accessed April 12, 2014].

Wen, J. et al., 2009. Parametrized BRDF for atmospheric and topographic correction and albedo estimation in Jiangxi rugged terrain, China. *International Journal of Remote Sensing*, 30(11), pp.2875–2896.

Wickham, J.D. et al., 2010. Thematic accuracy of the NLCD 2001 land cover for the conterminous United States. *Remote Sensing of Environment*, 114(6), pp.1286–1296.

Wu, Z. [Hrsg, 1999. *Flora of China*, Beijing: Science Press.

8 Acknowledgement

Writing this master thesis would not have been possible without the assistance and contribution of some people and friends. Therefore at this place I would like to express my appreciation and thanks in first place to the members of the Lin4carbon project team as well as employees of the Chair of Forest Inventory and Remote Sensing (AWF) institute at the University of Göttingen in Germany. Especially to Prof. Dr Christoph Kleinn as the supervisor of the thesis who provided me with the opportunity to work together with his team on this interesting topic. Also, Dr. Hans Fuchs whose instructions and advices were of big importance for this me and the research. My big gratitude to the rest of the project team as well: Sabine for the organization and being the best host; Dengkui, Xiaolu, Ezequil and Ruben for the field work support; Julia for sharing information and experience.

I would also like to acknowledge the support I received during the whole period of my Masters studies from Prof. Strobl, Stefan Prüller, Dr. Wallentin and the complete UNIGIS team.

Thanks to my colleagues from UNIQUE forestry and land use GmbH who supported my master studies and offered enough understanding and space for me to successfully finish all obligations.

Finally thanks to my friends and family who have provided moral support throughout the whole time.

9 Annex

9.1 Annex 1 - Land Cover Statistics

Class	Original		Original + AD	
Topographic correctio	Not corrected			
area	ha	%	ha	%
Broadleaved Forest	15,848	25.4%	15,311	24.5%
Conifer Forest	13,232	21.2%	15,293	24.5%
Bamboo Forest	5,022	8.0%	2,565	4.1%
Shrubs and grass	17,204	27.5%	20,015	32.0%
Tea	1,221	2.0%	822	1.3%
Agriculture	4,948	7.9%	4,887	7.8%
Water	398	0.6%	488	0.8%
Urban/Infrastructure	2,349	3.8%	2,369	3.8%
Bare Land	2,277	3.6%	750	1.2%
Total	**62,500**	**100%**	**62,500**	**100%**

Class	No separation		No separation + AD		No separation		No separation + AD		No separation		No separation + AD	
Topographic corr.	C-correction				Minnaert				Rotation			
Area	ha	%	ha	%	ha	%	ha	%	ha	%	ha	%
Broadleaved Forest	15,736	25.2%	13,803	22.1%	16,527	26.4%	16,826	26.9%	15,712	25.1%	16,906	27.0%
Conifer Forest	11,909	19.1%	14,151	22.6%	12,247	19.6%	12,996	20.8%	12,182	19.5%	13,768	22.0%
Bamboo Forest	3,302	5.3%	3,269	5.2%	4,762	7.6%	3,924	6.3%	3,959	6.3%	2,508	4.0%
Shrubs and grass	20,127	32.2%	21,498	34.4%	17,786	28.5%	18,951	30.3%	19,623	31.4%	19,881	31.8%
Tea	1,302	2.1%	1,189	1.9%	1,090	1.7%	1,135	1.8%	1,042	1.7%	994	1.6%
Agriculture	5,042	8.1%	4,847	7.8%	4,948	7.9%	5,081	8.1%	4,913	7.9%	4,800	7.7%
Water	403	0.6%	446	0.7%	399	0.6%	444	0.7%	421	0.7%	442	0.7%
Urban/Infrastructure	2,426	3.9%	2,490	4.0%	2,433	3.9%	2,396	3.8%	2,300	3.7%	2,429	3.9%
Barre Land	2,253	3.6%	807	1.3%	2,308	3.7%	711	1.1%	2,349	3.8%	737	1.2%
Not classified	0	0.0%	0	0.0%	0	0.0%	37	0.1%	0	0.0%	36	0.1%
Total	**62,500**	**100.0%**	**62,500**	**100.0%**	**62,500**	**100.0%**	**62,500**	**100.0%**	**62,500**	**100.0%**	**62,500**	**100.0%**

Class	NDVI		NDVI + AD		NDVI		NDVI + AD		NDVI		NDVI + AD	
Topographic corr.	C-correction				Minnaert				Rotation			
Area	ha	%	ha	%	ha	%	ha	%	ha	%	ha	%
Broadleaved Forest	17,474	28.0%	15,031	24.1%	14,696	23.5%	14,678	23.5%	15,930	25.5%	15,302	24.5%
Conifer Forest	12,986	20.8%	15,316	24.5%	12,969	20.7%	15,474	24.8%	12,528	20.0%	15,741	25.2%
Bamboo Forest	3,618	5.8%	3,228	5.2%	5,111	8.2%	2,216	3.5%	4,282	6.9%	3,196	5.1%
Shrubs and grass	15,133	24.2%	19,160	30.7%	17,802	28.5%	19,875	31.8%	18,553	29.7%	18,669	29.9%
Tea	1,096	1.8%	1,139	1.8%	1,420	2.3%	1,289	2.1%	987	1.6%	993	1.6%
Agriculture	7,334	11.7%	4,978	8.0%	5,123	8.2%	5,294	8.5%	4,808	7.7%	5,011	8.0%
Water	384	0.6%	454	0.7%	400	0.6%	449	0.7%	417	0.7%	464	0.7%
Urban/Infrastructure	2,129	3.4%	2,488	4.0%	2,411	3.9%	2,440	3.9%	2,540	4.1%	2,496	4.0%
Bare Land	2,345	3.8%	704	1.1%	2,565	4.1%	747	1.2%	2,455	3.9%	629	1.0%
Not classified	0	0.0%	0	0.0%	3	0.0%	38	0.1%	0	0.0%	0	0.0%
Total	**62,500**	**100.0%**	**62,500**	**100.0%**	**62,500**	**100.0%**	**62,500**	**100.0%**	**62,500**	**100.0%**	**62,500**	**100.0%**

Class	Slope		Slope + AD		Slope		Slope + AD		Slope		Slope + AD	
Topographic corr.	C-correction				Minnaert				Rotation			
Area	ha	%	ha	%	ha	%	ha	%	ha	%	ha	%
Broadleaved Forest	15,864	25.4%	13,784	22.1%	14,721	23.6%	14,719	23.6%	15,712	25.1%	16,878	27.0%
Conifer Forest	11,921	19.1%	13,813	22.1%	12,999	20.8%	15,547	24.9%	12,205	19.5%	13,726	22.0%
Bamboo Forest	3,377	5.4%	3,253	5.2%	5,106	8.2%	2,210	3.5%	4,027	6.4%	2,468	3.9%
Shrubs and grass	19,989	32.0%	21,982	35.2%	17,677	28.3%	19,777	31.6%	19,523	31.2%	19,968	31.9%
Tea	1,282	2.1%	1,113	1.8%	1,407	2.3%	1,261	2.0%	1,036	1.7%	1,006	1.6%
Agriculture	5,028	8.0%	4,839	7.7%	5,113	8.2%	5,282	8.5%	4,922	7.9%	4,799	7.7%
Water	403	0.6%	445	0.7%	400	0.6%	453	0.7%	421	0.7%	441	0.7%
Urban/Infrastructure	2,387	3.8%	2,482	4.0%	2,414	3.9%	2,458	3.9%	2,296	3.7%	2,423	3.9%
Bare Land	2,250	3.6%	790	1.3%	2,661	4.3%	755	1.2%	2,358	3.8%	755	1.2%
Not classified	0	0.0%	0	0.0%	3	0.0%	38	0.1%	0	0.0%	36	0.1%
Total	**62,500**	**100.0%**	**62,500**	**100.0%**	**62,500**	**100.0%**	**62,500**	**100.0%**	**62,500**	**100.0%**	**62,500**	**100.0%**

Class	Illumination		Illumination + AD		Illumination		Illumination + AD		Illumination		Illumination + AD	
Topographic corr.	C-correction				Minnaert				Rotation			
Area	ha	%	ha	%	ha	%	ha	%	ha	%	ha	%
Broadleaved Forest	20,974	33.6%	16,489	26.4%	14,906	23.8%	14,888	23.8%	17,239	27.6%	16,135	25.8%
Conifer Forest	9,065	14.5%	12,469	20.0%	12,798	20.5%	15,657	25.1%	11,206	17.9%	12,753	20.4%
Bamboo Forest	2,519	4.0%	4,617	7.4%	5,112	8.2%	2,143	3.4%	3,742	6.0%	4,006	6.4%
Shrubs and grass	18,207	29.1%	19,215	30.7%	17,602	28.2%	19,641	31.4%	18,787	30.1%	19,913	31.9%
Tea	1,324	2.1%	1,255	2.0%	1,407	2.3%	1,232	2.0%	1,110	1.8%	1,243	2.0%
Agriculture	4,643	7.4%	4,910	7.9%	5,127	8.2%	5,234	8.4%	5,025	8.0%	4,856	7.8%
Water	378	0.6%	441	0.7%	400	0.6%	444	0.7%	433	0.7%	453	0.7%
Urban/Infrastructure	2,669	4.3%	2,526	4.0%	2,405	3.8%	2,449	3.9%	2,433	3.9%	2,469	4.0%
Bare Land	2,721	4.4%	542	0.9%	2,739	4.4%	773	1.2%	2,525	4.0%	637	1.0%
Not classified	0	0.0%	36	0.1%	3	0.0%	38	0.1%	0	0.0%	36	0.1%
Total	**62,500**	**100.0%**	**62,500**	**100.0%**	**62,500**	**100.0%**	**62,500**	**100.0%**	**62,500**	**100.0%**	**62,500**	**100.0%**

9.2 Accuracy assessment

Class	Original		Original + AD	
Topographic corr.	Not corrected			
Overall accuracy	89.10%		91.4	
	PA	UA	PA	UA
Broadleaved Forest	66.3	77.2	67.2	81.4
Conifer Forest	84.6	86.5	87.6	86.9
Bamboo Forest	96.7	91.6	99.2	97.2
Shrubs and grass	83.4	67.6	91.2	68.8
Tea	95.9	94.5	97.4	97.4
Agriculture	92.4	97.5	93.1	97.5
Water	96.2	100	98.2	100
Urban/Infrastructure	82.6	23.3	84.7	34.8
Bare Land	100	87.8	100	97.2

Class	No separation		No separation + AD		No separation		No separation + AD		No separation		No separation + AD	
Topographic corr.	C-correction				Minnaert				Rotation			
Overall accuracy	91.90%		92.1		89.70%		91.1		91.70%		91.9	
	PA	UA	PA	UA	PA	UA	PA	UA	PA	UA	PA	UA
Broadleaved Forest	75.4	87.3	68.7	88.1	68.4	75	64	80.7	73.9	85.6	68.2	83.2
Conifer Forest	89.3	92.7	90.6	91.1	84	89	88.2	89.2	88.7	92.8	87.7	88.5
Bamboo Forest	97.9	96.9	97.5	96.4	98.5	95.5	99.3	96	98.3	95.5	99.3	96.6
Shrubs and grass	91.8	68.1	94.3	65.4	86.7	67	90.7	62.7	91.5	66.1	95.5	68.1
Tea	96.4	86.8	96.4	83.1	95.9	93.6	96.9	96	96.4	94.5	97.9	98.9
Agriculture	91.7	95.6	91.9	98.2	91.5	96.6	92.2	98.2	92.2	96.4	92.2	98.2
Water	96.4	100	98.5	100	96.2	100	98.2	100	96.5	100	98.4	100
Urban/Infrastr.	84.7	23.4	84.7	35.1	82.6	22.7	86.9	34	84.7	24.8	86.9	35.7
Barre Land	100	92.3	100	97.2	100	81.8	100	100	100	92.3	100	100

Class	NDVI		NDVI + AD		NDVI		NDVI + AD		NDVI		NDVI + AD	
Topographic corr.	C-correction				Minnaert				Rotation			
Overall accuracy	88.70%		92.2		88.80%		89.2		91.40%		92.3	
	PA	UA	PA	UA	PA	UA	PA	UA	PA	UA	PA	UA
Broadleaved Forest	68.2	81.7	70.1	87.3	66.4	75.1	59.6	76.2	71	85.1	70.6	86.4
Conifer Forest	87.4	89.4	90	89.3	83.7	87	84.9	82.5	88.3	92.8	89.4	89.5
Bamboo Forest	97.5	92	97.6	95.4	96.3	93.3	95.3	96.1	98.1	94.4	98.5	95.6
Shrubs and grass	88.7	80	92.1	72.5	82.3	63.6	90.7	61.8	88.7	64	92.6	70.3
Tea	90.4	86.1	95.9	84.1	95.9	93.6	97.4	99.4	96.4	95	95.4	94.05
Agriculture	87.6	88.2	91.2	98.2	92.4	97.3	92.6	97.8	91	96.3	91.7	97.7
Water	93	100	98.7	100	96.2	100	98.3	100	97.6	100	98.8	100
Urban/Infrastr.	78.2	16.6	89.1	34.1	80.4	22.4	86.9	35.3	89.1	26.7	86.9	34.7
Bare Land	100	35.6	100	100	100	83.7	100	100	100	83.7	100	100

Class	Slope		Slope + AD		Slope		Slope + AD		Slope		Slope + AD	
Topographic correctio	C-correction				Minnaert				Rotation			
Overall accuracy	91.70%		92.40%		88.90%		89.5		91.70%		91.8	
	PA	UA	PA	UA	PA	UA	PA	UA	PA	UA	PA	UA
Broadleaved Forest	75	87	70.7	88.5	67.1	75.5	60.2	77.3	73.5	85.3	67.9	83.2
Conifer Forest	88.6	92.5	90.4	90.9	84	87.1	85.5	83	88.7	92.5	87.8	88
Bamboo Forest	98.1	96.3	97.6	96.5	96.2	93.4	95.4	96.2	98.2	95.6	99.2	96.7
Shrubs and grass	91.5	67.2	94.9	67.8	82	63.8	90.7	61.9	91.8	66	95.2	68.6
Tea	96.4	87.6	95.9	83.4	95.9	94	97.9	100	96.4	95	98.4	98.4
Agriculture	91.7	95.4	91.9	98.2	92.4	97.3	92.6	97.8	92.2	96.4	92.2	98.5
Water	96.2	100	98.5	100	96.2	100	98.2	100	96.5	100	98.3	100
Urban/Infrastr.	84.7	23.4	84.7	35.1	80.4	22.4	86.9	35	84.7	24.8	86.9	35
Bare Land	100	92.3	100	97.2	100	83.7	100	100	100	92.3	100	100

Class	Illumination		Illumination + AD		Illumination		Illumination + AD		Illumination		Illumination + AD	
Topographic corr.	C-correction				Minnaert				Rotation			
Overall accuracy	89.70%		92.4		89.20%		90.6		91.04%		92.4	
	PA	UA	PA	UA	PA	UA	PA	UA	PA	UA	PA	UA
Broadleaved Forest	66.5	79.7	70.2	86.1	68.3	75.8	65	78.5	71.9	80.7	67.9	85
Conifer Forest	87.9	95.8	89.5	91.3	84.1	88.1	84.8	86.5	86.5	91	88.7	90.5
Bamboo Forest	94.2	95.9	99.5	95.7	96.5	92.7	98.7	96.6	99.1	95.4	99.5	95.4
Shrubs and grass	81.7	48.9	94.1	66	81.7	65.2	92.4	64.3	86.2	65.4	93.2	64
Tea	96.9	81	96.9	97.6	96.4	95.5	99.4	99.4	95.4	94	97.4	98.9
Agriculture	100	97.7	92.2	98.5	92.4	97.3	92.6	98.2	91.9	97.3	92.2	98.2
Water	95.9	100	98.5	100	96.2	100	98.2	100	96.9	100	98.6	100
Urban/Infrastr.	86.9	28.5	84.7	35	84.7	23	86.9	35	86.9	26.8	84.7	37.1
Bare Land	100	73.4	100	97	100	85.7	100	100	100	92.3	100	97.2

9.3 Error matrix

9.3.1 Class: original images

Class: Original

ID	1	2	3	4	5	6	7	8	9	Total
1	594	127	2	46	0	0	0	0	0	769
2	155	1245	34	5	0	0	0	0	0	1439
3	34	64	1120	4	0	0	0	0	0	1222
4	109	32	0	297	1	0	0	0	0	439
5	3	2	2	4	191	0	0	0	0	202
6	0	0	0	0	7	403	0	3	0	413
7	0	0	0	0	0	0	2355	0	0	2355
8	0	0	0	0	0	33	92	38	0	163
9	0	0	0	0	0	0	0	5	36	41
Total	895	1470	1158	356	199	436	2447	46	36	7043

Class: Original + Ancillary data

ID	1	2	3	4	5	6	7	8	9	Total
1	602	120	1	16	0	0	0	0	0	739
2	181	1288	8	4	0	0	0	0	0	1481
3	6	20	1149	6	1	0	0	0	0	1182
4	106	41	0	325	0	0	0	0	0	472
5	0	0	0	5	194	0	0	0	0	199
6	0	0	0	0	4	406	0	6	0	416
7	0	0	0	0	0	0	2405	0	0	2405
8	0	1	0	0	0	30	42	39	0	112
9	0	0	0	0	0	0	0	1	36	37
Total	895	1470	1158	356	199	436	2447	46	36	7043

ID	Land cover type
1	Broadleaved Forest
2	Conifer Forest
3	Bamboo Forest
4	Shrubs and grass
5	Tea
6	Agriculture
7	Water
8	Urban/Infrastr.
9	Barre Land

9.3.2 Class: no separation

Class: No separation
Topographic normalization: c-correction

ID	0	1	2	3	4	5	6	7	8	9	Total
0	0	0	0	0	0	0	0	0	0	0	0
1	0	675	85	7	6	0	0	0	0	0	773
2	0	96	1314	7	0	0	0	0	0	0	1417
3	0	10	20	1134	6	0	0	0	0	0	1170
4	0	103	50	0	327	0	0	0	0	0	480
5	0	5	1	10	13	192	0	0	0	0	221
6	0	3	0	0	4	7	400	0	4	0	418
7	0	0	0	0	0	0	0	2359	0	0	2359
8	0	3	0	0	0	0	36	88	39	0	166
9	0	0	0	0	0	0	0	0	3	36	39
Total	0	895	1470	1158	356	199	436	2447	46	36	7043

Class: No separation
Topographic normalization: minnaert

ID	0	1	2	3	4	5	6	7	8	9	Total
0	0	0	0	0	0	0	0	0	0	0	0
1	0	613	174	9	21	0	0	0	0	0	817
2	0	146	1236	6	0	0	0	0	0	0	1388
3	0	16	26	1141	10	1	0	0	0	0	1194
4	0	119	33	0	309	0	0	0	0	0	461
5	0	1	1	2	9	191	0	0	0	0	204
6	0	0	0	0	4	7	399	0	3	0	413
7	0	0	0	0	0	0	0	2355	0	0	2355
8	0	0	0	0	0	0	37	92	38	0	167
9	0	0	0	0	3	0	0	0	5	36	44
Total	0	895	1470	1158	356	199	436	2447	46	36	7043

Class: No separation
Topographic normalization: rotation

ID	0	1	2	3	4	5	6	7	8	9	Total
0	0	0	0	0	0	0	0	0	0	0	0
1	0	662	95	11	5	0	0	0	0	0	773
2	0	93	1305	8	0	0	0	0	0	0	1406
3	0	16	24	1139	13	0	0	0	0	0	1192
4	0	122	45	0	326	0	0	0	0	0	493
5	0	2	1	0	8	192	0	0	0	0	203
6	0	0	0	0	4	7	402	0	4	0	417
7	0	0	0	0	0	0	0	2363	0	0	2363
8	0	0	0	0	0	0	34	84	39	0	157
9	0	0	0	0	0	0	0	0	3	36	39
Total	0	895	1470	1158	356	199	436	2447	46	36	7043

Class: No separation + ancillary data
Topographic normalization: c-correction

ID	0	1	2	3	4	5	6	7	8	9	Total
0	0	0	0	0	0	0	0	0	0	0	0
1	0	615	79	3	1	0	0	0	0	0	698
2	0	125	1332	5	0	0	0	0	0	0	1462
3	0	16	14	1130	7	5	0	0	0	0	1172
4	0	132	44	0	336	0	0	0	1	0	513
5	0	7	0	20	12	192	0	0	0	0	231
6	0	0	0	0	0	2	401	0	5	0	408
7	0	0	0	0	0	0	0	2411	0	0	2411
8	0	0	1	0	0	0	35	36	39	0	111
9	0	0	0	0	0	0	0	0	1	36	37
Total	0	895	1470	1158	356	199	436	2447	46	36	7043

Class: No separation + ancillary data
Topographic normalization: minnaert

ID	0	1	2	3	4	5	6	7	8	9	Total
0	0	0	0	0	0	0	0	0	0	0	0
1	0	573	124	4	9	0	0	0	0	0	710
2	0	152	1297	4	0	0	0	0	0	0	1453
3	0	16	10	1150	17	4	0	0	0	0	1197
4	0	153	38	0	323	0	0	0	1	0	515
5	0	1	0	0	7	193	0	0	0	0	201
6	0	0	0	0	0	2	402	0	5	0	409
7	0	0	0	0	0	0	0	2405	0	0	2405
8	0	0	1	0	0	0	34	42	40	0	117
9	0	0	0	0	0	0	0	0	0	36	36
Total	0	895	1470	1158	356	199	436	2447	46	36	7043

Class: No separation + ancillary data
Topographic normalization: rotation

ID	0	1	2	3	4	5	6	7	8	9	Total
0	0	0	0	0	0	0	0	0	0	0	0
1	0	611	120	1	2	0	0	0	0	0	734
2	0	159	1290	7	1	0	0	0	0	0	1457
3	0	3	24	1150	10	3	0	0	0	0	1190
4	0	122	36	0	340	0	0	0	1	0	499
5	0	0	0	0	2	195	0	0	0	0	197
6	0	0	0	0	1	1	402	0	5	0	409
7	0	0	0	0	0	0	0	2409	0	0	2409
8	0	0	0	0	0	0	34	38	40	0	112
9	0	0	0	0	0	0	0	0	0	36	36
Total	0	895	1470	1158	356	199	436	2447	46	36	7043

9.3.3 Class: NDVI

Class: NDVI
Topographic normalization: c-correction

ID	1	2	3	4	5	6	7	8	9	Total
1	611	111	2	20	3	0	0	0	0	747
2	132	1285	12	0	8	0	0	0	0	1437
3	58	35	1130	5	0	0	0	0	0	1228
4	51	27	0	316	1	0	0	0	0	395
5	10	0	14	4	180	1	0	0	0	209
6	26	5	0	8	7	382	0	5	0	433
7	0	0	0	0	0	0	2277	0	0	2277
8	4	6	0	0	0	0	170	36	0	216
9	3	1	0	3	0	53	0	5	36	101
Total	895	1470	1158	356	199	436	2447	46	36	7043

Class: NDVI
Topographic normalization: minnaert

ID	0	1	2	3	4	5	6	7	8	9	Total
0	0	0	0	0	0	0	0	0	0	0	0
1	0	595	146	1	49	1	0	0	0	0	792
2	0	139	1231	39	5	0	0	0	0	0	1414
3	0	23	55	1116	2	0	0	0	0	0	1196
4	0	131	36	0	293	0	0	0	0	0	460
5	0	4	2	2	5	191	0	0	0	0	204
6	0	0	0	0	0	7	403	0	4	0	414
7	0	0	0	0	0	0	0	2355	0	0	2355
8	0	3	0	0	0	0	33	92	37	0	165
9	0	0	0	0	2	0	0	0	5	36	43
Total	0	895	1470	1158	356	199	436	2447	46	36	7043

Class: NDVI
Topographic normalization: rotation

ID	1	2	3	4	5	6	7	8	9	Total
1	636	81	12	18	0	0	0	0	0	747
2	91	1299	9	0	0	0	0	0	0	1399
3	22	33	1137	12	0	0	0	0	0	1204
4	132	45	0	316	0	0	0	0	0	493
5	3	0	0	6	192	0	0	1	0	202
6	0	0	0	4	7	397	0	4	0	412
7	0	0	0	0	0	0	2390	0	0	2390
8	8	9	0	0	0	38	57	41	0	153
9	3	3	0	0	0	1	0	0	36	43
Total	895	1470	1158	356	199	436	2447	46	36	7043

Class: NDVI + ancillary data
Topographic normalization: c-correction

ID	1	2	3	4	5	6	7	8	9	Total
1	628	78	6	7	0	0	0	0	0	719
2	151	1324	7	0	0	0	0	0	0	1482
3	22	15	1131	11	6	0	0	0	0	1185
4	82	42	0	328	0	0	0	0	0	452
5	12	0	14	10	191	0	0	0	0	227
6	0	0	0	0	2	398	0	5	0	405
7	0	0	0	0	0	0	2417	0	0	2417
8	0	11	0	0	0	38	30	41	0	120
9	0	0	0	0	0	0	0	0	36	36
Total	895	1470	1158	356	199	436	2447	46	36	7043

Class: NDVI + ancillary data
Topographic normalization: minnaert

ID	0	1	2	3	4	5	6	7	8	9	Total
0	0	0	0	0	0	0	0	0	0	0	0
1	0	534	149	0	17	0	0	0	0	0	700
2	0	199	1247	53	11	0	0	0	0	0	1510
3	0	8	29	1104	5	2	0	0	0	0	1148
4	0	154	45	0	323	0	0	0	0	0	522
5	0	0	0	1	0	194	0	0	0	0	195
6	0	0	0	0	0	3	404	0	6	0	413
7	0	0	0	0	0	0	0	2406	0	0	2406
8	0	0	0	0	0	0	32	41	40	0	113
9	0	0	0	0	0	0	0	0	0	36	36
Total	0	895	1470	1158	356	199	436	2447	46	36	7043

Class: NDVI + ancillary data
Topographic normalization: rotation

ID	1	2	3	4	5	6	7	8	9	Total
1	632	81	11	7	0	0	0	0	0	731
2	149	1315	5	0	0	0	0	0	0	1469
3	17	19	1141	10	6	0	0	0	0	1193
4	95	44	0	330	0	0	0	0	0	469
5	2	0	1	9	190	0	0	0	0	202
6	0	0	0	0	3	400	0	6	0	409
7	0	0	0	0	0	0	2419	0	0	2419
8	0	11	0	0	0	36	28	40	0	115
9	0	0	0	0	0	0	0	0	36	36
Total	895	1470	1158	356	199	436	2447	46	36	7043

9.3.4 Class: slope

Class: Slope
Topographic normalization: c-correction

ID	1	2	3	4	5	6	7	8	9	Total
1	672	88	5	7	0	0	0	0	0	772
2	98	1303	7	0	0	0	0	0	0	1408
3	8	26	1136	9	0	0	0	0	0	1179
4	107	52	0	326	0	0	0	0	0	485
5	6	1	10	10	192	0	0	0	0	219
6	4	0	0	4	7	400	0	4	0	419
7	0	0	0	0	0	0	2356	0	0	2356
8	0	0	0	0	0	36	91	39	0	166
9	0	0	0	0	0	0	0	3	36	39
Total	895	1470	1158	356	199	436	2447	46	36	7043

Class: Slope
Topographic normalization: minnaert

ID	0	1	2	3	4	5	6	7	8	9	Total
0	0	0	0	0	0	0	0	0	0	0	0
1	0	601	143	1	50	1	0	0	0	0	796
2	0	137	1235	40	5	0	0	0	0	0	1417
3	0	21	55	1115	2	0	0	0	0	0	1193
4	0	129	36	0	292	0	0	0	0	0	457
5	0	4	1	2	5	191	0	0	0	0	203
6	0	0	0	0	0	7	403	0	4	0	414
7	0	0	0	0	0	0	0	2355	0	0	2355
8	0	3	0	0	0	0	33	92	37	0	165
9	0	0	0	0	2	0	0	0	5	36	43
Total	0	895	1470	1158	356	199	436	2447	46	36	7043

Class: Slope
Topographic normalization: rotation

ID	1	2	3	4	5	6	7	8	9	Total
1	658	95	12	6	0	0	0	0	0	771
2	97	1304	8	0	0	0	0	0	0	1409
3	15	25	1138	12	0	0	0	0	0	1190
4	123	45	0	327	0	0	0	0	0	495
5	2	1	0	7	192	0	0	0	0	202
6	0	0	0	4	7	402	0	4	0	417
7	0	0	0	0	0	0	2363	0	0	2363
8	0	0	0	0	0	34	84	39	0	157
9	0	0	0	0	0	0	0	3	36	39
Total	895	1470	1158	356	199	436	2447	46	36	7043

Class: Slope + ancillary data
Topographic normalization: c-correction

ID	1	2	3	4	5	6	7	8	9	Total
1	633	80	2	0	0	0	0	0	0	715
2	127	1330	5	0	0	0	0	0	0	1462
3	13	15	1131	7	6	0	0	0	0	1172
4	115	44	0	338	0	0	0	1	0	498
5	7	0	20	11	191	0	0	0	0	229
6	0	0	0	0	2	401	0	5	0	408
7	0	0	0	0	0	0	2411	0	0	2411
8	0	1	0	0	0	35	36	39	0	111
9	0	0	0	0	0	0	0	1	36	37
Total	895	1470	1158	356	199	436	2447	46	36	7043

Class: Slope + ancillary data
Topographic normalization: minnaert

ID	0	1	2	3	4	5	6	7	8	9	Total
0	0	0	0	0	0	0	0	0	0	0	0
1	0	539	141	0	17	0	0	0	0	0	697
2	0	193	1257	53	11	0	0	0	0	0	1514
3	0	8	29	1105	5	1	0	0	0	0	1148
4	0	155	43	0	323	0	0	0	0	0	521
5	0	0	0	0	0	195	0	0	0	0	195
6	0	0	0	0	0	3	404	0	6	0	413
7	0	0	0	0	0	0	0	2405	0	0	2405
8	0	0	0	0	0	0	32	42	40	0	114
9	0	0	0	0	0	0	0	0	0	36	36
Total	0	895	1470	1158	356	199	436	2447	46	36	7043

Class: Slope + ancillary data
Topographic normalization: rotation

ID	0	1	2	3	4	5	6	7	8	9	Total
0	0	0	0	0	0	0	0	0	0	0	0
1	0	608	118	1	3	0	0	0	0	0	730
2	0	166	1292	8	1	0	0	0	0	0	1467
3	0	3	24	1149	10	2	0	0	0	0	1188
4	0	118	36	0	339	0	0	0	1	0	494
5	0	0	0	0	3	196	0	0	0	0	199
6	0	0	0	0	0	1	402	0	5	0	408
7	0	0	0	0	0	0	0	2407	0	0	2407
8	0	0	0	0	0	0	34	40	40	0	114
9	0	0	0	0	0	0	0	0	0	36	36
Total	0	895	1470	1158	356	199	436	2447	46	36	7043

9.3.5 Class: Illumination

Class: Illumination
Topographic normalization: c-correction

ID	0	1	2	3	4	5	6	7	8	9	Total
0	0	0	0	0	0	0	0	0	0	0	0
1	0	596	76	29	46	0	0	0	0	0	747
2	0	50	1291	4	0	0	0	0	0	0	1345
3	0	8	38	1091	0	0	0	0	0	0	1137
4	0	238	65	0	291	0	0	0	0	0	594
5	0	0	0	34	11	193	0	0	0	0	238
6	0	0	0	0	0	6	436	0	4	0	446
7	0	0	0	0	0	0	0	2347	0	0	2347
8	0	0	0	0	0	0	0	100	40	0	140
9	0	3	0	0	8	0	0	0	2	36	49
Total	0	895	1470	1158	356	199	436	2447	46	36	7043

Class: Illumination
Topographic normalization: minnaert

ID	0	1	2	3	4	5	6	7	8	9	Total
0	0	0	0	0	0	0	0	0	0	0	0
1	0	612	143	1	51	0	0	0	0	0	807
2	0	124	1237	37	5	0	0	0	0	0	1403
3	0	32	53	1118	3	0	0	0	0	0	1206
4	0	119	36	0	291	0	0	0	0	0	446
5	0	3	1	2	3	192	0	0	0	0	201
6	0	0	0	0	0	7	403	0	4	0	414
7	0	0	0	0	0	0	0	2355	0	0	2355
8	0	5	0	0	0	0	33	92	39	0	169
9	0	0	0	0	3	0	0	0	3	36	42
Total	0	895	1470	1158	356	199	436	2447	46	36	7043

Class: Illumination
Topographic normalization: rotation

ID	0	1	2	3	4	5	6	7	8	9	Total
0	0	0	0	0	0	0	0	0	0	0	0
1	0	644	122	2	30	0	0	0	0	0	798
2	0	117	1273	8	0	0	0	0	0	0	1398
3	0	18	28	1148	7	2	0	0	0	0	1203
4	0	116	46	0	307	0	0	0	0	0	469
5	0	0	1	0	11	190	0	0	0	0	202
6	0	0	0	0	0	7	401	0	4	0	412
7	0	0	0	0	0	0	0	2373	0	0	2373
8	0	0	0	0	0	0	35	74	40	0	149
9	0	0	0	0	1	0	0	0	2	36	39
Total	0	895	1470	1158	356	199	436	2447	46	36	7043

Class: Illumination + ancillary data
Topographic normalization: c-correction

ID	0	1	2	3	4	5	6	7	8	9	Total
0	0	0	0	0	0	0	0	0	0	0	0
1	0	629	98	1	2	0	0	0	0	0	730
2	0	119	1316	4	1	0	0	0	0	0	1440
3	0	10	19	1153	17	5	0	0	0	0	1204
4	0	134	37	0	335	0	0	0	1	0	507
5	0	3	0	0	1	193	0	0	0	0	197
6	0	0	0	0	0	1	402	0	5	0	408
7	0	0	0	0	0	0	0	2411	0	0	2411
8	0	0	0	0	0	0	34	36	39	0	109
9	0	0	0	0	0	0	0	0	1	36	37
Total	0	895	1470	1158	356	199	436	2447	46	36	7043

Class: Illumination + ancillary data
Topographic normalization: minnaert

ID	0	1	2	3	4	5	6	7	8	9	Total
0	0	0	0	0	0	0	0	0	0	0	0
1	0	582	151	0	8	0	0	0	0	0	741
2	0	167	1248	14	13	0	0	0	0	0	1442
3	0	8	27	1144	5	0	0	0	0	0	1184
4	0	138	44	0	329	0	0	0	0	0	511
5	0	0	0	0	1	198	0	0	0	0	199
6	0	0	0	0	0	1	404	0	6	0	411
7	0	0	0	0	0	0	0	2405	0	0	2405
8	0	0	0	0	0	0	32	42	40	0	114
9	0	0	0	0	0	0	0	0	0	36	36
Total	0	895	1470	1158	356	199	436	2447	46	36	7043

Class: Illumination + ancillary data
Topographic normalization: rotation

ID	0	1	2	3	4	5	6	7	8	9	Total
0	0	0	0	0	0	0	0	0	0	0	0
1	0	608	104	2	1	0	0	0	0	0	715
2	0	131	1304	3	2	0	0	0	0	0	1440
3	0	9	22	1153	21	3	0	0	0	0	1208
4	0	145	40	0	332	0	0	0	1	0	518
5	0	2	0	0	0	194	0	0	0	0	196
6	0	0	0	0	0	2	402	0	5	0	409
7	0	0	0	0	0	0	0	2415	0	0	2415
8	0	0	0	0	0	0	34	32	39	0	105
9	0	0	0	0	0	0	0	0	1	36	37
Total	0	895	1470	1158	356	199	436	2447	46	36	7043

9.4 Datasets for land cover classification

The table presents the datasets which were used for the land cover classification and and forest type mapping. It describes which components and bands does it include as well and contains information about the topographic normalization method used for the imagery and which criteria was used for the separation in vegetation classes (class).

All forest maps are presented afterwards in the order as given in the table.

ID	Class	Topographic normalization	Bands
1	Original	Not corrected	Bands 1-5 RE spring; Bands 1-5 RE Autumn
2			Bands 1-5 RE spring; Bands 1-5 RE Autumn; Ancillary data
3		C-correction	Bands 1-5 RE spring; Bands 1-5 RE Autumn
4			Bands 1-5 RE spring; Bands 1-5 RE Autumn; Ancillary data
5		Minnaert	Bands 1-5 RE spring; Bands 1-5 RE Autumn
6			Bands 1-5 RE spring; Bands 1-5 RE Autumn; Ancillary data
7		Rotation	Bands 1-5 RE spring; Bands 1-5 RE Autumn
8			Bands 1-5 RE spring; Bands 1-5 RE Autumn; Ancillary data
9	NDVI	C-correction	Bands 1-5 RE spring; Bands 1-5 RE Autumn
10			Bands 1-5 RE spring; Bands 1-5 RE Autumn; Ancillary data
11		Minnaert	Bands 1-5 RE spring; Bands 1-5 RE Autumn
12			Bands 1-5 RE spring; Bands 1-5 RE Autumn; Ancillary data
13		Rotation	Bands 1-5 RE spring; Bands 1-5 RE Autumn
14			Bands 1-5 RE spring; Bands 1-5 RE Autumn; Ancillary data
15	Slope	C-correction	Bands 1-5 RE spring; Bands 1-5 RE Autumn
16			Bands 1-5 RE spring; Bands 1-5 RE Autumn; Ancillary data
17		Minnaert	Bands 1-5 RE spring; Bands 1-5 RE Autumn
18			Bands 1-5 RE spring; Bands 1-5 RE Autumn; Ancillary data
19		Rotation	Bands 1-5 RE spring; Bands 1-5 RE Autumn
20			Bands 1-5 RE spring; Bands 1-5 RE Autumn; Ancillary data
21	Illumination	C-correction	Bands 1-5 RE spring; Bands 1-5 RE Autumn
22			Bands 1-5 RE spring; Bands 1-5 RE Autumn; Ancillary data
23		Minnaert	Bands 1-5 RE spring; Bands 1-5 RE Autumn
24			Bands 1-5 RE spring; Bands 1-5 RE Autumn; Ancillary data
25		Rotation	Bands 1-5 RE spring; Bands 1-5 RE Autumn
26			Bands 1-5 RE spring; Bands 1-5 RE Autumn; Ancillary data

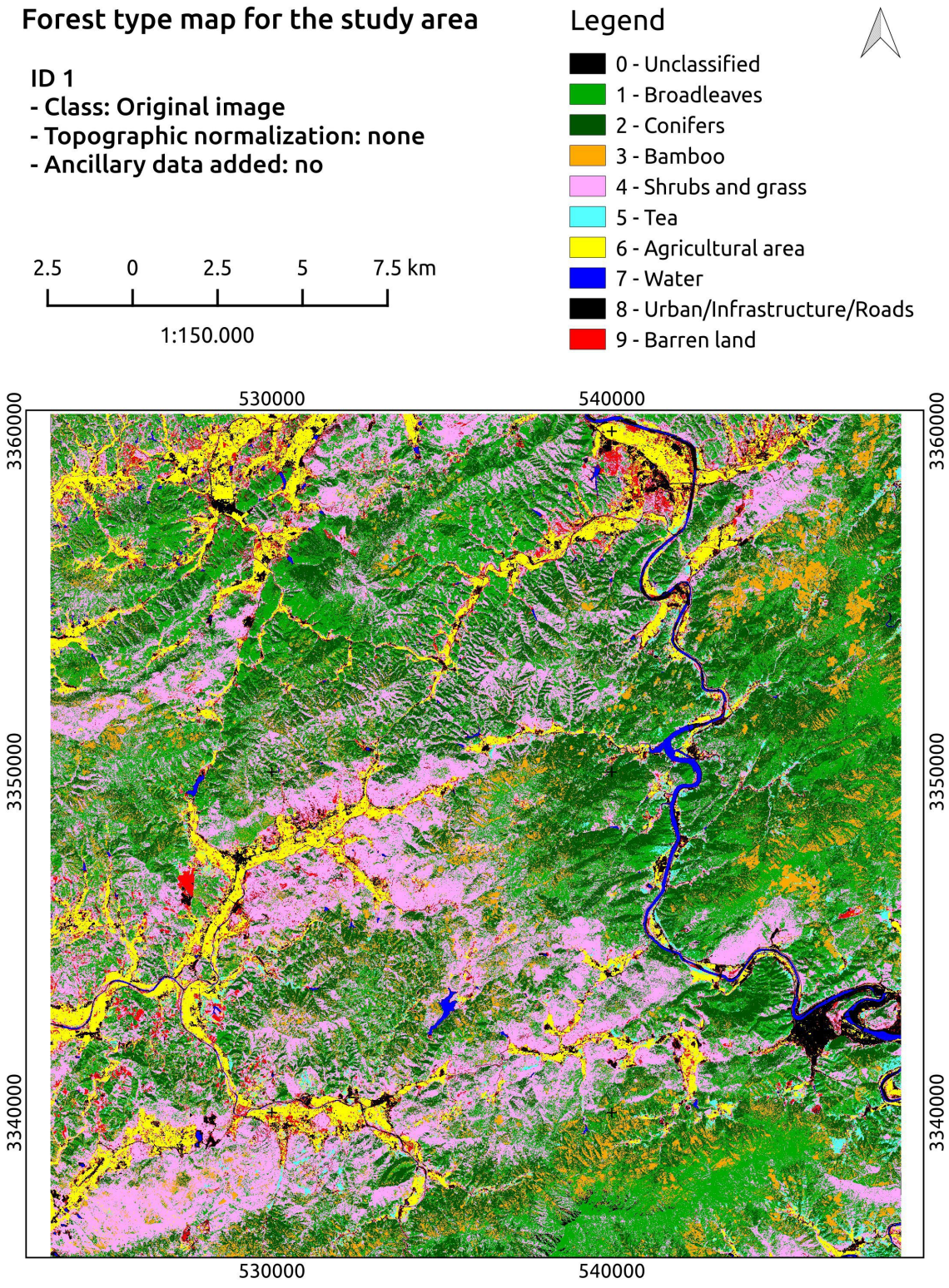
Forest type map for the study area
ID 1
- Class: Original image
- Topographic normalization: none
- Ancillary data added: no
2.5 0 2.5 5 7.5 km
1:150.000
Legend
0 - Unclassified
1 - Broadleaves
2 - Conifers
3 - Bamboo
4 - Shrubs and grass
5 - Tea
6 - Agricultural area
7 - Water
8 - Urban/Infrastructure/Roads
9 - Barren land
530000
540000
3360000
3350000
3340000

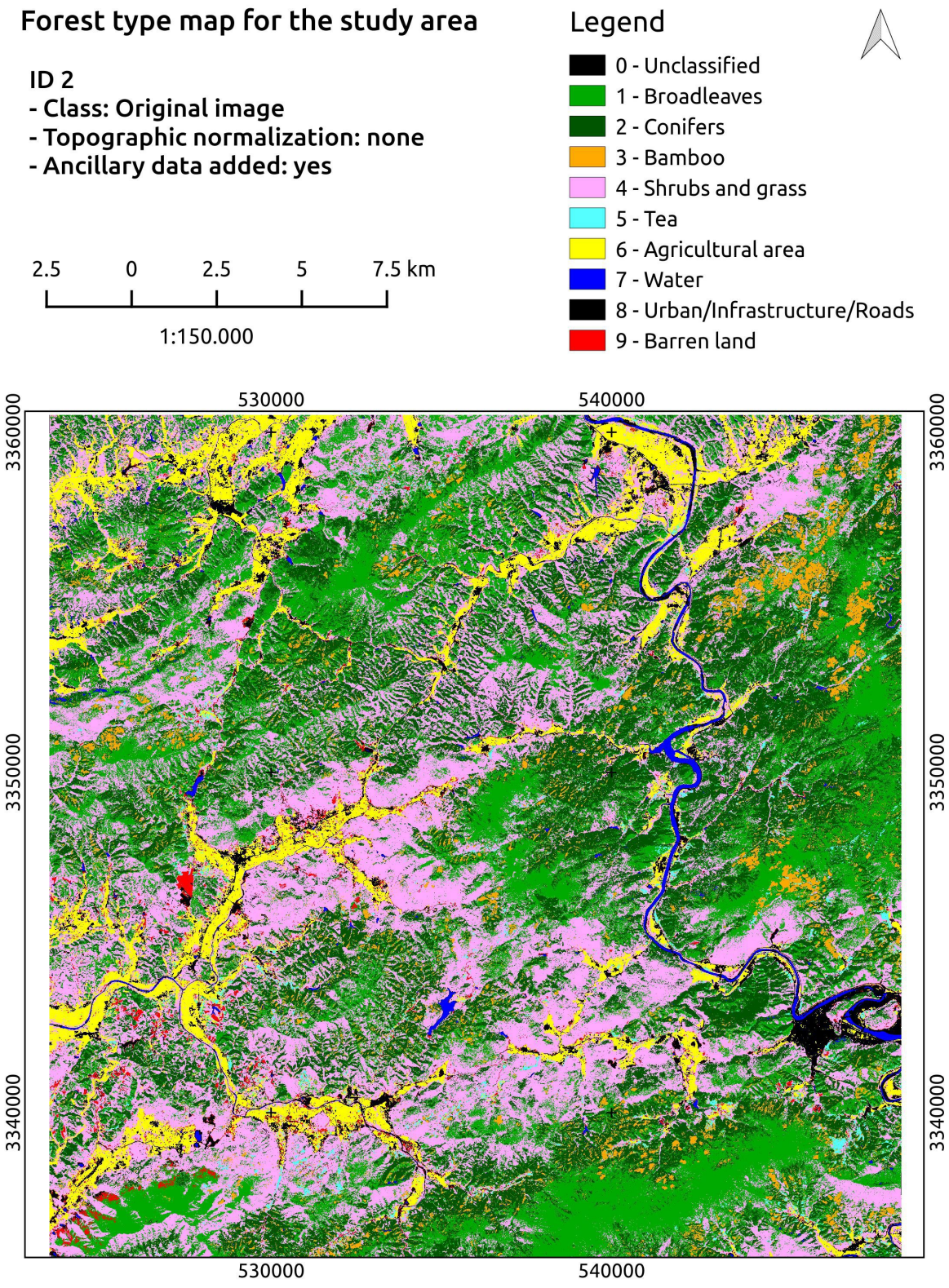
Forest type map for the study area
ID 2
- Class: Original image
- Topographic normalization: none
- Ancillary data added: yes
2.5 0 2.5 5 7.5 km
1:150.000
Legend
0 - Unclassified
1 - Broadleaves
2 - Conifers
3 - Bamboo
4 - Shrubs and grass
5 - Tea
6 - Agricultural area
7 - Water
8 - Urban/Infrastructure/Roads
9 - Barren land
530000
540000
3360000
3350000
3340000

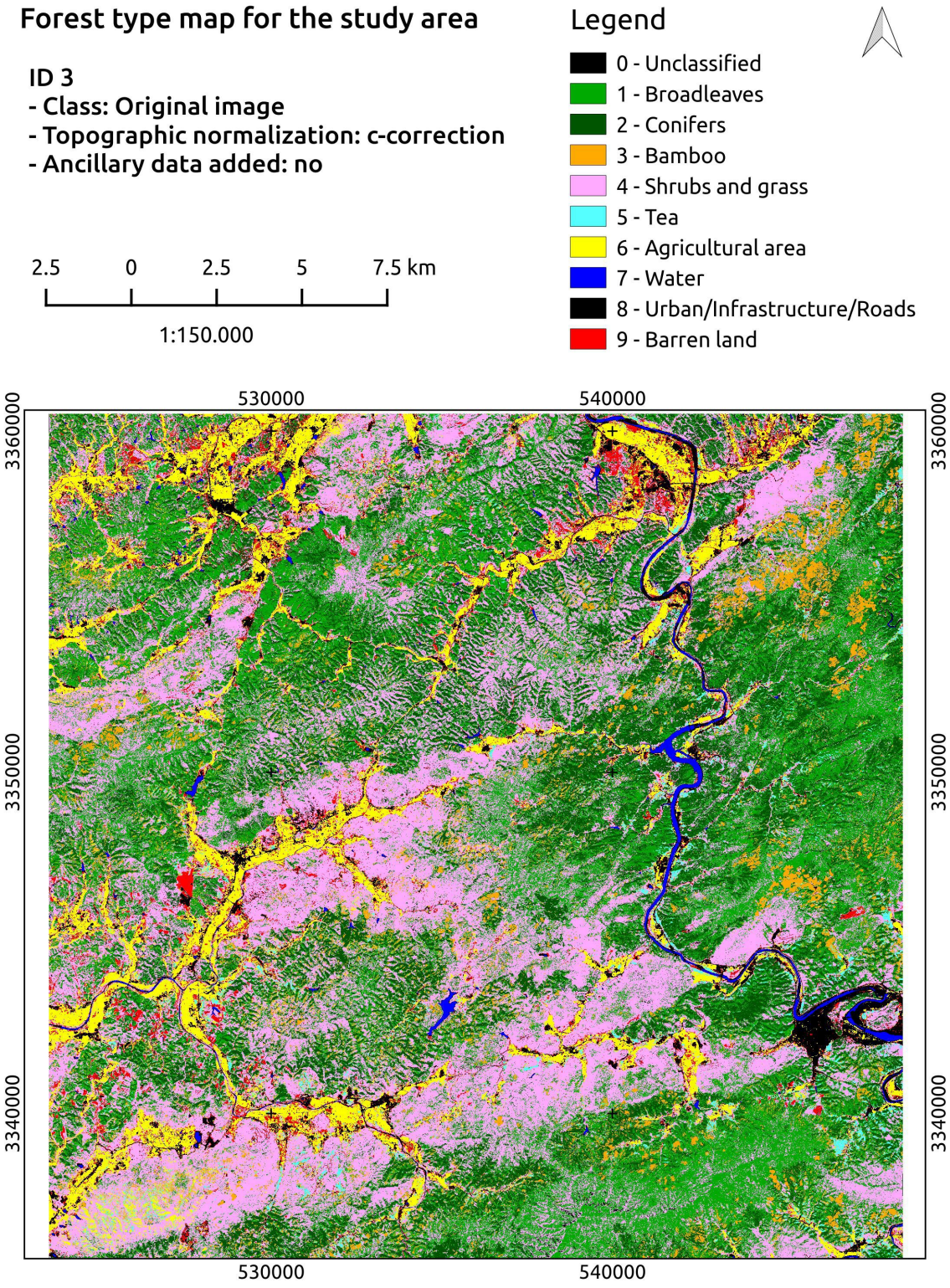
Forest type map for the study area
ID 3
- Class: Original image
- Topographic normalization: c-correction
- Ancillary data added: no
2.5 0 2.5 5 7.5 km
1:150.000
Legend
0 - Unclassified
1 - Broadleaves
2 - Conifers
3 - Bamboo
4 - Shrubs and grass
5 - Tea
6 - Agricultural area
7 - Water
8 - Urban/Infrastructure/Roads
9 - Barren land
530000
540000
3360000
3350000
3340000

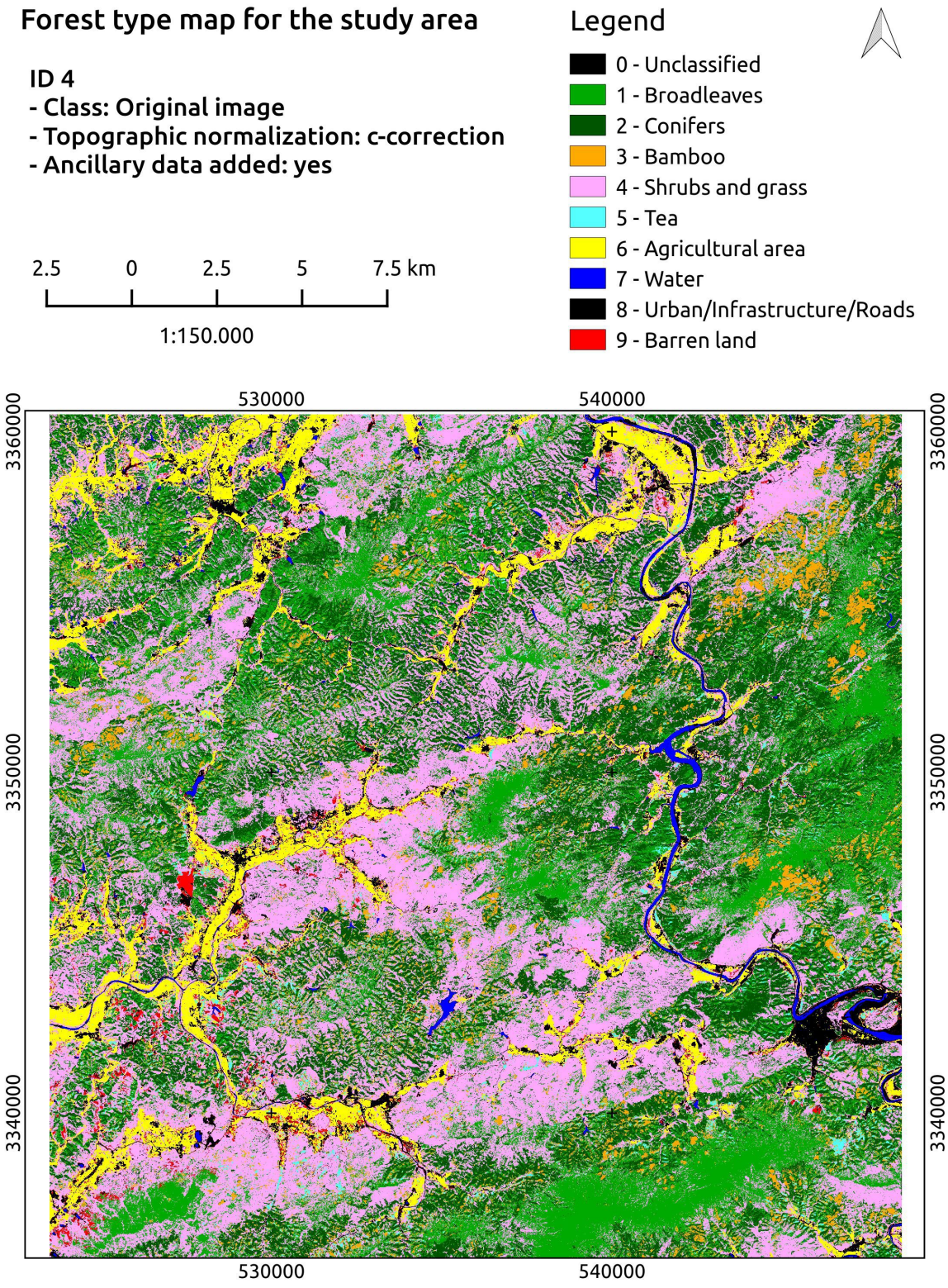
Forest type map for the study area
ID 4
- Class: Original image
- Topographic normalization: c-correction
- Ancillary data added: yes
2.5 0 2.5 5 7.5 km
1:150.000
Legend
0 - Unclassified
1 - Broadleaves
2 - Conifers
3 - Bamboo
4 - Shrubs and grass
5 - Tea
6 - Agricultural area
7 - Water
8 - Urban/Infrastructure/Roads
9 - Barren land
530000
540000
3360000
3350000
3340000

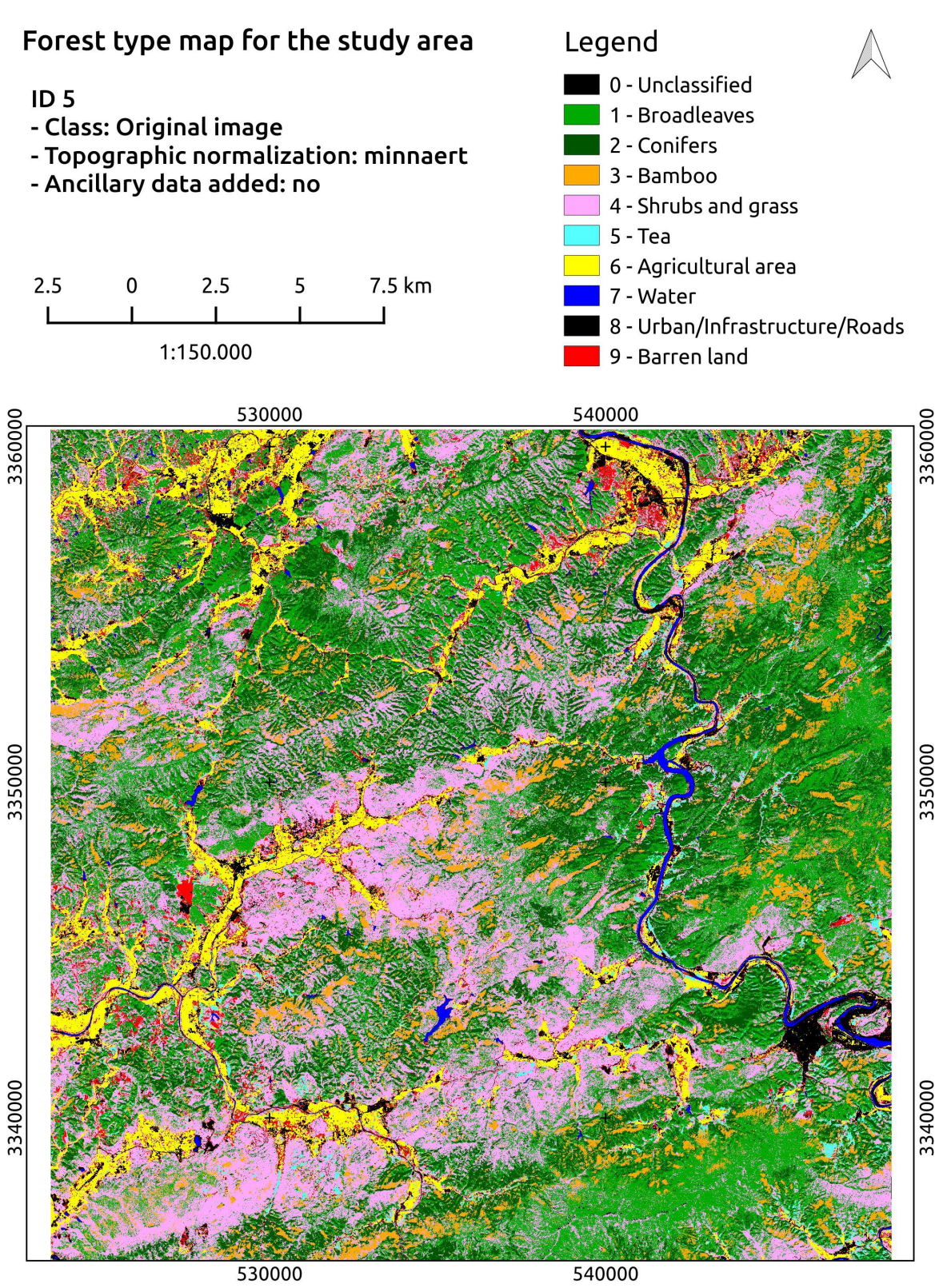
Forest type map for the study area
ID 5
- Class: Original image
- Topographic normalization: minnaert
- Ancillary data added: no
2.5 0 2.5 5 7.5 km
1:150.000
Legend
0 - Unclassified
1 - Broadleaves
2 - Conifers
3 - Bamboo
4 - Shrubs and grass
5 - Tea
6 - Agricultural area
7 - Water
8 - Urban/Infrastructure/Roads
9 - Barren land
530000
540000
3360000
3350000
3340000

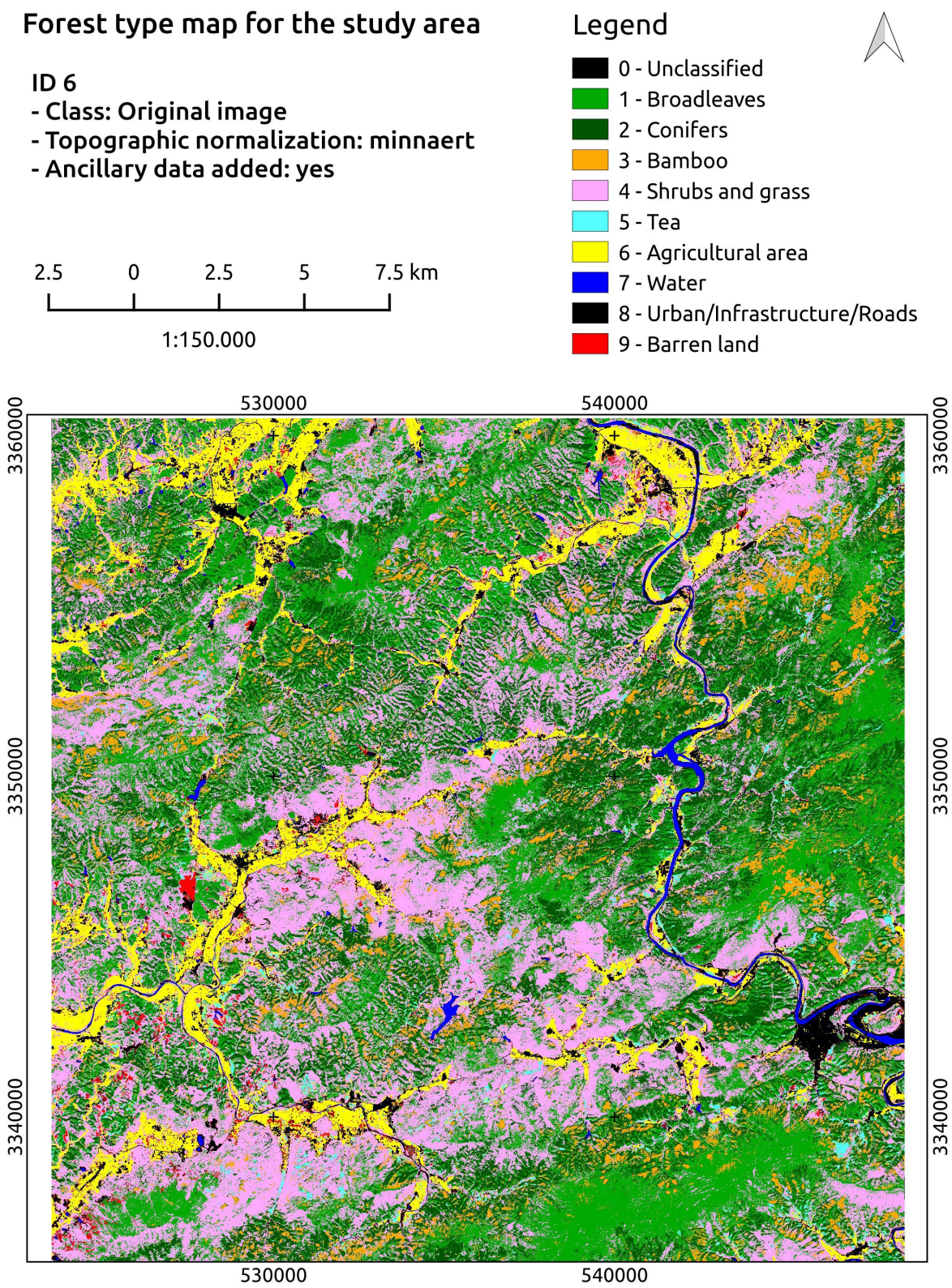
Forest type map for the study area
ID 6
- Class: Original image
- Topographic normalization: minnaert
- Ancillary data added: yes
2.5 0 2.5 5 7.5 km
1:150.000
Legend
0 - Unclassified
1 - Broadleaves
2 - Conifers
3 - Bamboo
4 - Shrubs and grass
5 - Tea
6 - Agricultural area
7 - Water
8 - Urban/Infrastructure/Roads
9 - Barren land
530000
540000
3360000
3350000
3340000

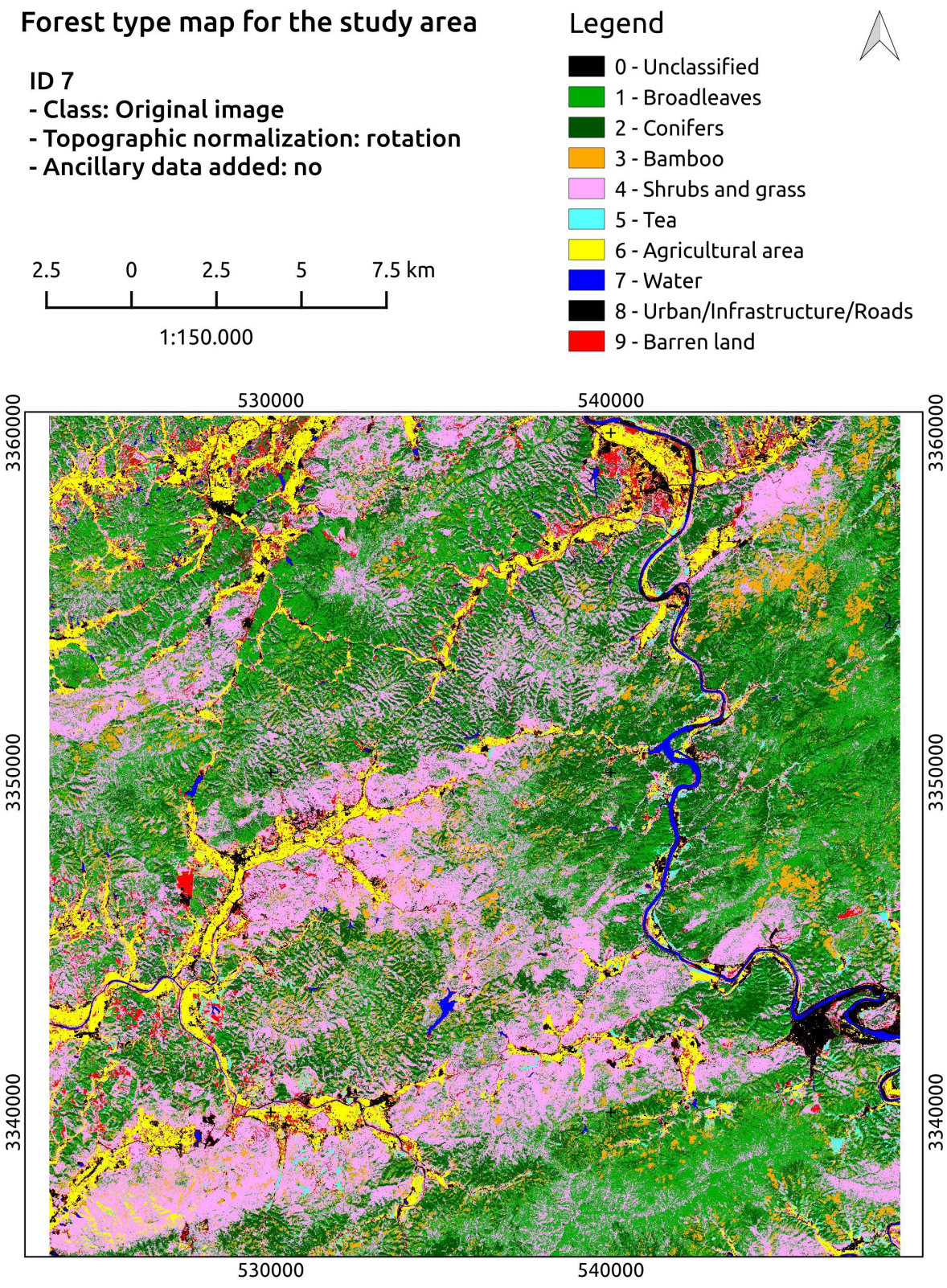
Forest type map for the study area
ID 7
- Class: Original image
- Topographic normalization: rotation
- Ancillary data added: no
2.5 0 2.5 5 7.5 km
1:150.000
Legend
0 - Unclassified
1 - Broadleaves
2 - Conifers
3 - Bamboo
4 - Shrubs and grass
5 - Tea
6 - Agricultural area
7 - Water
8 - Urban/Infrastructure/Roads
9 - Barren land
530000
540000
3360000
3350000
3340000

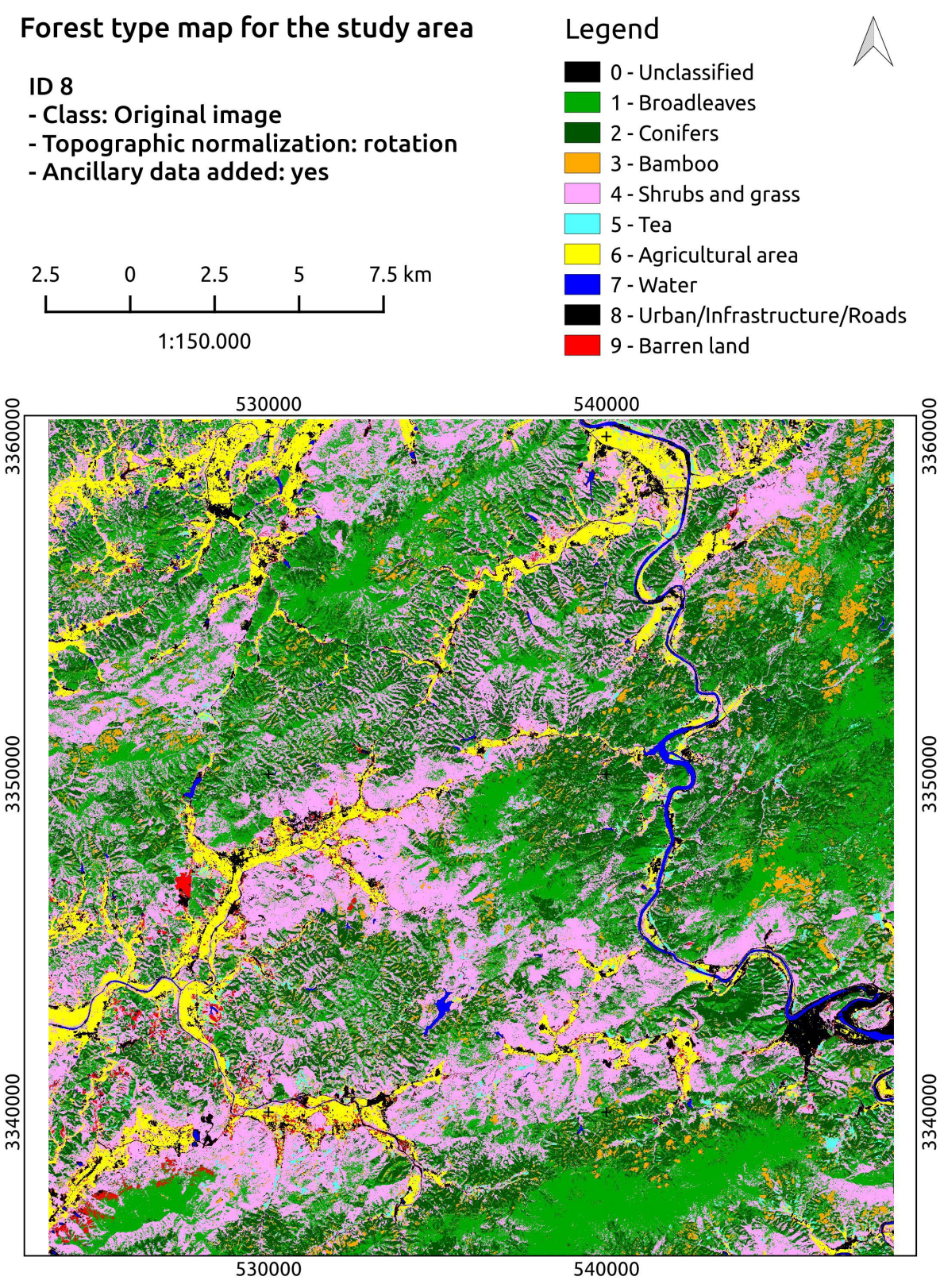
Forest type map for the study area
ID 8
- Class: Original image
- Topographic normalization: rotation
- Ancillary data added: yes
2.5 0 2.5 5 7.5 km
1:150.000
Legend
0 - Unclassified
1 - Broadleaves
2 - Conifers
3 - Bamboo
4 - Shrubs and grass
5 - Tea
6 - Agricultural area
7 - Water
8 - Urban/Infrastructure/Roads
9 - Barren land
530000
540000
3360000
3350000
3340000

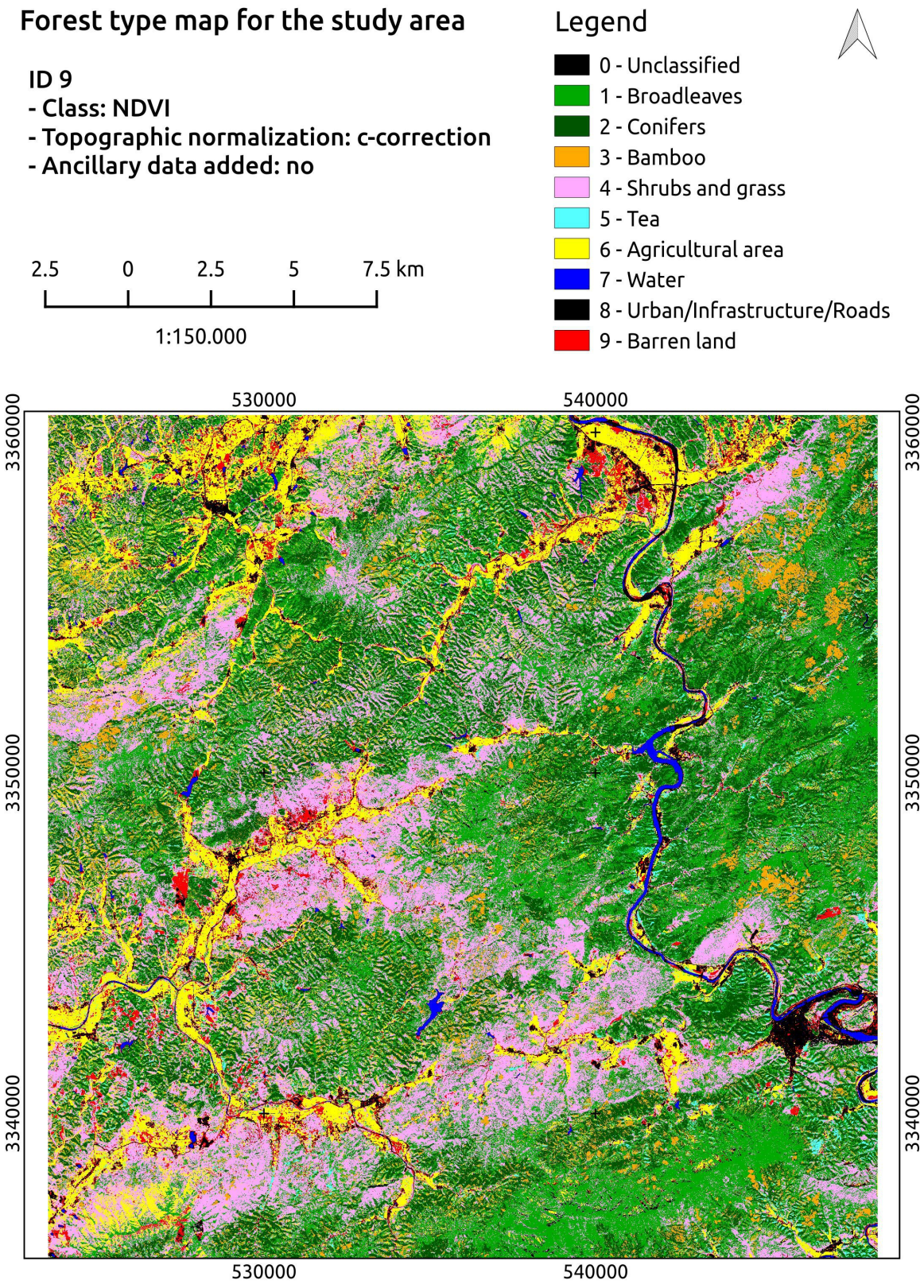
Forest type map for the study area
ID 9
- Class: NDVI
- Topographic normalization: c-correction
- Ancillary data added: no
2.5 0 2.5 5 7.5 km
1:150.000
Legend
0 - Unclassified
1 - Broadleaves
2 - Conifers
3 - Bamboo
4 - Shrubs and grass
5 - Tea
6 - Agricultural area
7 - Water
8 - Urban/Infrastructure/Roads
9 - Barren land
530000
540000
3360000
3350000
3340000

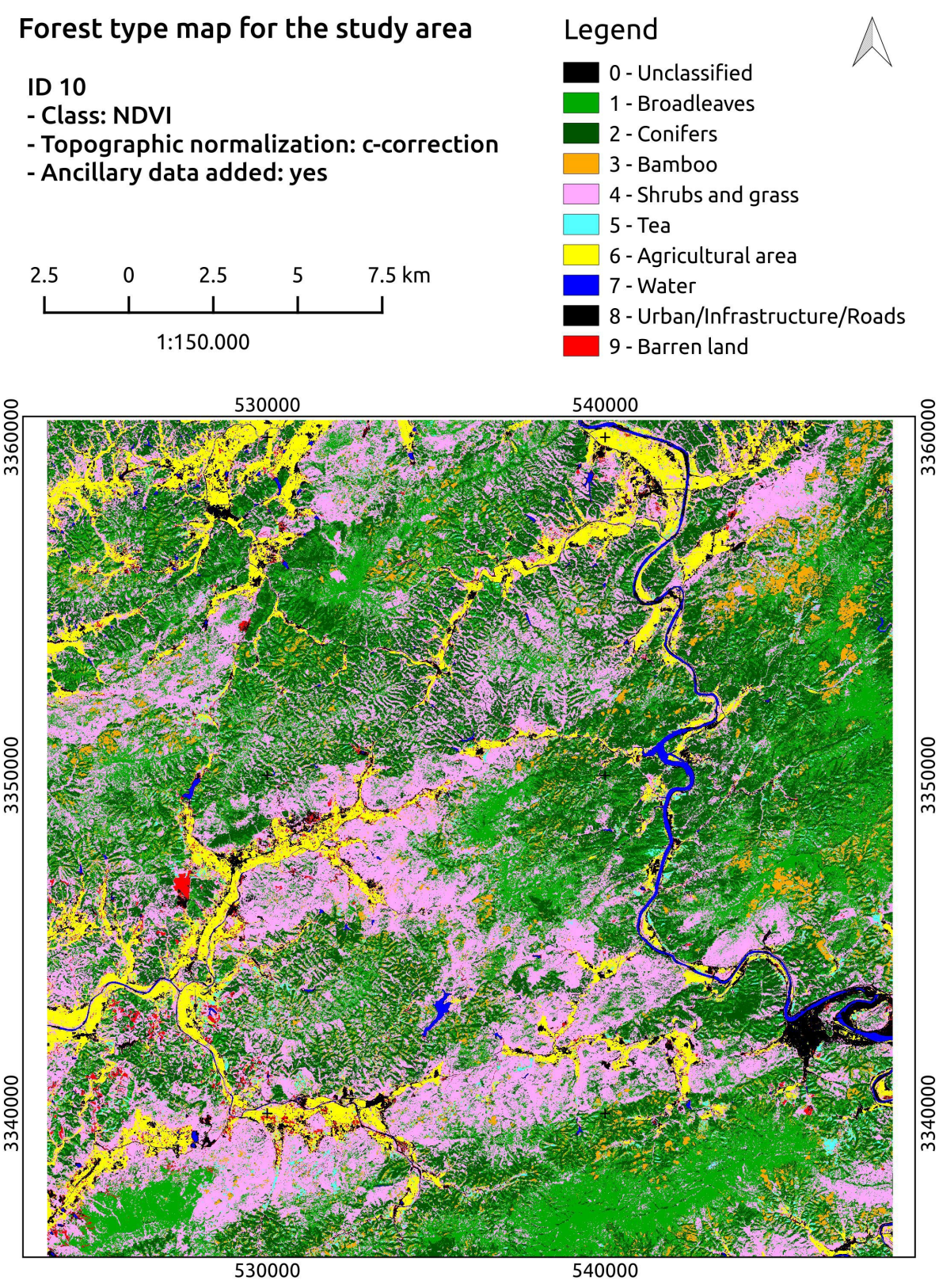
Forest type map for the study area
ID 10
- Class: NDVI
- Topographic normalization: c-correction
- Ancillary data added: yes
2.5 0 2.5 5 7.5 km
1:150.000
Legend
0 - Unclassified
1 - Broadleaves
2 - Conifers
3 - Bamboo
4 - Shrubs and grass
5 - Tea
6 - Agricultural area
7 - Water
8 - Urban/Infrastructure/Roads
9 - Barren land
530000
540000
3360000
3350000
3340000

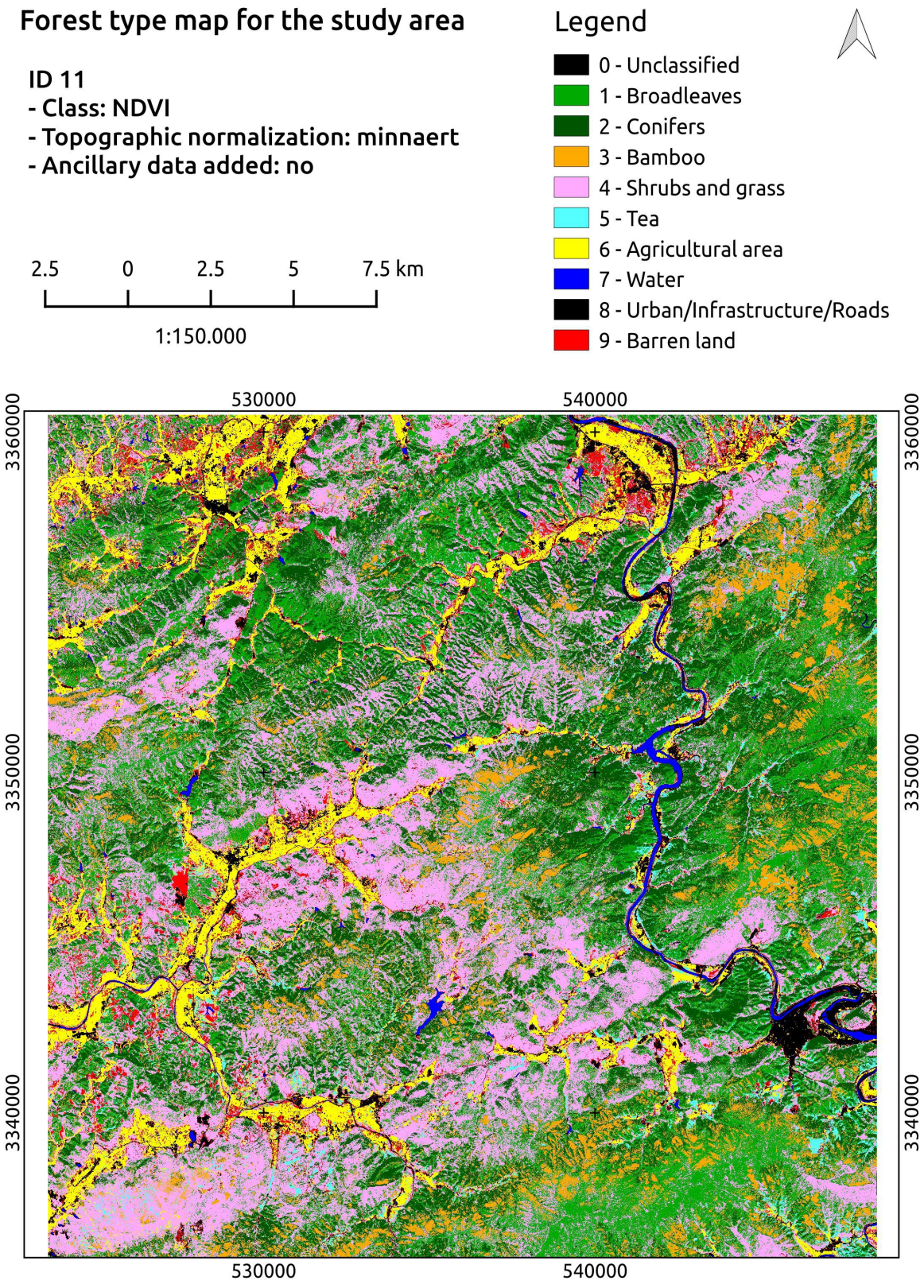
Forest type map for the study area
ID 11
- Class: NDVI
- Topographic normalization: minnaert
- Ancillary data added: no
2.5 0 2.5 5 7.5 km
1:150.000
Legend
0 - Unclassified
1 - Broadleaves
2 - Conifers
3 - Bamboo
4 - Shrubs and grass
5 - Tea
6 - Agricultural area
7 - Water
8 - Urban/Infrastructure/Roads
9 - Barren land
530000
540000
3360000
3350000
3340000

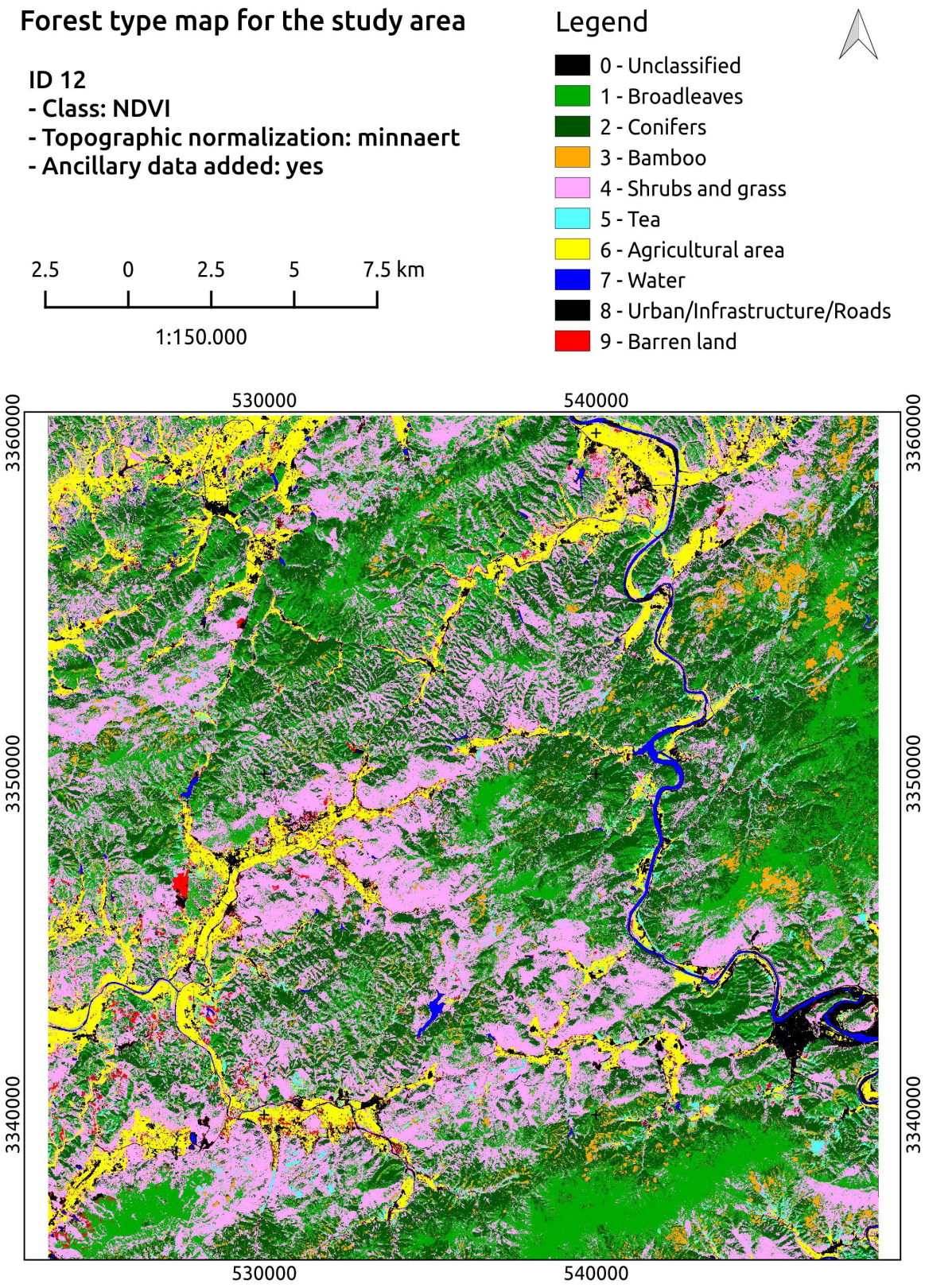
Forest type map for the study area
ID 12
- Class: NDVI
- Topographic normalization: minnaert
- Ancillary data added: yes
2.5 0 2.5 5 7.5 km
1:150.000
Legend
0 - Unclassified
1 - Broadleaves
2 - Conifers
3 - Bamboo
4 - Shrubs and grass
5 - Tea
6 - Agricultural area
7 - Water
8 - Urban/Infrastructure/Roads
9 - Barren land
530000
540000
3360000
3350000
3340000

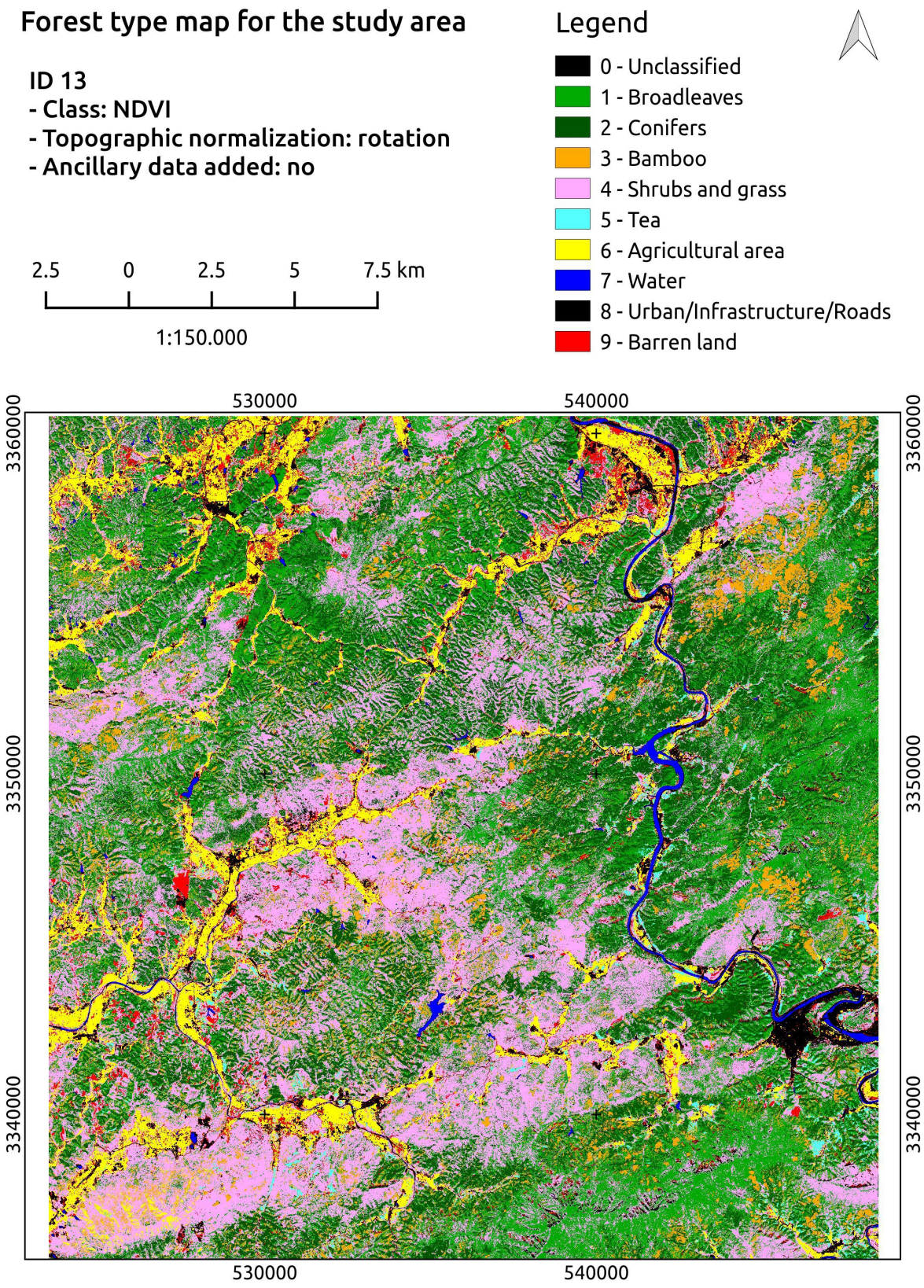
Forest type map for the study area
ID 13
- Class: NDVI
- Topographic normalization: rotation
- Ancillary data added: no
2.5 0 2.5 5 7.5 km
1:150.000
Legend
0 - Unclassified
1 - Broadleaves
2 - Conifers
3 - Bamboo
4 - Shrubs and grass
5 - Tea
6 - Agricultural area
7 - Water
8 - Urban/Infrastructure/Roads
9 - Barren land
530000
540000
3360000
3350000
3340000

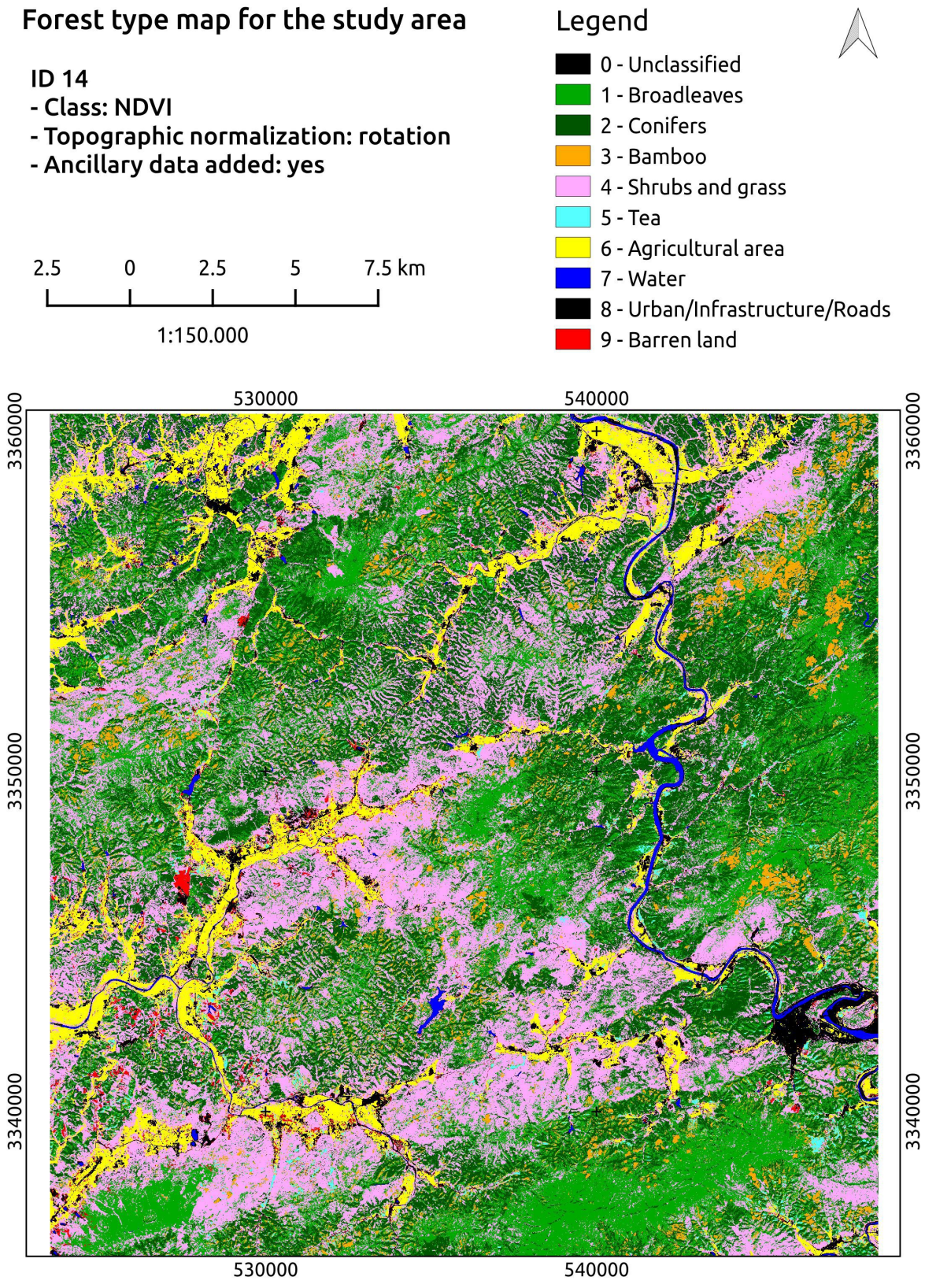
Forest type map for the study area
ID 14
- Class: NDVI
- Topographic normalization: rotation
- Ancillary data added: yes
2.5 0 2.5 5 7.5 km
1:150.000
Legend
0 - Unclassified
1 - Broadleaves
2 - Conifers
3 - Bamboo
4 - Shrubs and grass
5 - Tea
6 - Agricultural area
7 - Water
8 - Urban/Infrastructure/Roads
9 - Barren land
530000
540000
3360000
3350000
3340000

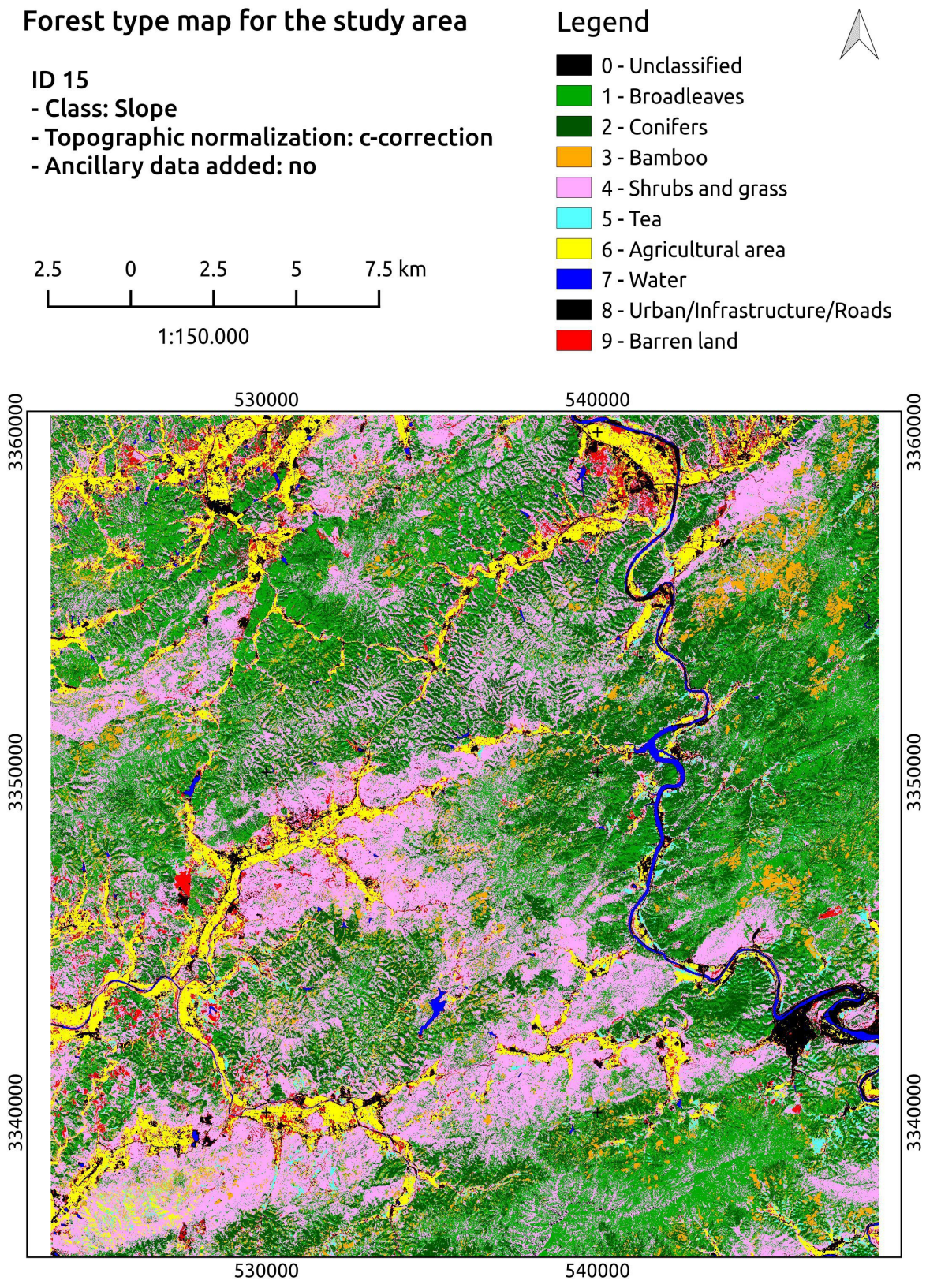
Forest type map for the study area
ID 15
- Class: Slope
- Topographic normalization: c-correction
- Ancillary data added: no
2.5 0 2.5 5 7.5 km
1:150.000
Legend
0 - Unclassified
1 - Broadleaves
2 - Conifers
3 - Bamboo
4 - Shrubs and grass
5 - Tea
6 - Agricultural area
7 - Water
8 - Urban/Infrastructure/Roads
9 - Barren land
530000
540000
3360000
3350000
3340000

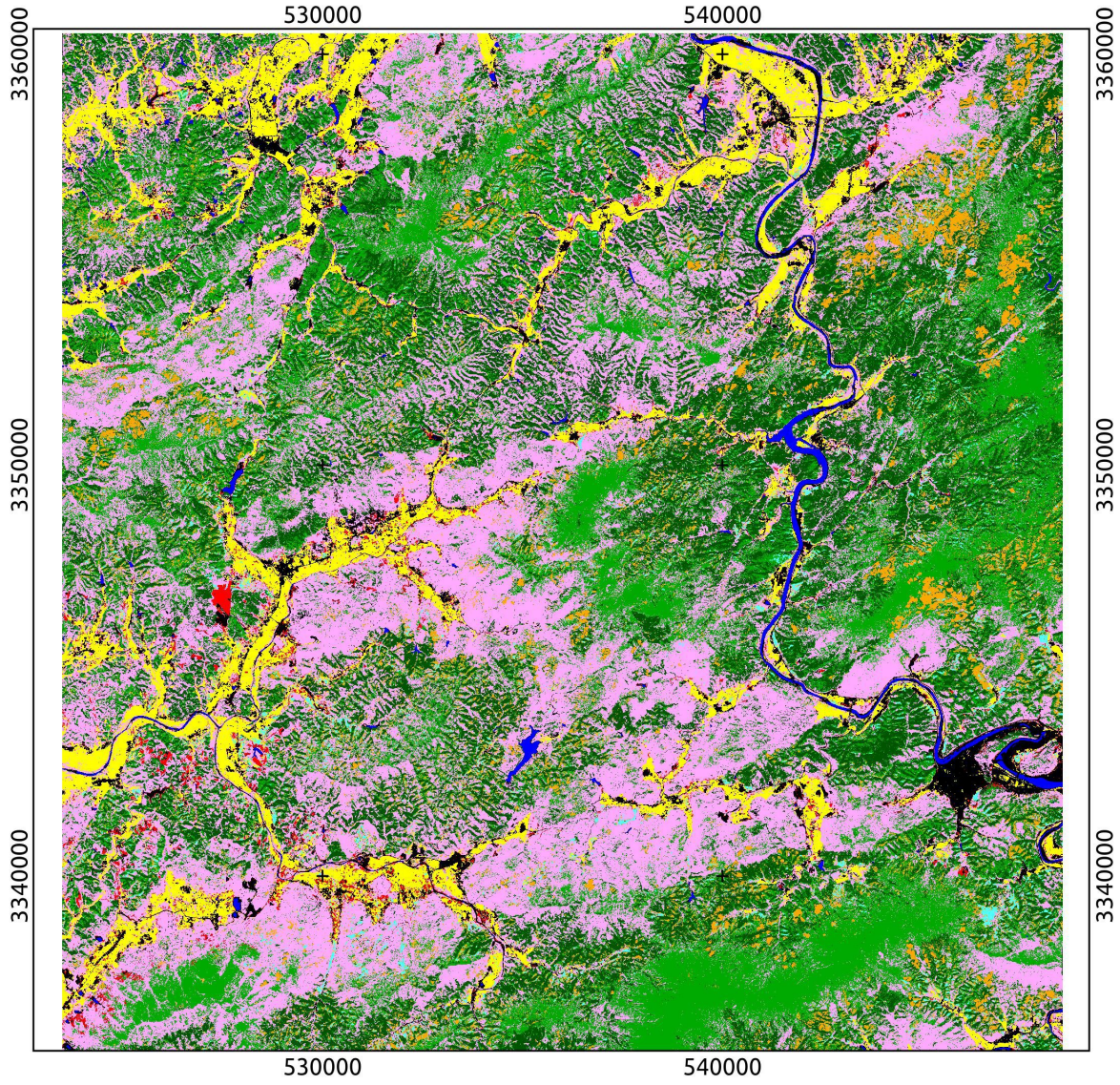
Forest type map for the study area
ID 16
- Class: Slope
- Topographic normalization: c-correction
- Ancillary data added: yes
2.5 0 2.5 5 7.5 km
1:150.000
Legend
0 - Unclassified
1 - Broadleaves
2 - Conifers
3 - Bamboo
4 - Shrubs and grass
5 - Tea
6 - Agricultural area
7 - Water
8 - Urban/Infrastructure/Roads
9 - Barren land
530000
540000
3360000
3350000
3340000

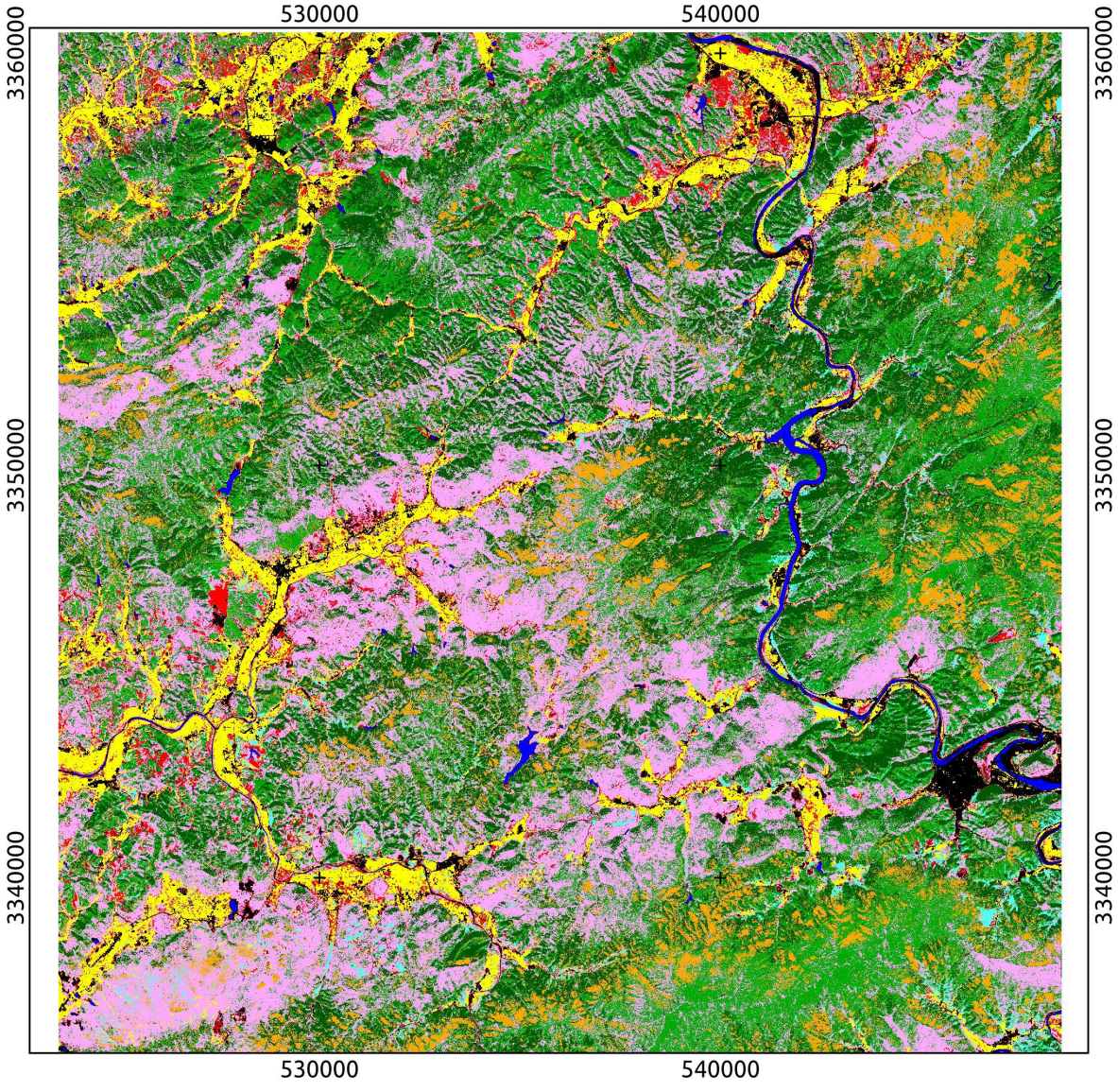
Forest type map for the study area
ID 17
- Class: Slope
- Topographic normalization: minnaert
- Ancillary data added: no
2.5 0 2.5 5 7.5 km
1:150.000
Legend
0 - Unclassified
1 - Broadleaves
2 - Conifers
3 - Bamboo
4 - Shrubs and grass
5 - Tea
6 - Agricultural area
7 - Water
8 - Urban/Infrastructure/Roads
9 - Barren land
530000
540000
3360000
3350000
3340000

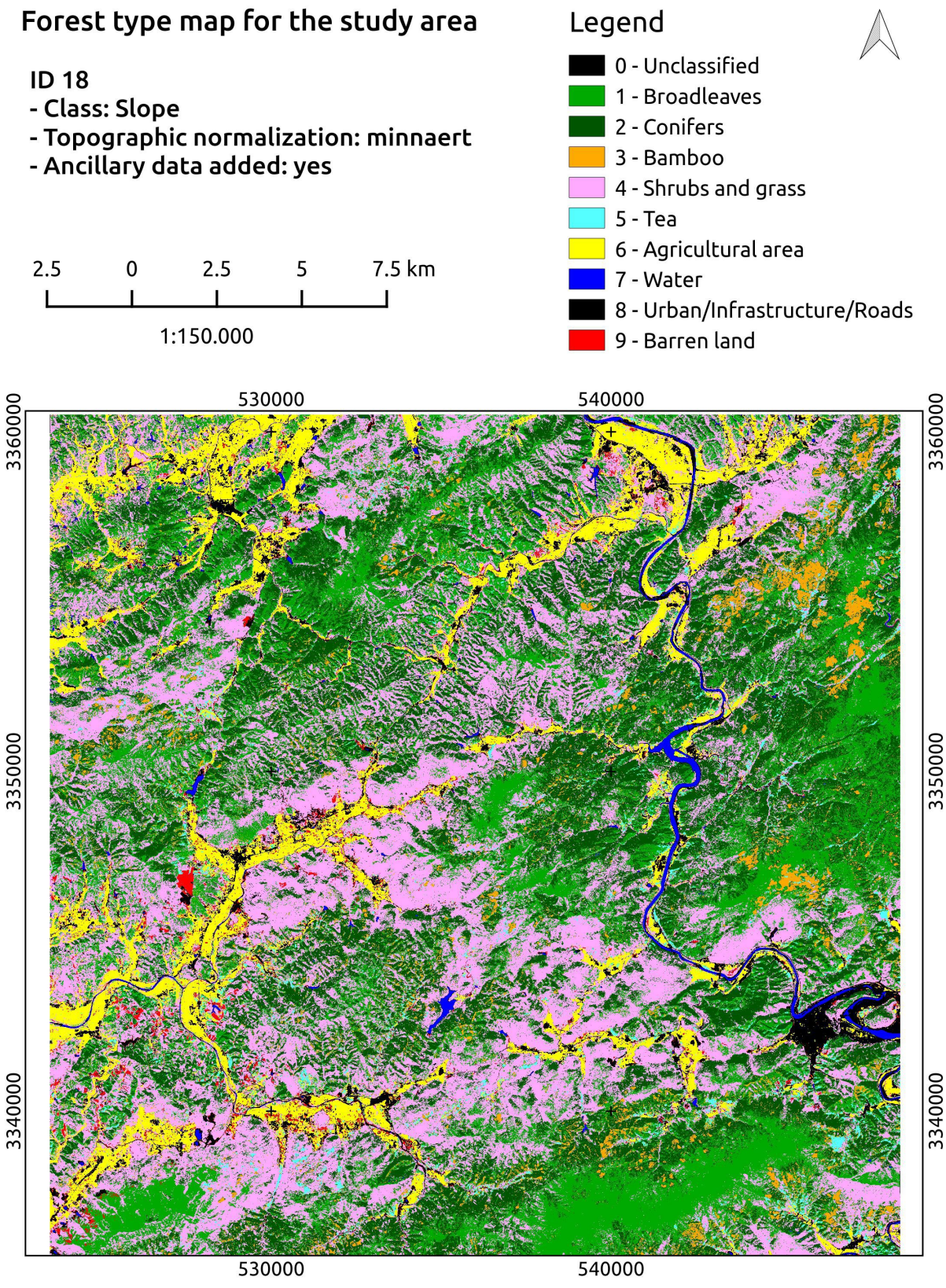
Forest type map for the study area
ID 18
- Class: Slope
- Topographic normalization: minnaert
- Ancillary data added: yes
2.5 0 2.5 5 7.5 km
1:150.000
Legend
0 - Unclassified
1 - Broadleaves
2 - Conifers
3 - Bamboo
4 - Shrubs and grass
5 - Tea
6 - Agricultural area
7 - Water
8 - Urban/Infrastructure/Roads
9 - Barren land
530000
540000
3360000
3350000
3340000

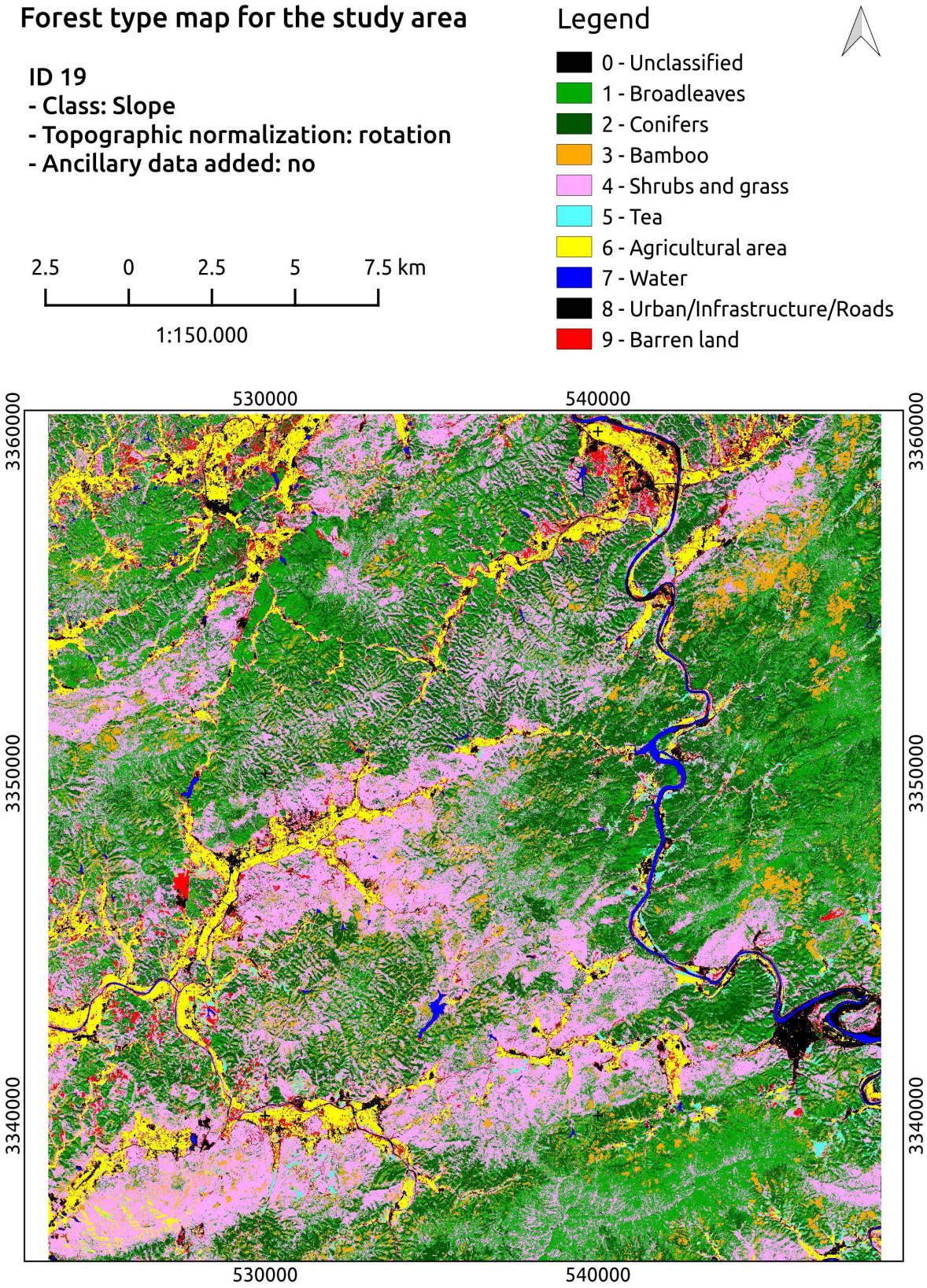
Forest type map for the study area
ID 19
- Class: Slope
- Topographic normalization: rotation
- Ancillary data added: no
2.5 0 2.5 5 7.5 km
1:150.000
Legend
0 - Unclassified
1 - Broadleaves
2 - Conifers
3 - Bamboo
4 - Shrubs and grass
5 - Tea
6 - Agricultural area
7 - Water
8 - Urban/Infrastructure/Roads
9 - Barren land
530000
540000
3360000
3350000
3340000

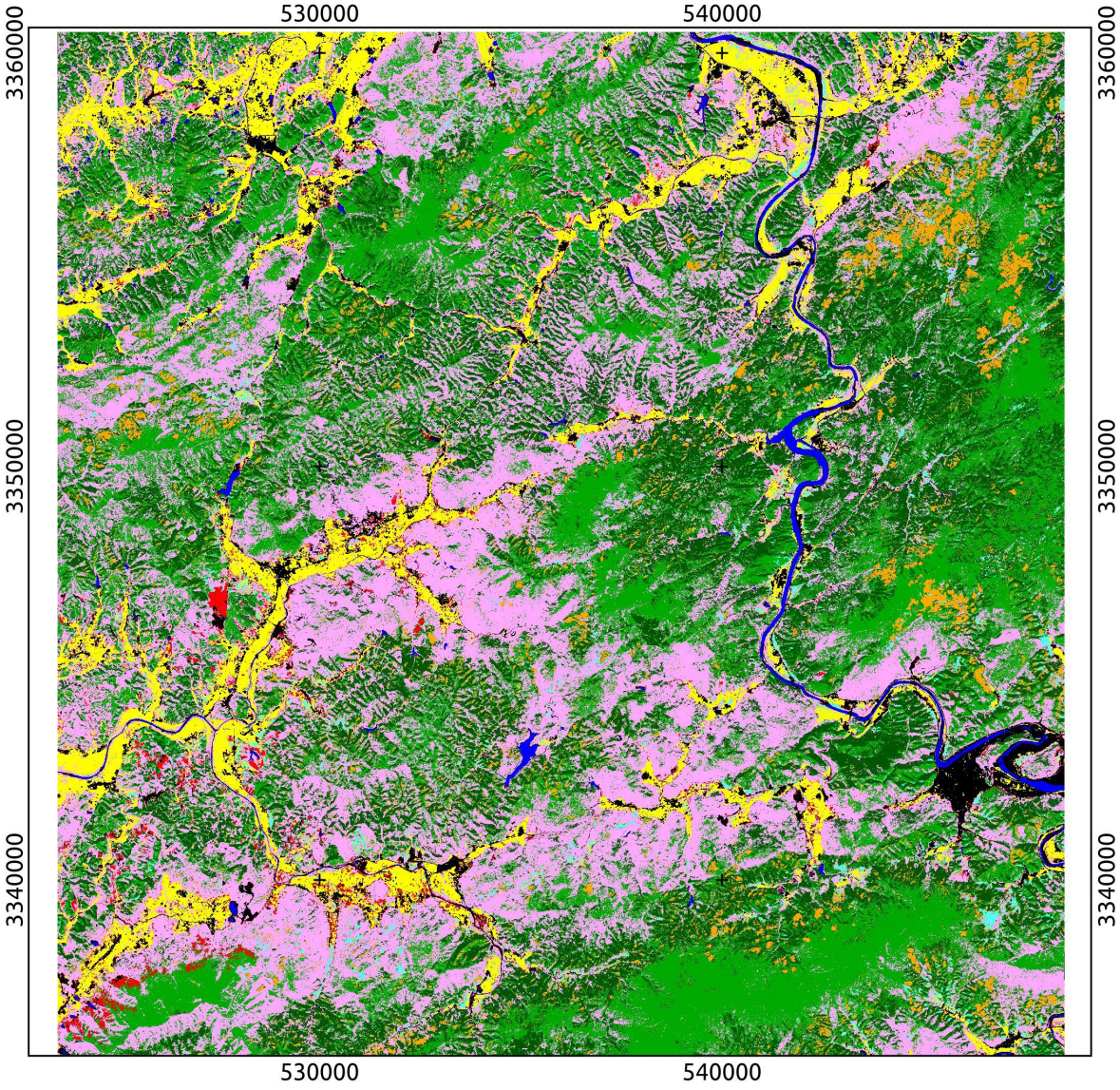
Forest type map for the study area
ID 20
- Class: Slope
- Topographic normalization: rotation
- Ancillary data added: yes
2.5 0 2.5 5 7.5 km
1:150.000
Legend
0 - Unclassified
1 - Broadleaves
2 - Conifers
3 - Bamboo
4 - Shrubs and grass
5 - Tea
6 - Agricultural area
7 - Water
8 - Urban/Infrastructure/Roads
9 - Barren land
530000
540000
3360000
3350000
3340000

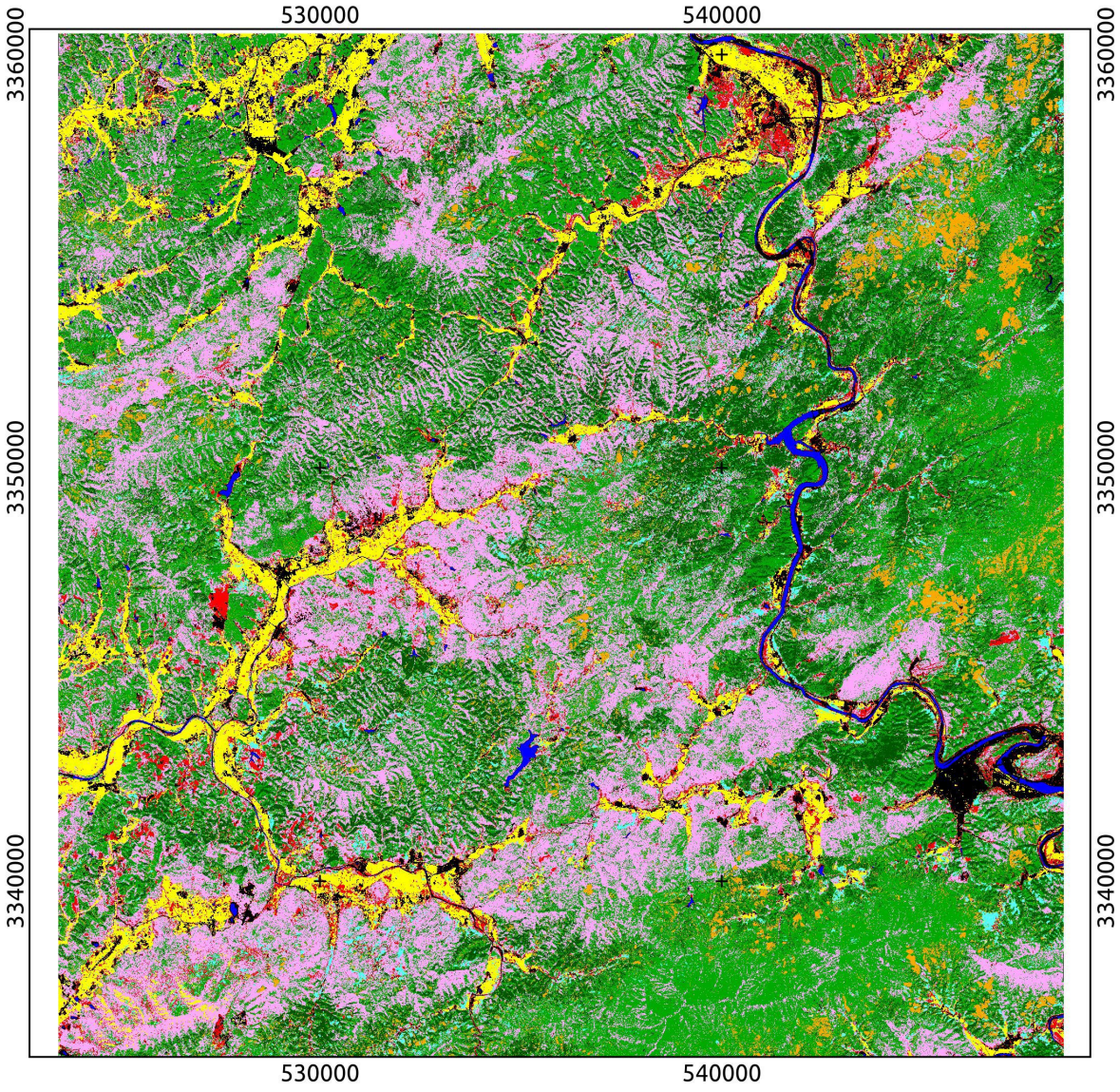
Forest type map for the study area
ID 21
- Class: Illumination
- Topographic normalization: c-correction
- Ancillary data added: no
2.5 0 2.5 5 7.5 km
1:150.000
Legend
0 - Unclassified
1 - Broadleaves
2 - Conifers
3 - Bamboo
4 - Shrubs and grass
5 - Tea
6 - Agricultural area
7 - Water
8 - Urban/Infrastructure/Roads
9 - Barren land
530000
540000
3360000
3350000
3340000

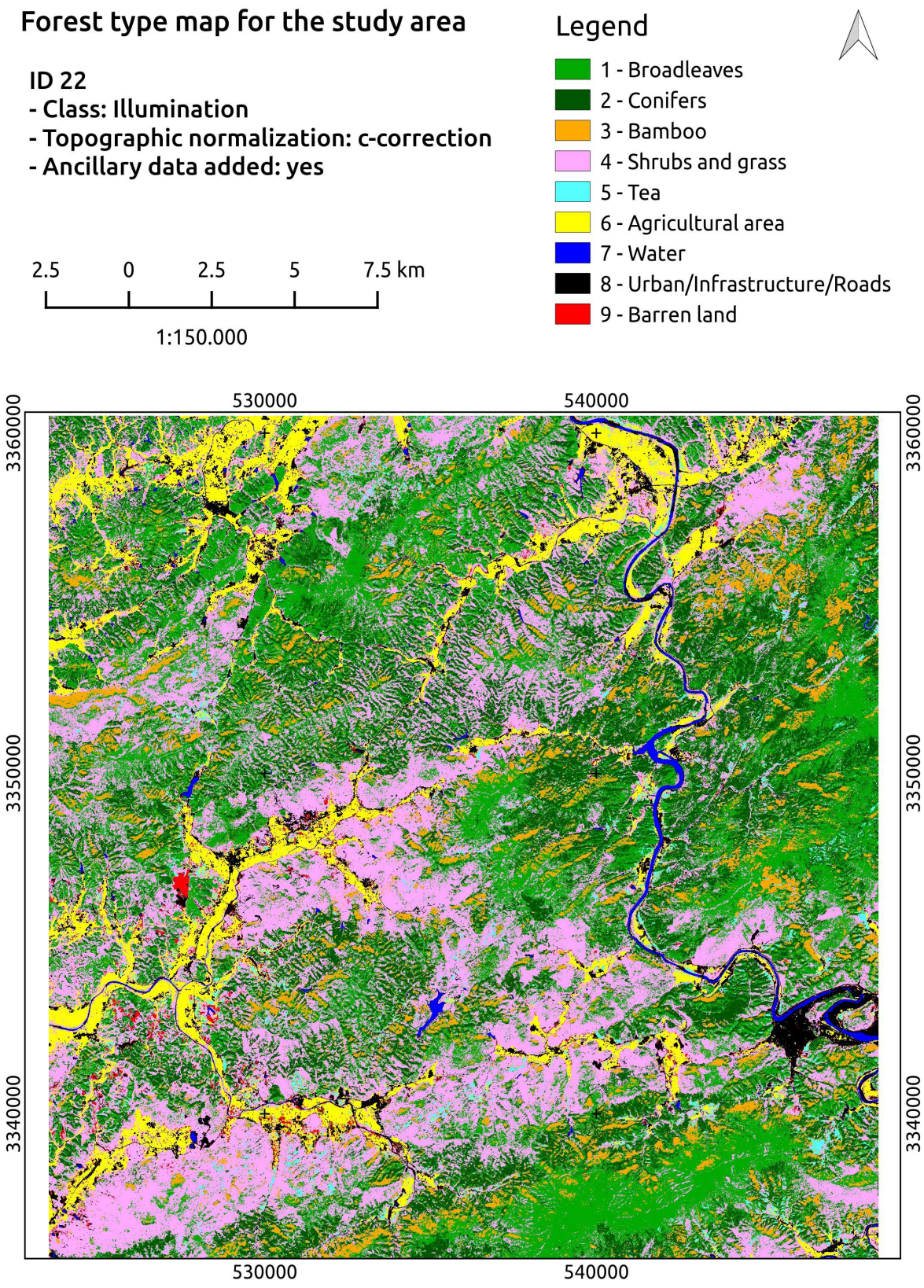
Forest type map for the study area
ID 22
- Class: Illumination
- Topographic normalization: c-correction
- Ancillary data added: yes
2.5 0 2.5 5 7.5 km
1:150.000
Legend
1 - Broadleaves
2 - Conifers
3 - Bamboo
4 - Shrubs and grass
5 - Tea
6 - Agricultural area
7 - Water
8 - Urban/Infrastructure/Roads
9 - Barren land
530000
540000
3360000
3350000
3340000

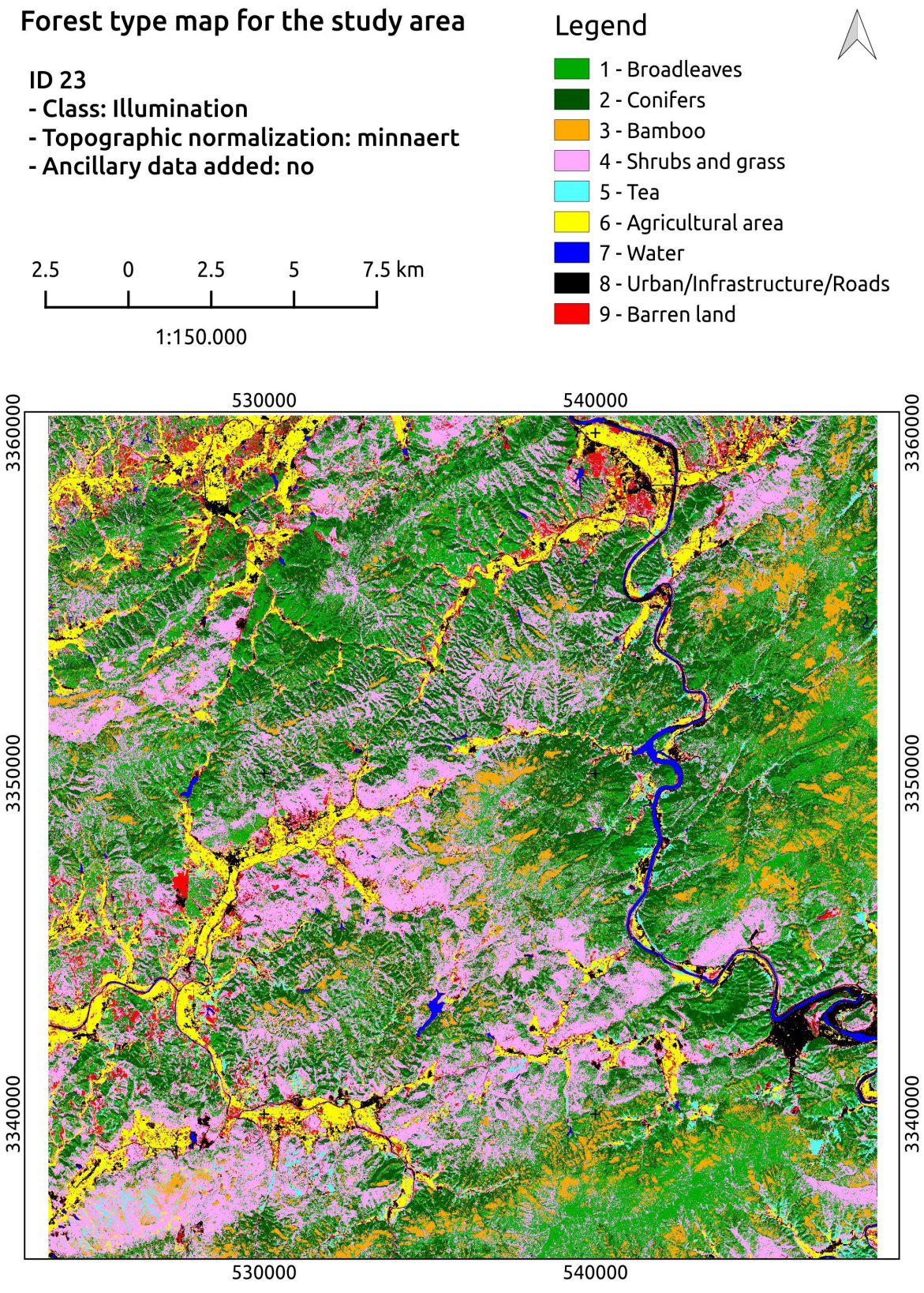
Forest type map for the study area
ID 23
- Class: Illumination
- Topographic normalization: minnaert
- Ancillary data added: no
2.5 0 2.5 5 7.5 km
1:150.000
Legend
1 - Broadleaves
2 - Conifers
3 - Bamboo
4 - Shrubs and grass
5 - Tea
6 - Agricultural area
7 - Water
8 - Urban/Infrastructure/Roads
9 - Barren land
530000
540000
3360000
3350000
3340000

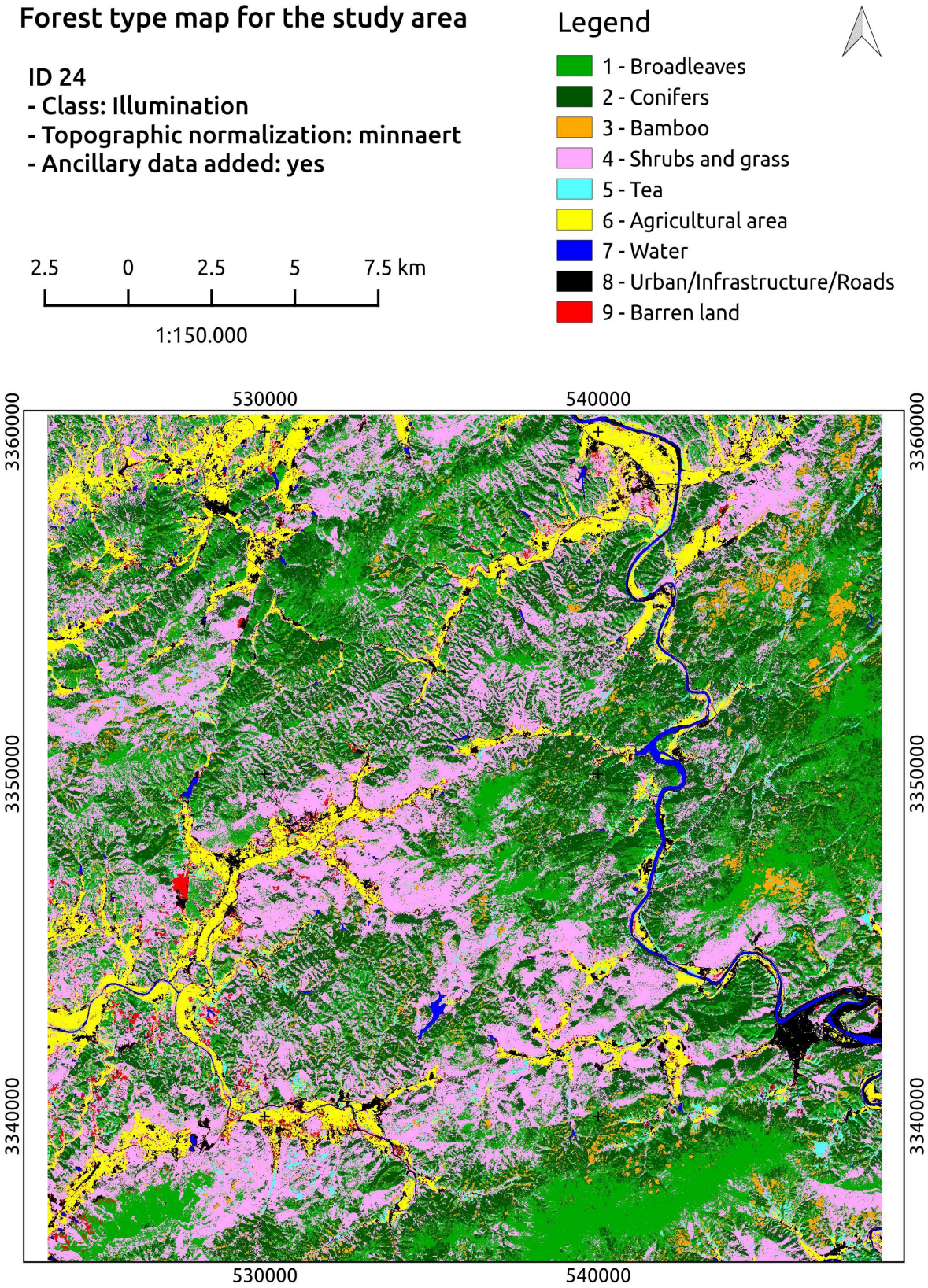
Forest type map for the study area
ID 24
- Class: Illumination
- Topographic normalization: minnaert
- Ancillary data added: yes
2.5 0 2.5 5 7.5 km
1:150.000
Legend
1 - Broadleaves
2 - Conifers
3 - Bamboo
4 - Shrubs and grass
5 - Tea
6 - Agricultural area
7 - Water
8 - Urban/Infrastructure/Roads
9 - Barren land
530000
540000
3360000
3350000
3340000

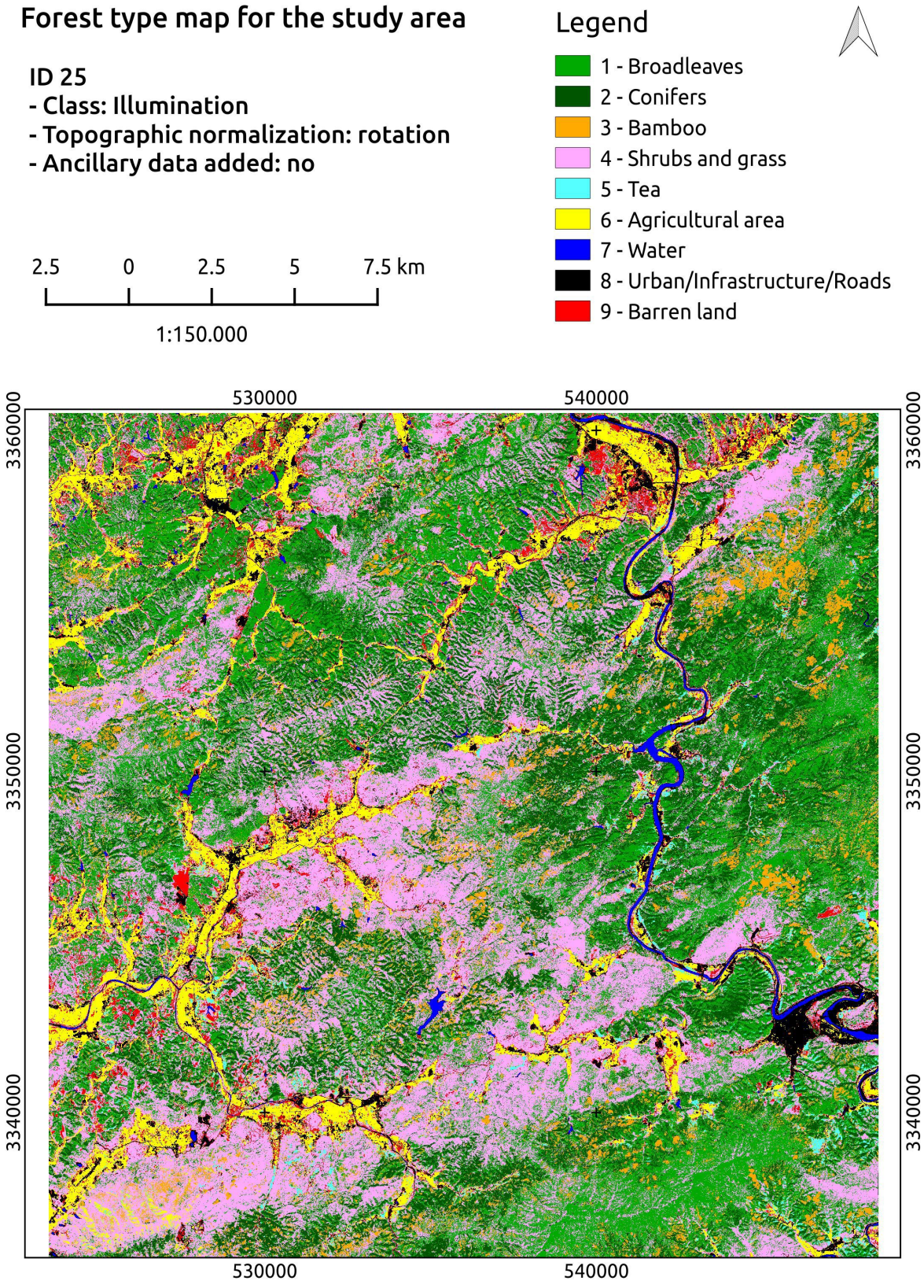
Forest type map for the study area
ID 25
- Class: Illumination
- Topographic normalization: rotation
- Ancillary data added: no
2.5 0 2.5 5 7.5 km
1:150.000
Legend
1 - Broadleaves
2 - Conifers
3 - Bamboo
4 - Shrubs and grass
5 - Tea
6 - Agricultural area
7 - Water
8 - Urban/Infrastructure/Roads
9 - Barren land
530000
540000
3360000
3350000
3340000

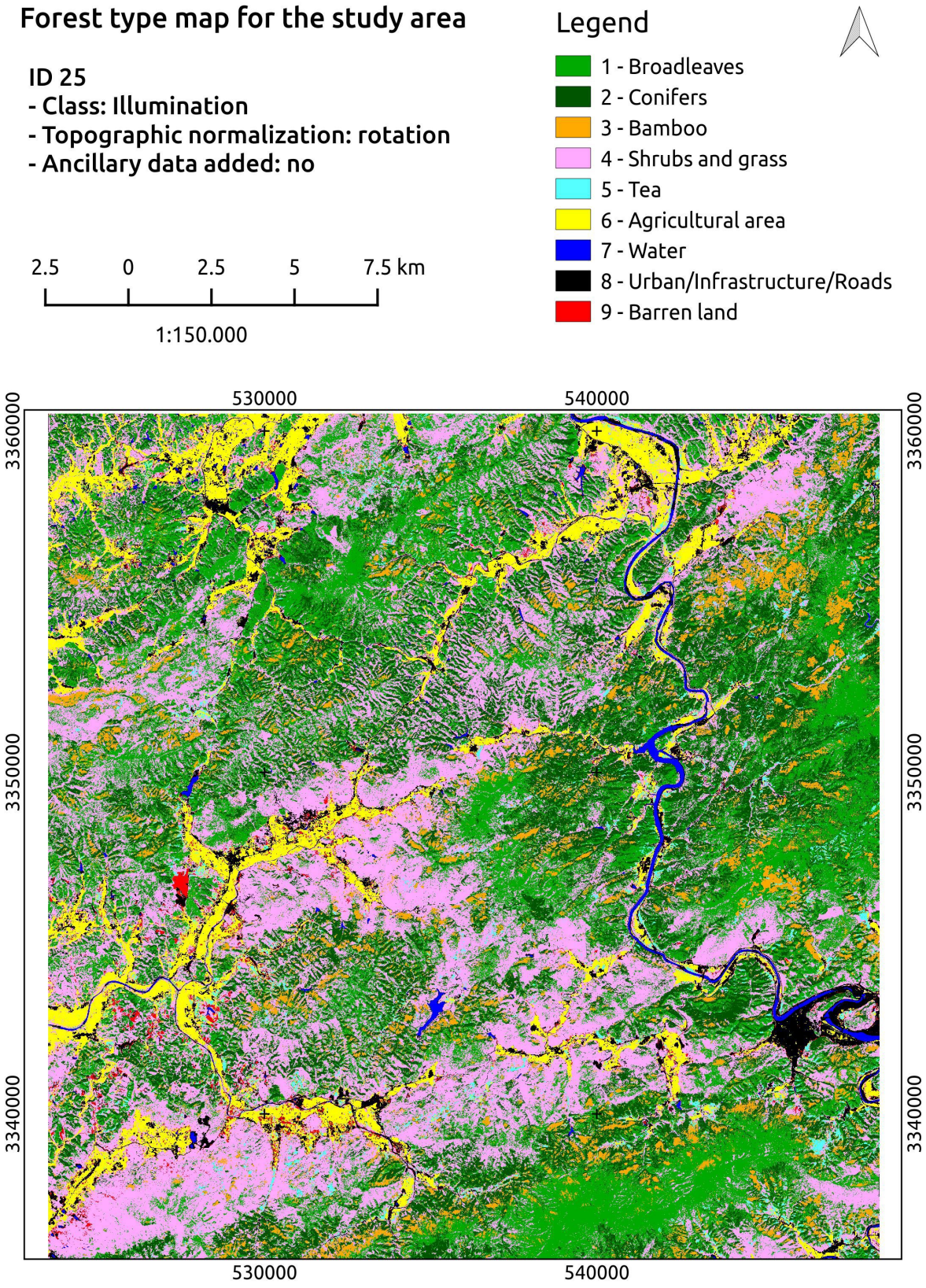
Forest type map for the study area
ID 25
- Class: Illumination
- Topographic normalization: rotation
- Ancillary data added: no
2.5 0 2.5 5 7.5 km
1:150.000
Legend
1 - Broadleaves
2 - Conifers
3 - Bamboo
4 - Shrubs and grass
5 - Tea
6 - Agricultural area
7 - Water
8 - Urban/Infrastructure/Roads
9 - Barren land
530000
540000
3360000
3350000
3340000

"Approaches to topographic normalization for forest type mapping in Shitai County, Anhui Province, China"

Universitätslehrganges „Geographical Information Science & Systems“
(UNIGIS MSc) am Interfakultären Fachbereich für GeoInformatik (Z_GIS)
der Paris Lodron-Universität Salzburg

Declaration of Authorship

I certify that the material contained in this degree dissertation is my own work and does not contain any significant amount of unacknowledged work of others.

1. Where I have consulted the published work of others this is always clearly attributed.

2. Where I have quoted from the work of others the source is always given. With the exception of such quotation, the work of this dissertation is entirely my own work.

3. This dissertation has not been submitted for the award of any other degree or diploma in any tertiary institution.

MSc Metodi Panev

10662, UNIGIS MSc Jahrgang 2012

Freiburg, January 2015